The characterization of the *Atxn2*-CAG42-knock-in mouse as a model for Spinocerebellar Ataxia Type 2

Dissertation

zur Erlangung des Grades

“Doktor der

Naturwissenschaften“

am Fachbereich Biologie

der Johannes Gutenberg-Universität

in Mainz

(D77)

Ewa Maria Damrath

geboren in Hannover

Mainz, 2012

Dekan: ……...

1. Berichterstatter: …….

2. Berichterstatter: …….

Tag der mündlichen Prüfung: 25.09.2012

Table of contents

1 Introduction

1.1 Autosomal dominant cerebellar ataxias type I

The cerebellar ataxias are a large group of neurodegenerative diseases that can be divided into inherited and sporadic forms. The inherited ataxias are further divided into episodic, X-linked, autosomal recessive and autosomal dominant ataxias (Manto & Marmolino 2009). The latter manifest with a loss of balance and motor coordination due to a dysfunction of the cerebellar neurons and their afferent and efferent connections (Duenas *et al.* 2006). The classification of the autosomal dominant cerebellar ataxias (ADCA), though clinically and genetically very heterogeneous, was made in 1993 by Harding on the basis of clinical symptoms and encompasses 3 groups (Harding 1993). ADCA type I includes accessory symptoms known from, among others, the Spinocerebellar ataxias SCA1, SCA2, SCA3 and DRPLA (dentatorubral-pallidoluysian atrophy) that are described in detail further below. The type II class includes accessory symptoms like macular degeneration, e.g. in SCA7, while type III is comprised of pure cerebellar syndromes as known from e.g. SCA5 and SCA6. The phenotype of ADCA type I patients manifests with a disordered voluntary movement of the gait, limbs and stance, leading to dyschronometria (rate of initiation and cessation), dysmetria (amplitude), dysdiadochokinesia (speed of alternating movements), dyssynergia (coordination of single movements) and action tremors. Nystagmus, saccadic abnormalities and dysarthria are further common symptoms (Whaley *et al.* 2011). The involvement of degenerated basal ganglia, cerebral cortex, optic nerve, pontomedullary systems, spinal tracts or peripheral nerves can also contribute to the disease (Duenas *et al*. 2006).
The incidence of SCAs worldwide is around 3:100,000 inhabitants, however, regional differences are common. A putative founder effect contributed to the prevalence of SCA2 in the province Holguín in Cuba to approximately 183:100,000 inhabitants (Velazquez-Perez *et al.* 2011). Among the triplet repeat disorders (section 1.1.1), SCA3 is the most frequent worldwide, followed by SCA2, SCA1 and SCA8 (Whaley *et al*. 2011).

1.1.1 Triplet repeat disorders

The triplet repeat disorders comprise three main classes of diseases which are all caused by an expansion of a repeated microsatellite sequence. Firstly, the expansion can lead to a loss of the protein function as e.g. known from the Fragile-X-Syndrome that manifests with a mental retardation of the affected patient. An expanded CGG repeat (above 200) in the 5' UTR region of the *FMR1* gene causes an increased methylation of the CpG islands in the 5' promoter region of *FMR1* leading to decreased histone acetylation and thus to inhibited

FMR1 expression and FMRP protein function (Coffee *et al.* 1999, Fu *et al.* 1992, Verkerk *et al.* 1991). Secondly, an RNA-mediated gain-of-function can lead to disease, e.g. in Myotonic Dystrophy, which is caused by a CTG-repeat in the 3' UTR of *DMPK* (Brook *et al.* 1992, Mahadevan *et al.* 1992). The expansion leads to a misregulated alternative splicing of other RNAs; its own splicing is not affected (Ranum & Cooper 2006). Thirdly, the gain of protein function is thought to be the main cause for the polyglutamine diseases. This class includes Huntington's disease, SBMA (spinal bulbar muscle atrophy) and also several ADCAs: SCA1-3, SCA6, SCA7, SCA17 and DRPLA (David *et al.* 1997, Imbert *et al.* 1996, Kawaguchi *et al.* 1994, Koide *et al.* 1994, Nagafuchi *et al.* 1994, Nakamura *et al.* 2001, Orr *et al.* 1993, Pulst *et al.* 1996, Sanpei *et al.* 1996, Zhuchenko *et al.* 1997). These polyglutamine disorders (currently 9 are known) are caused by an expanded CAG-triplet repeat in the coding region of the mutant gene that is thus translated with an expansion domain (Table 1). When a certain repeat number is reached, the disease will manifest. Furthermore, when a certain threshold is passed, the repeat becomes unstable and tends to expand further in successive generations, leading to a more severe disease course. This phenomenon is called anticipation (Schols *et al*. 2004). An inverse correlation between age at onset and CAG repeat number is common (Schols *et al*. 2004).

Table 1. Polyglutamine disorders. (adapted from Hands, 2008 and Verbeek, 2011)

Disease	Protein	Locus	CAG repeat normal	CAG repeat affected
Huntington's disease	Huntingtin	4p16.3	6-34	36-121
SBMA	Androgen receptor	Xq11-q12	9-36	38-62
DRPLA	Atrophin-1	12p13.31	7-34	49-88
SCA 1	Ataxin-1	6p23	6-44	39-82
SCA 2	Ataxin-2	12q24	15-24	32-200
SCA 3	Ataxin-3	14q21	13-36	61-84
SCA 6	CACNA1A	19p13	4-19	10-33
SCA 7	Ataxin-7	3p21.1-p12	4-35	37-306
SCA 17	TATA binding protein	6q27	25-42	47-63

1.1.2 Pathomechanism of polyglutamine disorders

One similarity of the polyglutamine disorders is the expansion of a polyglutamine tract in the diseased protein, making a common pathway likely to be involved in the disease course. The impact of the polyglutamine tract itself was investigated in a mouse model with an expansion of 146 CAGs in a novel genetic context, the murine *Hprt* locus. This mouse showed late-onset neurological symptoms with neuronal intranuclear inclusions (NII) (Ordway *et al.* 1997). Beside that fact, the affected proteins are completely unrelated and it is the protein

context itself that plays the critical role in the disease course. Despite the ubiquitous expression, only neurons in the CNS are affected. While the medium sized spiny neurons of the striatum are affected in Huntington's disease, in the SCAs the cerebellar Purkinje cells are prone to degeneration. Each disease shows different repeat-length dependence. While SCA17 does not manifest before a repeat length of 47 CAGs, the threshold in SCA6 is considerably lower (Table 1). Furthermore, the phosphorylation state and interaction partners are specific to a polyglutamine protein and have been shown to also influence the disease course. The phosphorylation at position S776 of ATXN1 is critical for the formation of intranuclear inclusions, as the substitution to A776 in transgenic mice leads to reduced phosphorylation at this site and to a reduced number of NIIs as well as extenuated pathogenesis. Also, the inhibition of the interaction between ATXN1 and Gfi-1 via deletion of the AXH domain (see below) reduces neurodegeneration in flies and mice (Emamian *et al.* 2003, Tsuda *et al.* 2005).

The main cause for the degeneration of the neurons in polyglutamine disorders is thought to be mediated by a toxic gain-of-function mechanism on the protein level (Orr & Zoghbi 2007). The neuropathological hallmark of the polyglutamine diseases are mainly nuclear but also cytoplasmic aggregates of the disease protein and are commonly found in neurons of the affected areas of patients' brains. The aggregation is a consequence of the aberrant conformation of the expanded protein, with longer expansions being more prone to aggregation and being more robust. This probably leads to neuronal dysfunction and eventually cell death (Orr & Zoghbi 2007). However, whether these aggregates are in fact toxic or protective to the cell is still a matter of debate. Current views support the concept that small oligomeric species and microaggregates are directly toxic, whereas the larger aggregates are rather a by-product or even cytoprotective (Arrasate *et al.* 2004, Saudou *et al.* 1998, Slow *et al.* 2005). Chaperones, ubiquitin and subunits of the proteasome, all components of the protein quality system necessary to degrade misfolded proteins, were also found to be sequestered into the aggregates (Cummings *et al.* 1998, Schmidt *et al.* 2002). The fact that the phenotypes of transgenic and knock-in mouse models mimic the respective disease well (Clark *et al.* 1997, Huynh *et al.* 2000), whereas knock-out mice show different phenotypes with no ataxia or neurodegeneration (Lastres-Becker *et al.* 2008a, Matilla *et al.* 1998), further supports the concept of a gain-of-function mechanism as the main cause for the pathogenesis. In addition, the expansion can alter protein interactions, thus contributing to the disease. While the overexpression of either wild-type or expanded ATXN1 in transgenic mice decreased the expression levels of the ATXN1 interactor and transcription factor Gfi-1, the loss of Gfi-1 itself mimicked the SCA1 phenotype including ataxia and Purkinje cell degeneration (Tsuda *et al*. 2005). However, also partial loss-of-function mechanisms likely contribute to disease progression as has been shown in one study, where

the removal of the wild-type copy in Atxn1Q154 worsened the phenotype (Lim *et al.* 2008). Another study documented that the overexpression of the ATXN1 paralog ATXN1L, which shares several conserved domains and its interaction partners with ATXN1, could partially suppress the phenotype and neuropathology in the Atxn1Q154 mouse model with ATXN1L duplication (Bowman *et al.* 2007). Furthermore, Atxn1-deficient and Atxn1Q154 mice share 197 dysregulated genes (Crespo-Barreto *et al.* 2010).

Recent advances in defining other possible pathomechanisms of polyglutamine diseases denominate RNA as another driver of toxicity. Studies in *D. melanogaster* demonstrate that flies expressing a truncated version of Ataxin-3 with 78 CAGs ($Sca3tr78_{CAG}$) have stronger retinal degeneration, reduced lifespan and reduced ability to climb in comparison to control and $Sca3tr78_{CAA/G}$ flies whose polyglutamine expansion is encoded by a CAG triplet interrupted with CAAs (Li *et al.* 2008).

Further mechanisms leading to disease manifestation include transcriptional dysregulation (Lin *et al.* 2000), impaired axonal transport (Liu-Yesucevitz *et al.* 2011), aberrant neural signaling (Koch *et al.* 2011), repeat associated non-ATG translation initiation (RAN-translation) (Pearson 2011) and autophagy (Heng *et al.* 2010a, Heng *et al.* 2010b, Ravikumar *et al.* 2006, Zhuchenko *et al*. 1997).

1.1.3 Spinocerebellar ataxia type 2

The first description of SCA2 was made in 1971 in India by Wadia and Swami reporting patients with spinocerebellar degeneration who also showed noticeable slowed saccadic eye movements (Wadia & Swami 1971). Nowadays it is known that more than 90% of SCA2 patients manifest with these characteristic slowed saccadic eye movements (Velazquez-Perez *et al*. 2011). Other characteristics besides the cerebellar syndrome (section 1.1) of SCA2 are altered sleep (e.g. restless legs syndrome), reduced deep tendon reflexes, myoclonus and cramps due to an early affection of the thalamus, brainstem, cranial nerves, spinal cord and muscles (Estrada *et al.* 1999, Gierga *et al.* 2005, Orozco Diaz *et al.* 1990, Tuin *et al.* 2006, Velazquez-Perez *et al*. 2011). Early involvement of the midbrain can also lead to a manifestation as Parkinsonism (Charles *et al.* 2007, Gwinn-Hardy *et al.* 2000, Shan *et al.* 2001). Cognitive impairment includes reduction of attention and concentration (Burk *et al.* 2003, Reynaldo-Arminan *et al.* 2002). Later in the disease course, immobility with distal amyotrophy, dysphagia, ophthalmoplegia, incontinence and mental deficiencies are common (Lastres-Becker *et al.* 2008b). The disease takes a progressive course with worsening of, among others, the cerebellar syndrome and saccade slowing, and patients mostly die 15-20 years after the appearance of initial symptoms due to respiratory failure (Auburger 2012, Velazquez-Perez *et al*. 2011). Therapeutic treatment includes physical therapy and

logopedics to improve e.g. coordination, normal gait speed and speech (Perez-Avila *et al.* 2004). Besides, levodopa treatment is used to alleviate rigidity and bradykinesia, while muscle cramps can be ameliorated by magnesium administration. An effect of deep brain stimulation on postural tremor was reported in one case (Freund *et al.* 2007). In a recent study it was shown that riluzole, a drug currently used to ameliorate ALS, was beneficial for patients with cerebellar ataxia (Ristori *et al.* 2010). Other approaches include the administration of lithium, which is thought to exert neuroprotective effects (Watase *et al.* 2007), RNAi technique to inhibit the expression of the mutant allele (Xia *et al.* 2004), overexpression of chaperones (Muchowski & Wacker 2005) and histone deacetylase inhibitors to regulate gene expression (Thomas *et al.* 2008).

Disease onset is on average in the 3rd decade of life, whereas a case with a repeat length of > 200 CAGs was reported to manifest SCA2 shortly after birth. The parent carried a repeat in the normal disease range of around 40 CAGs, illustrating that the repeat transmitted was extremely unstable (Babovic-Vuksanovic *et al.* 1998, Mao *et al.* 2002).

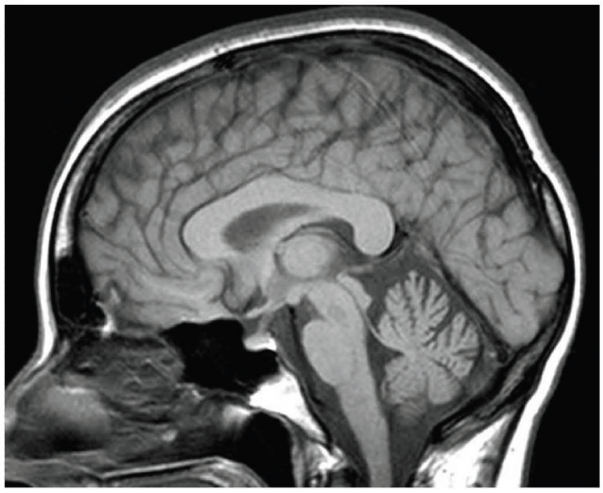

Figure 1. Sagittal MR (T1) scan of a 54 year old African-American SCA2 patient. The patient displays a clear cerebellar and brainstem atrophy (Whaley *et al*. 2011).

Pathological observations in SCA2 include a marked atrophy of the cerebellum, pons, frontal lobe, medulla oblongata, cranial nerves and the substantia nigra in the midbrain (Estrada *et al*. 1999, Gierga *et al*. 2005). Microscopic findings in the cerebellum of SCA2 patients include early loss of the large Purkinje neurons, preceded by a reduction in their dendritic arborisation and in the thickness of the molecular layer where the synaptic contacts and neuronal processes are located (Estrada *et al*. 1999). While pathological NIIs containing polyQ aggregates in SCA2 are detectable only in a minority of olivary and pontine neurons, they were never observed in cerebellar Purkinje neurons. Still, cytoplasmic expanded

polyglutamine-containing microaggregates were found within SCA2 brains and rarely also in Purkinje neurons (Huynh *et al*. 2000, Koyano *et al.* 2002, Pang *et al.* 2002).

1.2 Ataxin-2: gene, protein and function

1.2.1 The *Atxn2* gene

The Ataxin-2 (*ATXN2*) gene was detected independently by three groups in 1996 and is located on chromosome 12q24 (Imbert *et al*. 1996, Pulst *et al*. 1996, Sanpei *et al*. 1996). It consists of 25 exons, carrying a polyglutamine encoding tract in its first exon. More than 90% of the human population carry a repeat size of 22-23 triplets, composed of a CAG-sequence interrupted by CAA triplets, usually $(CAG)_8$-CAA-$(CAG)_4$-CAA-$(CAG)_8$ (Pulst *et al*. 1996). Alleles between 27 and 33 are considered intermediate size expansions and have recently been shown to result in a higher risk for related neurodegenerative diseases such as ALS and Progressive supranuclear palsy (Elden *et al.* 2010, Gispert *et al.* 2012, Ross *et al.* 2011). Individuals having a polyQ-repeat of 32 CAGs or more may develop SCA2 (Auburger 2012). The role of the CAA interruptions is critical. They stabilize the repeat size during replication and/or repair by maintaining proper DNA structure (McMurray 1999), while their loss causes an unstable transmission (usually paternal) to successive generations (Pujana *et al.* 1999). The intermediate sized *ATXN2*-repeats mostly bear at least one CAA interruption, while SCA2 patients have a pure CAG repeat. Several studies documented that CAA-interruptions in the pathological expansion range of > 32 manifest with Parkinsonism (Charles *et al*. 2007, Kim *et al.* 2007, Payami *et al.* 2003, Shan *et al*. 2001), while recent data also document an ALS phenotype associated with interrupted pathological expansions of > 31 in size (Corrado *et al.* 2011).

Alternative splice variants of *ATXN2* were reported for human and mouse (Table 2), possibly existing to exert different functions (Affaitati *et al.* 2001, Lastres-Becker *et al*. 2008b, Sahba *et al.* 1998).

Table 2. Alternative splice variants of *Ataxin-2.* (Affaitati 2001, Lastres-Becker 2008, Sahba 1998).

Isoform	Affected exon	Species	Tissue
Type I	Full-length	Human and mouse	Brain, spinal cord, cerebellum, heart, placenta
Type II	Exon 10	Human and mouse	not determined
Type III	Exon 10 and 11	Mouse	not determined
Type IV	Exon 21	Mouse	Brain, spinal cord, cerebellum, heart, placenta
Type V	Exon 12	Mouse	not determined
Type VI	Exon 24	Mouse	not determined

The *ATXN2* gene is expressed as early as embryonal day 8 in mice (Nechiporuk *et al.* 1998). In humans its expression was found throughout the brain in cerebellum, cerebral cortex, medulla, spinal cord, occipital pole, frontal lobe, striatum (putamen and nucleus caudatus), amygdala, corpus callosum, hippocampus, hypothalamus, substantia nigra and thalamus. *ATXN2* expression in peripheral tissue was detected in heart, placenta, liver, skeletal muscle and pancreas (Imbert *et al*. 1996, Pulst *et al*. 1996, Sanpei *et al*. 1996).

1.2.2 The ATXN2 protein

The *ATXN2* gene encodes the 1312 residue long ATXN2 protein, including a 22 glutamine repeat spanning the amino acids 166-187 in humans (Figure 2). Its molecular mass is around 140 kDa. It is a highly basic protein, except for one acidic region built up by two predicted globular domains, the Lsm (Like Sm, amino acids 254-345) and LsmAD domain (Lsm-asssociated domain, amino acids 353-475), spanning exons 2-7. The LsmAD domain further bears a clathrin-mediated *trans*-Golgi signal (amino acids 414-416) and an ER exit signal (amino acids 426-428). The PAM2 motif (amino acids 908-925) mediates the interaction to the Poly(A)-binding protein (PABPC1) and is conserved throughout eukaryotes. Outside of these domains, ATXN2 is only weakly conserved (Albrecht *et al.* 2004, Satterfield & Pallanck 2006). Four proline-rich domains (PRDI and PRDII) were found across the ATXN2 sequence, making interactions with SH3 domains of cytoskeleton and endocytosis related proteins possible. ATXN2 can be phosphorylated at S860 and S864 (La Spada & Taylor 2010, Turnbull *et al.* 2004).

Figure 2. ATXN2 protein structure. Characteristic domains of ATXN2 are indicated. Arrows indicate *trans*-Golgi and ER exit signal.

The expression of the ATXN2 protein is widely throughout neuronal cells of the adult mouse brain in conjunction with the mRNA expression pattern. A high ATXN2 expression is detected in the Purkinje cells of the cerebellum and in neurons from the brain stem, while it is only weakly expressed in the cerebellar granule layer and the cerebral cortex. It is further found in hippocampus, thalamus and hypothalamus, while it is undetectable in glial cells. A cytoplasmic and perinuclear distribution and a granular pattern with no nuclear staining are characteristic for the ATXN2 localization (Nechiporuk *et al*. 1998, van de Loo *et al.* 2009). More precisely, ATXN2 was shown to co-sediment with the rough ER membranes in the mouse brain (van de Loo *et al*. 2009).

1.2.3 The function of ATXN2

Yeast and mouse studies showed that ATXN2 is a non-essential gene, whereas *D. melanogaster* and *C. elegans* are not viable upon ATXN2 loss (Kiehl *et al.* 2000, Lastres-Becker *et al*. 2008a, Mangus *et al.* 1998, Satterfield *et al.* 2002). Phenotypic observations describe a role of ATXN2 in RNA metabolism that is nowadays well established; however its exact function still remains to be elucidated. The previously described domains found in ATXN2 gave first clues about its function. The PAM2 domain is found in proteins that interact with the Poly(A)-binding protein (PABPC1), thus making a role of ATXN2 in translation likely. Proteins that function in RNA processing such as RNA modification, pre-mRNA splicing, mRNA decapping and degradation bear the conserved LSm domains (Albrecht *et al*. 2004). Furthermore, the proline-rich domains (PRD) suggest an ATXN2 role in endocytosis.

1.2.3.1 ATXN2 function in translation initiation

Protein synthesis is mainly regulated at the initiation step of translation, to allow for rapid, reversible and spatial control of gene expression (Jackson *et al.* 2010). Translation initiation in eukaryotes includes initiator Met-tRNA (Met-tRNA$_i$) assembly to the 40S ribosomal subunit and binding to a 5' cap-mRNA, ready to scan the mRNA. Upon ATG-start codon recognition the 60S subunit joins this complex to form the 80S initiation complex to start translation. Energy expenditure and at least nine eukaryotic initiation factors are required for this highly complex process (Jackson *et al*. 2010).

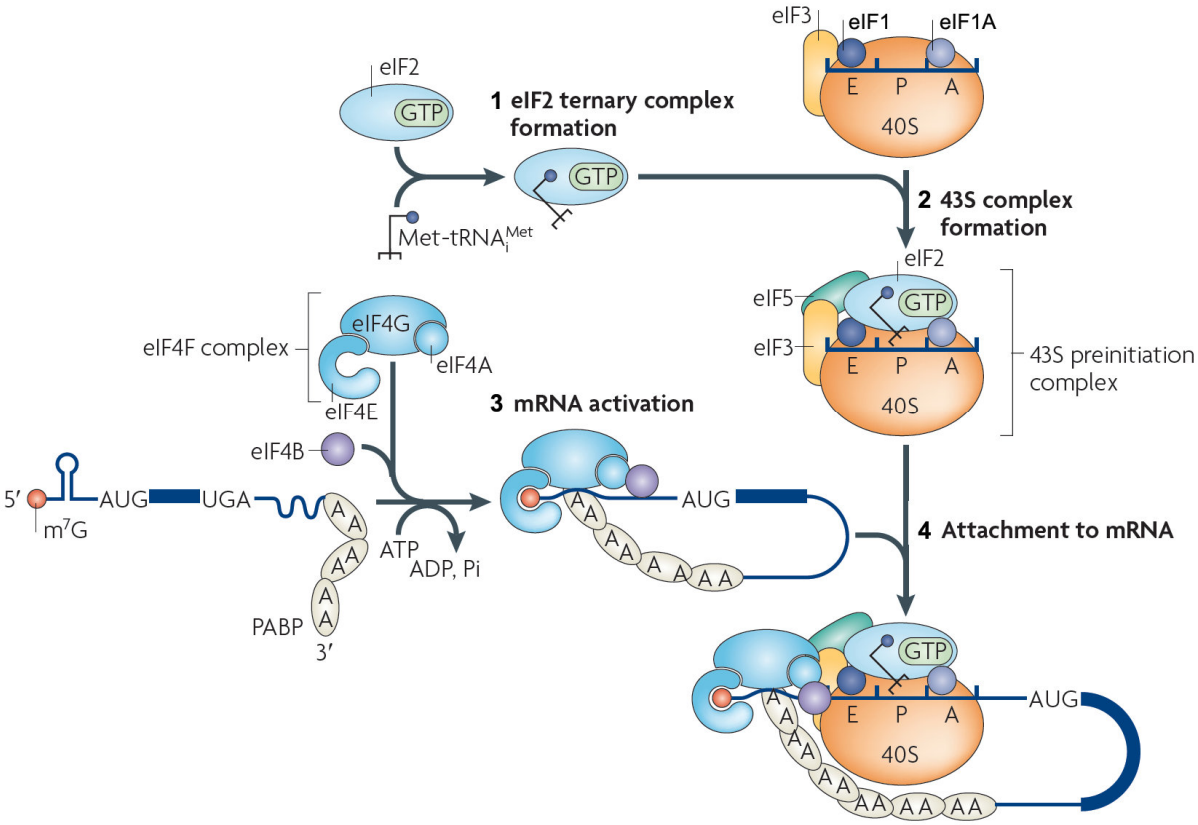

Figure 3. 43S preinitiation complex formation and mRNA binding during translation initiation. The four stages for the formation of the 43S preinitiation complex and its binding to 5'-capped mRNA are indicated. 1: eIF2 ternary complex formation, 2: 43S complex formation, 3: mRNA activation, 4: 43S preinitiation complex attachment to mRNA. Adapted from (Jackson *et al*. 2010)

The first stage of translation initiation is the formation of the 43S preinitiation complex (Figure 3, Table 3). During 80S ribosome recycling, the eukaryotic initiation factors eIF3, eIF1 and eIF1A are recruited to the 40S ribosomal subunit. The binding of eIF1 and eIF1A induce conformational changes of the 40S subunit to prepare it for mRNA binding. GTP-bound eIF2 binds Met-tRNA$_i$ (step 1) and attaches then together with eIF5 to the 40S subunit building the 43S preinitiation complex (step 2). The eIF4F complex is composed of the RNA helicase eIF4A, eIF4E that binds to the 5'-cap structure of the mRNA and the scaffold protein eIF4G.

eIF4G binds to eIF4A, eIF4E and mRNA-bound PABP, thus enhancing the affinity of eIF4E to the cap and promoting circularization of the mRNA. The recruitment of eIF4B further enhances the RNA-helicase activity of eIF4A. The mRNA activation occurs under ATP hydrolysis (step 3). The eIF4F complex together with eIF4B helps to unwind the 5'-cap region of the mRNA allowing the 43S preinitiation complex to attach to it (step 4) (Jackson *et al*. 2010).

Table 3. Eukaryotic initiation factors. Adapted from (Jackson *et al*. 2010)

Name	Function
Core initiation factors	
eIF1	Ensures the fidelity of initiation codon selection; Promotes ribosomal scanning; Stimulates binding of eIF2–GTP–Met-tRNA$_i$ to 40S subunits; Prevents premature eIF5-induced hydrolysis of eIF2-bound GTP and P$_i$ release
eIF1A	Stimulates binding of eIF2–GTP–Met-tRNA$_i$ to 40S subunits and cooperates with eIF1 in promoting ribosomal scanning and initiation codon selection
eIF2	Forms an eIF2–GTP–Met-tRNA$_i$ ternary complex that binds to the 40S subunit, thus mediating ribosomal recruitment of Met-tRNA$_i$
eIF3	Binds 40S subunits, eIF1, eIF4G and eIF5; Stimulates binding of eIF2–GTP–Met-tRNA$_i$ to 40S subunits; Promotes attachment of 43S complexes to mRNA and subsequent scanning; Possesses ribosome dissociation and anti-association activities, preventing joining of 40S and 60S subunits
eIF4A	DEAD-box ATPase and ATP-dependent RNA helicase
eIF4B	An RNA-binding protein that enhances the helicase activity of eIF4A
eIF4E	Binds to the m7GpppG 5′-cap structure of mRNA
eIF4F	A cap-binding complex, comprising eIF4E, eIF4A and eIF4G; Unwinds the 5′ region of mRNA and mediates the attachment of 43S complexes to it; Assists ribosomal complexes during scanning
eIF4G	Binds eIF4E, eIF4A, eIF3, PABP and mRNA and enhances the helicase activity of eIF4A
eIF5	A GTPase-activating protein, specific for GTP-bound eIF2, that induces hydrolysis of eIF2-bound GTP on recognition of the initiation codon
Auxiliary factors	
PABP	Binds to the 3′-poly(A) tail of mRNA, eIF4G and eRF3; Enhances binding of eIF4F to the cap; Might facilitate recruitment of recycled post-termination 40S subunits back to the 5′ end of mRNA

PABPC1 belongs to a family of proteins that are characterized by their ability to bind to poly(A) RNA and are conserved throughout eukaryotes (Gorgoni & Gray 2004). Within the nucleus, poly(A) RNA is bound by PABPN1 to aid in adenylation and maturation of pre-mRNAs. In the cytoplasm PABPC1 is the best characterized member. It contains four RNA recognition motifs (RRM) through which binding to RNA is facilitated. RRM1 and RRM2 have the highest binding affinity to RNA, similar to that of full-length PABPC1. The proline-rich region is necessary for homodimerisation, while the PABC domain allows the interaction with

other PAM2 motif containing proteins (Figure 4) (Gorgoni & Gray 2004). And indeed, an interaction with ATXN2 via its PAM2 domain was confirmed (Mangus *et al*. 1998, Satterfield & Pallanck 2006).

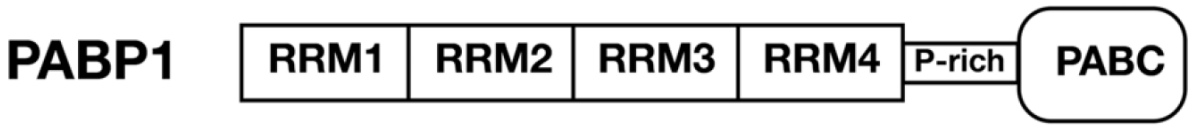

Figure 4. PABPC1 protein structure. PABPC1 is composed of four non-identical RNA recognition motifs (RRM), a proline-rich linker region (P-rich) and the C-terminal PABC domain through which binding to a PAM2 motif is mediated. PABPC1 synonyms: PABP1, PABP, PAB1, PAB (Gorgoni & Gray 2004).

Early studies documented PABPC1 to be an essential protein in yeast, as its deletion was shown to be lethal (Sachs *et al.* 1987). One function of PABPC1 certainly is the stimulation of translation of poly(A)-tail containing mRNAs by promoting a physical interaction of the 5'-cap with the poly(A)-tail. The binding of RRM1 and RRM2 of PABPC1 to eIF4G mediate the closed-loop structure of the mRNA which in turn enhances both, the affinity of PABPC1 to the mRNA and eIF4G to the 5'-cap (Gallie 1998, Haghighat & Sonenberg 1997, Imataka *et al.* 1998, Luo & Goss 2001). A role in 60S subunit joining was also assigned to PABPC1 (Gorgoni & Gray 2004). An increased mRNA stability mediated by PABPC1 binding to the mRNA and thus protecting the 3'-poly(A)-tail from degradation from the 3' end was also reported. Furthermore, PABPC1 interacts with the termination factor eRF3 that in turn interacts with eRF1 to enhance its translation termination activity. The PABPC1/eRF3 interaction enhances recycling of terminating ribosomes to initiate another round of mRNA translation without ribosome run-off (Uchida *et al.* 2002). However, eRF3 was shown to interfere with the PABPC1 multimerisation on poly(A)-mRNA, thus potentially leading to PABPC1 dissociation, deadenylation and finally mRNA decay (Gorgoni & Gray 2004, Hoshino *et al.* 1999). In yeast, Pab1p (PABPC1) controls the length of poly(A)-tails together with the Poly(A) nuclease (PAN) and upon loss of one of the PAN subunits, Pan2p or Pan3p, long poly(A) tail containing mRNAs accumulate (Mangus *et al*. 1998).

PABPC1 regulation primarily occurs at the mRNA translation level. As a member of the 5' TOP (terminal oligopyrimidine tract) containing mRNA family its translation is, as from other components of the protein synthesis machinery, growth dependent. The PABPC1 mRNAs contain two translation control elements: The oligopyrimidine tract at the 5' end followed by a conserved A-rich sequence. The TOP element serves to increase the PABPC1 expression, while PABPC1 itself can bind to its own mRNA through the A-rich sequence to repress its translation (Hornstein *et al.* 1999). PABPC1 activity is further regulated through the interaction with the Poly(A) binding protein interacting proteins (Paips). They bind

PABPC1 through a PAM1 and PAM2 motif. Paip1 stimulates PABPC1 action, whereas the two Paip2 homologues play an inhibitory role (Derry *et al.* 2006).

The first documentation of an interaction between PABPC1 and ATXN2 was performed in yeast with a two-hybrid screen (Mangus *et al*. 1998) and later confirmed by co-immunoprecipitation in *Drosophila* and mammalian COS-7 cells, where ATXN2 was found, as predicted, to bind PABPC1 through its PAM2 domain (Ralser *et al.* 2005a, Satterfield & Pallanck 2006). The studies could further show that wild-type and expanded ATXN2 co-sedimented with the polysomes in yeast and human HEK293 cell lines, an association mediated directly through the LSm domains and indirectly through the PABPC1 interaction (Mangus *et al*. 1998, Satterfield & Pallanck 2006). The involvement of ATXN2 in translation was first documented in yeast. A deletion of the yeast ATXN2 homologue Pbp1 was able to suppress the lethality caused upon the PABPC1 homologue *Pab1* deletion (Mangus *et al*. 1998) suggesting that Pbp1 was able to oppose Pab1 action. The same study further demonstrated that Pbp1 is necessary for proper polyadenylation, as Pbp1p deficient yeast strains showed a reduced polyadenylation phase followed by a considerably faster poly(A) trimming phase. Further experiments corroborated the hypothesis that Pbp1p negatively regulates the Pab1p-dependent 3'-to-5' poly(A) exonuclease Pan2p that trims long poly(A)-tails to their final size (Mangus *et al*. 1998, Mangus *et al.* 2004). Proper polyadenylation is important, as shortening of a poly(A)-tail is the initial step to mark an mRNA for degradation. It is further interesting to note that PABPC1 levels were decreased as a consequence to diminished ATXN2 levels in HEK293 cells and this decrease was rather on protein level than on mRNA level. Concordantly, the overexpression of wild-type (Q22) or expanded (Q79) ATXN2 diminished endogenous PABPC1 levels (Nonhoff *et al.* 2007). Together with the fact that ATXN2 has a RNA-dependent localization at the rER (van de Loo *et al*. 2009), these data involve ATXN2 in translation initiation, with the PABPC1 interaction being important in this regard.

1.2.3.2 Other functions related to RNA metabolism

Stress granules (SGs) are distinct foci within the cytoplasm, where untranslated mRNAs are translationally inhibited during conditions of cell stress (drug treatment, depletion of transcription factors, impaired translation initiation) (Anderson & Kedersha 2008). Thus, the major component of SGs is the translational initiation machinery including eukaryotic initiation factors, the 40S ribosomal subunit, PABPC1 and TIA-1, and also ATXN2 was found to co-localize to SGs (Ralser *et al*. 2005a). While the overexpression of normal (Q22) or pathogenic (Q79) ATXN2 does not affect stress granule formation, its absence leads to a

reduced number and size of SGs, resulting in impaired SG assembly (Nonhoff *et al*. 2007). Another RNA granule type found within cells are the Processing bodies (PBs), comprised of components from the mRNA decay machinery (Kedersha & Anderson 2009). Both, SGs and PBs, interact within a cell and transfer components from one to another. DDX6/Me31B was found to be present in SGs and PBs and to interact with ATXN2 by binding to its LSm/LSmAD-domains. Elevated normal or pathogenic ATXN2 levels can interfere with PB structures (Nonhoff *et al*. 2007).

The Ataxin-2 binding protein A2BP1 (FOX1) was identified as another interactor protein of ATXN2 at the C-terminus using a yeast two-hybrid system. A2BP1 bears a RNP motif known from highly conserved RNA-binding proteins, e.g. hnRNPs, and is predominantly expressed in brain and muscle (Shibata *et al.* 2000). As current data indicate, A2BP1 is mainly involved in neuronal specific splicing (Underwood *et al.* 2005). Interestingly, it was furthermore recently involved in autism (Voineagu *et al.* 2011).

While the ATXN2 protein was always thought to reside in the cytoplasm, a recent study described for the first time that ATXN2 exerts a function also in the nucleus. There it regulates its own transcription through complex formation with the transcriptional regulator ZBRK1 (KRAB-containing zinc-finger) and binding within the *Atxn2* promoter region via ZBRK1 binding sites (Hallen *et al.* 2011).

A recent study involved the fly orthologue dAtx2 in the miRNA-mediated translational control of synaptic mRNAs to influence long-term memory in *Drosophila melanogaster*. dAtx2 does that by assuring proper repression of several miRNA-target mRNAs, most likely through its binding to PABPC1 or Me31B/DDX6 (McCann *et al.* 2011).

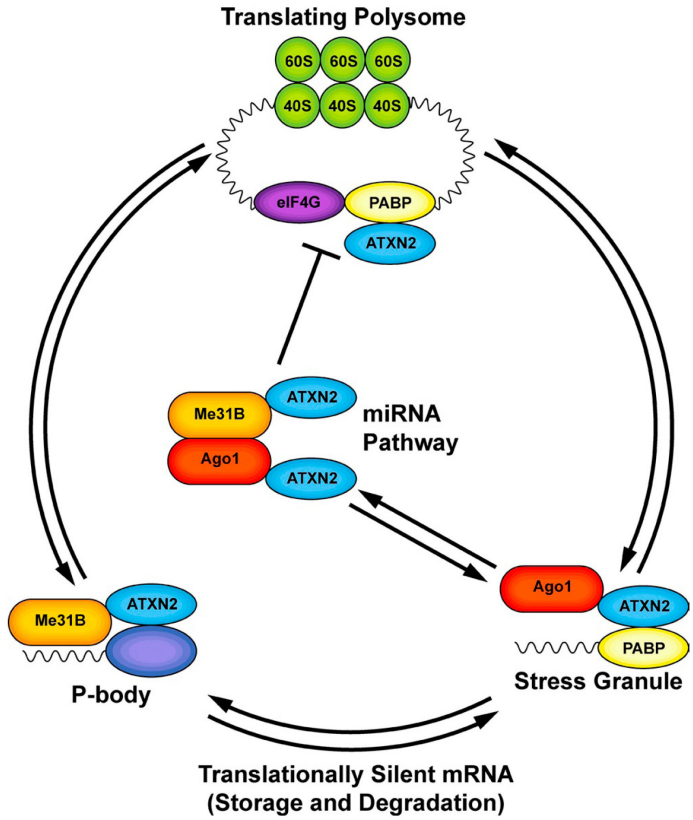

Figure 5. Proposed functions of ATXN2 in the regulation of mRNA translation. ATXN2 was found as a component of translating polysomes, in stress granules, in P-bodies and to play a role in the miRNA pathway. ATXN2 possibly functions in the trafficking of RNA/RNPs between actively translating polysomes and inactive stress granules and Processing bodies. (Orr 2012).

1.2.3.3 Other functions of ATXN2

The documentation that ATXN2 binds via a PRD/SH3 interaction to two members of the endophilin-A family, endophilin-A1 and endophilin-A3, gave first clues about its involvement in clathrin-mediated endocytosis (Ralser *et al.* 2005b). Further analyses showed that ATXN2 slows the EGF receptor internalization (Nonis *et al.* 2008). The direct association with T- and L-plastin implicated ATXN2 in plastin-associated pathways (Ralser *et al*. 2005b). Further research involves ATXN2 in embryonic development of *C. elegans*, leading to lethality when ATXN2 is absent (Kiehl *et al*. 2000). Increased expression of ATXN2 was reported to sensitize neuroblastoma cells for apoptosis (Wiedemeyer *et al.* 2003). Furthermore, in *Drosophila* dAtx2 is necessary for actin filament formation, leading to a germline defect with sterility or deformed eggs when dAtx2 function was disrupted (Satterfield *et al*. 2002).

1.3 ATXN2 implication in other neurodegenerative diseases

The involvement of ATXN2 in other neurodegenerative diseases was documented in several studies. Parkinson's disease (PD) (section 1.2.1), Progressive supranuclear palsy (section 1.2.1), ALS, SCA1 and SCA3 may be influenced by ATXN2, either through its triplet repeat length or its composition and/or ATXN2 expression levels.

1.3.1 ATXN2 implication in ALS

As described in section 1.2.1, intermediate sized polyQ expansions in *Atxn2* can increase the risk for ALS (Figure 6). In 4.7% of ALS patients, the ATXN2 repeat length was between 27 and 33 CAGs, whereas only 1.4% of the control group had that repeat size (Elden *et al*. 2010). But what is the cutoff expansion size that mediates risk interaction between these two diseases? Elden *et al*. identified ATXN2 to modify the TDP-43 mediated toxicity in yeast and *Drosophila* in a dose-dependent manner (Elden *et al*. 2010). While TDP-43 overexpression itself was toxic, the combined overexpression with ATXN2 led to an increased toxicity. Under normal conditions TDP-43 resides in the nucleus, but was found to relocalize to the cytoplasm under pathological conditions. Co-IP experiments validated that ATXN2 and TDP-43 occurred together in the same protein complex when both proteins are overexpressed, and in distinct foci within the cytoplasm when the nuclear localization signal (NLS) of TDP-43 was mutated, forcing it to reside in the cytoplasm. This colocalization was dependent on RNA. Furthermore, the ATXN2 localization in spinal cord neurons changed from diffuse in healthy individuals into distinct foci in ALS patients with normal *ATXN2* expansion, whereas TDP-43 was found to relocalize to the cytoplasm in SCA2 patients. The interaction of ATXN2 and TDP-43 seems to be a general component of ALS and SCA2, possibly defining a new target complex for therapeutic treatment (Elden *et al*. 2010). An elevated risk for SCA3 or sporadic PD due to intermediate expanded ATXN2 was not observed (Gispert *et al*. 2012). Furthermore, the CAG repeat length of Huntingtin does not exhibit an influence on ALS indicating a specific interaction between ATXN2 expansions and causes of ALS (Ramos *et al.* 2012).

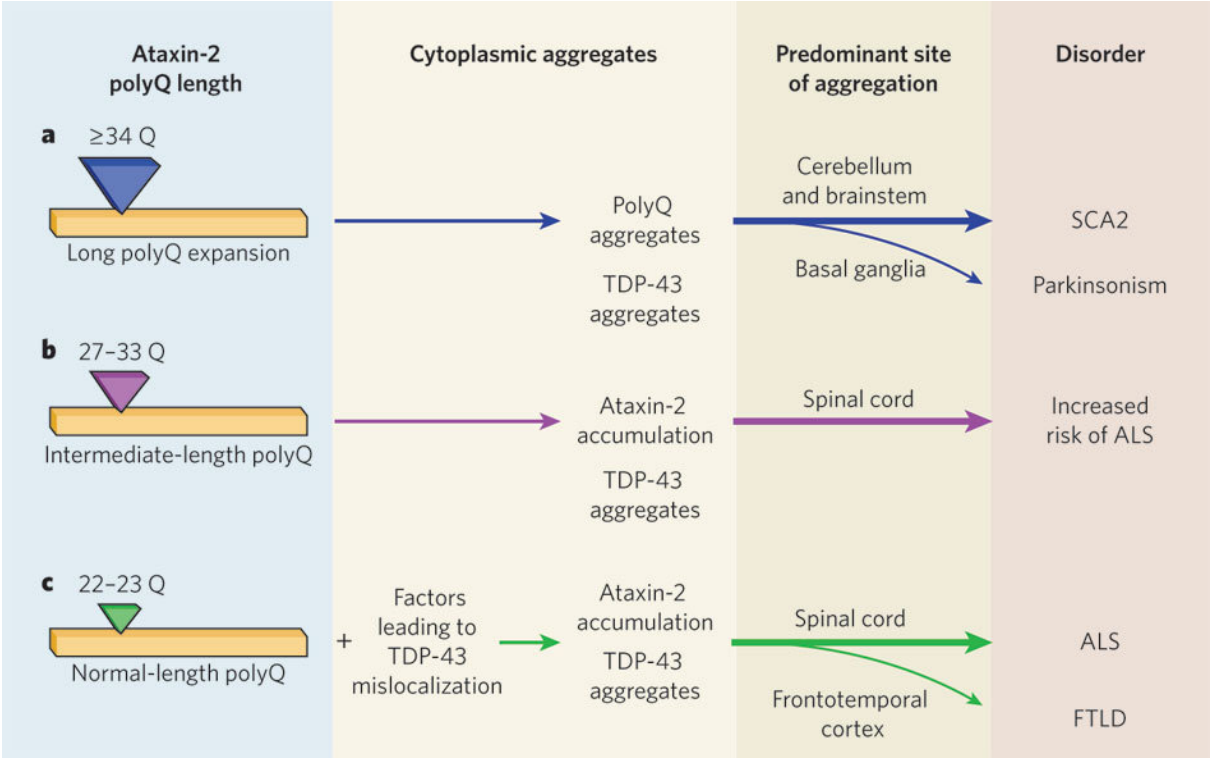

Figure 6. PolyQ size matters. Depending on the polyQ size of ATXN2 different diseases may develop. (a) Individuals having a polyQ-repeat of 32 CAGs or more may develop SCA2 and less frequently Parkinson's disease. (b) Alleles with 27-33 glutamines are associated with a higher risk for ALS. (c) The majority of the population carries 22-23 glutamines in ATXN2. Cytoplasmic aggregates containing ATXN2 and TDP-43 were observed in some SCA2 and ALS patients. Adapted from (Lagier-Tourenne & Cleveland 2010).

1.3.2 ATXN2 implication in other Spinocerebellar ataxias

As the polyglutamine diseases have several common features, one study was directed to identify possible pathways and modifiers that link these diseases. One interesting finding was that ATXN2 acted as an enhancer of retinal pathology in a *Drosophila* SCA1 and SCA3 model (Ghosh & Feany 2004).

Al-Ramahi *et al*. used different *Drosophila* mutants to describe the enhancing role of dAtx2, the *Drosophila* orthologue of ATXN2, in expanded Ataxin-1 driven neurotoxicity (Al-Ramahi *et al.* 2007). Sca1(82Q) expressing mutants were compared with dAtx2OE mutants that overexpressed wild-type dAtx2, the Sca1(Q82)/dAtx2OE double mutants and Sca1(Q82)/dAtx2^{X1} that expresses only reduced dAtx2 levels. The Sca1(Q82) single mutant led to retinal degeneration, neuronal dysfunction and premature death. Increased dAtx2 levels in the double mutant Sca1(Q82)/dAtx2OE led to enhanced phenotypes, while dAtx2 reduction in Sca1(Q82)/dAtx2^{X1} led to a suppression. Similar suppression due to reduced dAtx2 levels was observed in regard to loss of the proneural Sens protein and mechanoreceptor loss upon Sca1(Q82) expression. On the contrary, the neurodegeneration caused by expanded Huntingtin was not suppressed by reduced dAtx2 levels indicating the

specificity of this effect. A physical interaction between Ataxin-1 and dAtx2 or human ATXN2, respectively, was confirmed and was independent from the polyglutamine tract length, but in part dependent of the S776 phosphorylation of Ataxin-1. Furthermore, the interaction was compartment-independent and proved to occur in the cytoplasm as well as in the nucleus. Still, as in humans, dAtx2 normally localizes to the cytoplasm and Ataxin-1 to the nucleus. When co-expressed with expanded but not with normal Ataxin-1, dAtx2 localization shifted to the nucleus and was furthermore found in intranuclear inclusions in neurons. Also SCA1 patients showed NIIs containing ATXN2. Interestingly, dAtx2 itself, when forced to localize to the nucleus, induced retinal degeneration, mechanoreceptor loss and reduced Sens protein levels (Al-Ramahi *et al*. 2007).

A similar modulatory role of ATXN2 was also reported for SCA3 in another *Drosophila* study (Lessing & Bonini 2008). Here, the pathogenic effects of Sca3trQ78 flies expressing a truncated version of Ataxin-3 with an expansion of 78 glutamines, expression of dAtx2 alone and of the double mutants was investigated. While Sca3trQ78 expressing flies showed only an internal retinal disorganization, dAtx2 expression led to an obvious retinal degeneration. The double mutants on the contrary manifested a severe degeneration with collapse of the retina and pigmentation loss. Furthermore, the photoreceptors degenerated progressively in Sca3trQ78 flies, while dAtx2 expressing flies showed a milder phenotype. A dramatically enhanced degeneration was observed in Sca3trQ78/dAtx2 flies. A reduction of dAtx2 expression of ~ 50% in Sca3trQ78 flies mitigated the photoreceptor loss significantly. As NIIs are common in SCA3, the Sca3trQ78 flies also form NIIs. The additional dAtx2 expression accelerated inclusion formation. Again, while dAtx2 normally is cytoplasmic, it shifted its localization into nuclear Ataxin-3 positive inclusions in Sca3trQ78 flies. While the NIIs of pathogenic Ataxin-3 also contain Hsp70, the inclusions generated by dAtx2 expression alone were free of Hsp70. Using a PAM2-deletion construct that expresses dAtx2 without its PAM2 motif showed that even though its expression leads to retinal disorganization in the eye, it was intact and showed no signs of degeneration. Furthermore, its coexpression with Sca3trQ78 failed to enhance the toxicity known to be caused in Sca3trQ78/dAtx2 flies. The phenotypes resembled more that of Sca3trQ78 expressing flies in regard to eye degeneration, photoreceptor loss and inclusion formation. The PAM2 motif was required for the toxicity of upregulated dAtx2 alone or together with Sca3trQ78 (Lessing & Bonini 2008).

Thus, these results describe other possible mechanism by which ATXN2 plays a significant role in mediating neurodegeneration where the normal biological activity of ATXN2 modulates the toxicity in SCA1 and SCA3.

One study documented a modulator of SCA2 age of onset that was attributed to longer CAG repeat sizes in the *CACNA1A* gene, the disease gene of SCA6. The variation in the polyQ

repeat length accounted for ~ 6% of the age of onset variance when *ATXN2* repeat sizes were equal observed in a Cuban population (Pulst *et al*. 2005).

1.4 Mouse models

Cell culture experiments are indispensable nowadays and replace a vast majority of animal experiments; however, conclusions drawn from them are restricted, as they do not mimic the whole complexity of an organism and the progressive disease course cannot be studied over several years. Popular model organisms are among others *S. cerevisiae*, *D. melanogaster*, and *C. elegans* due to their easy genetic manipulation, high offspring number and low cost and time investment. With these models the function of conserved proteins, simple cellular processes and behaviours can be well studied. However, when studying e.g. neurodegenerative diseases, it is advisable, at least at a certain point, to change to a higher developed model like the mouse. Even though its long generation time and relatively small litter size make the work time and space consuming, they are more closely related to humans, not only in regard to the development of their central nervous system. Furthermore, the gene mutation in multiple individuals with homogenous background and in a highly controlled environment as well as early stages of disease before the appearance of overt symptoms can be studied relatively easy. Gain-of-function disorders can be modeled, by expressing the mutant protein that exerts an altered function or by overexpressing the wild-type protein. Inactivation of the endogenous gene and/or protein mimics loss-of-function diseases where the protein became non-functional (Picciotto & Wickman 1998).

1.4.1 SCA2 mouse models

Several mouse models for polyglutamine diseases exist, both knock-out models to get further insight into the function of a protein, and transgenic overexpressing and knock-in models to mimic the disease.

The loss-of-function models for SCA2 include two *Atxn2* knock-out models, both lacking a functional ATXN2 protein (Kiehl *et al.* 2006, Lastres-Becker *et al*. 2008a). Even though the ATXN2-deficient animals were viable, both studies reported a distorted ratio of genotypes. Less heterozygous and homozygous, mainly female, animals were born from heterozygous matings. The study from Lastres-Becker *et al*. further documented fertility problems in the knock-out animals leading to reduced number of litters and reduced animals per litter.

Histological examinations did not reveal any alterations in the CNS. At birth, the animals appeared normal, but constantly gained weight up to the age of 1 year, leading to increased abdominal and gonadal fat pads (Kiehl *et al*. 2006, Lastres-Becker *et al*. 2008a). This was not a result of hyperphagia or reduced movement, as the mice at 3 months showed increased activity in the open field test. Histological liver staining revealed hepatosteatosis, possibly as a cause of insulin resistance. Increased blood and pancreas insulin levels were accompanied by decreased insulin receptor protein levels even though its mRNA levels were increased (Lastres-Becker *et al*. 2008a).

Mice have only one CAG in the position of the human CAG repeat tract. Thus, the insertion of a CAG repeat expansion in the adjacent context is the approach to model SCA2 in mice. The first SCA2 mouse model was generated in 2000 by introducing a full-length human *ATXN2* cDNA with a repeat of 58 CAGs under the control of the Purkinje-cell-specific Pcp2 promoter (Huynh *et al*. 2000). Therefore, its expression was directed to the main site of pathology in SCA2, the Purkinje cells. This model mimicked well the pathological features observed in SCA2 patients that are attributed to the Purkinje cells. Reduced calbindin-immunoreactivity in Purkinje cells preceded a reduced stride length and reduced motor performance. Neuronal intranuclear inclusions were not observed while expanded polyglutamine-containing microaggregates were detected in the cytoplasm. Homozygous animals were more severely affected by the symptoms than heterozygotes (Huynh *et al*. 2000). Six years later, a second transgenic mouse model was published that expressed the full-length *ATXN2* cDNA with 75 CAGs under the human *ATXN2* promoter, thus directing a ubiquitous expression as in humans (Aguiar *et al.* 2006). Calbindin-immunoreactivity loss and reduced motor performance with homozygotes being more severely affected than heterozygotes were observed in this mouse model; however, first signs appeared earlier than in the transgenic mouse with 58 CAGs (Aguiar *et al*. 2006). Interestingly, both models did not mimic the instability of the CAG repeat as it occurs in humans. It was stably transmitted over generations.

One problem when working with transgenic mice is that they often only reproduce certain aspects of the human disease phenotype, they might be more severely affected or show artefacts that are irrelevant to the human disease (Watase & Zoghbi 2003) due to elevated dosage of the mutant protein on DNA, mRNA and protein level. These problems can be circumvented with the use of knock-in mice that have the following advantages: First, not heterologous but endogenous promoters are used to drive gene expression, thus leading to an expression of the protein of interest that will affect all tissues and cell types of an organism in a physiological way and in physiological amounts. This opens the possibility to examine, why certain groups of neurons are vulnerable to a mutation whereas others are not.

Second, the loss-of-function of the wild-type protein can be studied alongside with gain-of-function mechanisms affecting the organism. Third, in regard to polyglutamine diseases, disease severity can be triggered by introducing shorter or larger repeat tracts.

1.5 Aim of thesis

Insights into the pathomechanisms of SCA2 that are far-reaching enough to develop suitable medication to cure or ameliorate the neurodegenerative disease still do not exist. Even though current available SCA2 mouse models demonstrate well the phenotype observed in patients, the overexpression and tissue-specificity of expanded ATXN2 is unphysiological and might lead to unspecific effects within the cells. Only the gain-of-function mechanism of the disease can be described with these models, while possible loss-of-function mechanisms involved in SCA2 are inevitably disregarded. One problem when working with neurodegenerative diseases is that brain tissue can only be obtained post-mortem. Recruiting skin fibroblasts is a commonly used possibility to obtain material from living patients. As an equivalent in mouse, fibroblasts from embryos can be extracted and compared to human material. The first aim was to model SCA2 in mice as faithfully as possible. For this purpose a knock-in mouse with an expansion of 42 CAGs - a common repeat length in patients - was generated and to be characterized, which included:

1. The assessment of Ataxin-2 mRNA and protein expression levels.
2. The thorough assessment of the overall and neurological phenotype.
3. The characterization of *Atxn2*-CAG42-knock-in-MEFs to evaluate if they are a powerful tool to help unravel SCA2 disease mechanisms.

The second aim was to use the *Atxn2*-CAG42-knock-in mouse model to reveal and study pathomechanisms leading to SCA2. For this purpose, the following questions were to be investigated:

1. Evaluation of the impact of the Ataxin-2 expansion on its own expression levels and global mRNA levels by creating a transcriptome profile.
2. Is the well-characterized interaction partner PAPBC1 influenced by the Ataxin-2 expansion?
3. Does the Ataxin-2 expansion result in increased insolubility and aggregate formation and if so, are other proteins also involved?

4. Why is the cerebellum the most affected brain region in SCA2? Which differences between cerebellum and cortex allow the largely unaffected cortex to cope with the ATXN2 expansion?

Even though several studies involved ATXN2 to play a role in mRNA translation and especially in translation initiation, its function still remains to be elucidated. The third aim was to get further insight into the function of ATXN2 by performing studies in mouse tissue deficient of Ataxin-2 to answer the following questions:

1. Which function can be ascribed to ATXN2 in translation initiation? Is ATXN2 a translational repressor or an enhancer?

2 Material and Methods

2.1 Material

2.1.1 Laboratory equipment

Equipment	Company
96-well lid for microtest plate	Sarstedt, Newton, USA
Aluminium foil Alu pro	Ecopla, Le Touvet, France
Autoclave “Varioklav 400”	H+P Labortechnik, Oberschleißheim, Germany
BD Falcon conical tubes	BD Biosciences, Heidelberg, Germany
Bio Photometer	Eppendorf, Hamburg, Germany
BioMax MS films with BioMax intensifying screens	Kodak, Rochester, New York, USA
Cartridge for Labogaz 206	Camping Gaz, Hungen-Inheiden, Germany
Cell culture bench	Envirco, Sanford, USA
Cell culture bench Lamin Air HB2448	Heraeus Instruments, Hanau, Germany
Cell culture bench MSC Advantage	Thermo Scientific, Schwerte, Germany
Cell scraper	Sarstedt, Newton, USA
Cellstar Cell culture dishes	Greiner Bio-one, Frickenhausen, Germany
Cellstar cell culture flasks, different sizes	Greiner Bio-one, Frickenhausen, Germany
Centrifuge 5415 C	Eppendorf, Hamburg, Germany
Centrifuge 5415 D	Eppendorf, Hamburg, Germany
Centrifuge 5415 R	Eppendorf, Hamburg, Germany
Centrifuge 5702	Eppendorf, Hamburg, Germany
CO_2-Incubator MCO 18 AIC (UV)	Sanyo, Munich, Germany
Cryotubes	Sarstedt, Nürmberg, Germany
Developer	Curix 60, Agfa, Mortsel, Belgium
Digital kitchen balance	Zeitlos-Vertriebs GmbH, Breisach, Germany
Dounce homogenizer 7.0 ml	Wheaton, Millville, USA
Drying oven T 5028	Heraeus Instruments, Hanau, Germany
Dumont precision forceps #K344.1	Carl Roth, Karlsruhe, Germany
Easy Cast Electrophoresis System	Thermo Scientific, Schwerte, Germany
Falcon 14 ml	BD, Heidelberg, Germany
Fast optical 96-well reaction plate	Life Technologies, Darmstadt, Germany
Fast Start Universal Probe Master (Rox)	Roche, Penzberg, Germany
Feather disposable scalpel No. 10	Pfm medical, Cologne, Germany
Forceps #LH56.1	Carl Roth, Karlsruhe, Germany
Freezer AEG Artis	AEG, Nürnberg, Germany
Freezer Herafreeze (-80 ℃)	Thermo Scientific, Schwerte, Germany

Fujifilm instant Black & White FP-3000B professional	Fujifilm, Düsseldorf, Germany
Gene Amp PCR System 2700	Life Technologies, Darmstadt, Germany
Heracell 240i CO_2-Incubator	Thermo Scientific, Schwerte, Germany
Hypermount	Shandon, Pittsburgh, USA
Ice machine AF80	Scotsman, Vernon Hills, USA
Incubator	Memmert, Schwabach, Germany
Incubator Shaker	New Brunswick Scientific, Edison, USA
KimWipes	Kimberly-Clark Professional, Mainz, Germany
Labogaz 206	Camping Gaz, Hungen-Inheiden, Germany
Laboratory glassware	Fisherbrand, Schwerte, Germany
Magnetic stirrer REO basic C	IKA Werke, Staufen, Germany
Megafuge 1.0 R	Heraeus Instruments, Hanau, Germany
Micro tube rack	Carl Roth, Karlsruhe, Germany
Microplate reader	Tecan Group, Männedorf, Switzerland
Microscope “Axiovert 200 M”	Carl Zeiss AG, Oberkochen, Germany
Microtest Plate 96-well flat bottom	Sarstedt, Newton, USA
Microtome	Jung AG, Nußloch, Germany
Microtube Easy Cap	Sarstedt, Nümbrecht, Germany
Microwave R-234	Sharp, Hamburg, Germany
Milli-Q Synthesis	Millipore, Schwalbach, Germany
Mini Trans-Blot Cell	Biorad, Munich, Germany
Minigel Twin Electrophoresis System	Biometra, Göttingen, Germany
Miroscope Primo Star	Carl Zeiss AG, Oberkochen, Germany
Mountant, Perma Fluor	Thermo Scientific, Schwerte, Germany
MS1 Minishaker IKA	IKA Werke, Staufen, Germany
Multipette plus	Eppendorf, Hamburg, Germany
Multiply-µStrip 0.2 ml chain	Sarstedt, Nümbrecht, Germany
Nitrogen tank	MVE Cryosystem, Jüchen, Germany
Nitrogen tank	Welabo, Düsseldorf, Germany
Optical adhesive film	Life Technologies, Darmstadt, Germany
Original-Perfusor-Syringe OPS 50 ml	Braun, Melsungen, Germany
Paraffin Paraplast Plus X-tra	McCormick Scientific, Richmond, USA
Parafilm	Pechiney Plastic Packaging, Chicago, USA
Pasteur capillary pipettes	WU Mainz, Mainz Germany
Pehasoft nitrile	Hartmann, Heidenheim, Germany
Pellet Pestle Motor	Kontes Glass Company, Vineland, USA
Pestle	Kontes Glass Company, Vineland, USA
pH 210 Microprocessor pH Meter	Hanna instruments, Kehl, Germany
Pipet Boy accu-jet	Brand, Wertheim, Germany
Pipetman	Gilson, Middleton, USA

Pipette tips (0.5-1,000 µl)	Starlab, Ahrensberg, Germany
Pipette tips, sterile (0.5-1,000 µl)	Starlab, Ahrensberg, Germany
Plastic wrap	PapStar, Kall, Germany
Polaroid Direct Screen Instant Camera DS34	Polaroid, Minnetonka, USA
Power Pac 200	Biorad, Munich, Germany
Power pack Consort E122	Consort, Turnhout, Belgien
Precision balance Sartorius analytic	Sartorius, Göttingen, Germany
Precision scissors #3534.1	Carl Roth, Karlsruhe, Germany
PVDF membrane	Biorad, Munich, Germany
Radiographic cassette	Dr. Goos-Suprema, Heidelberg, Germany
RNase Zap Wipes	Life Technologies, Darmstadt, Germany
Rotator 34528E	Neolab, Heidelberg, Germany
Scissors #3577.1	Carl Roth, Karlsruhe, Germany
Serological pipet, non-sterile, different sizes	Sigma-Aldrich, Munich, Germany
Serological pipet, sterile, different sizes	Sigma-Aldrich, Munich, Germany
Shaker Polymax 1040	Heidolph instruments, Schwabach, Germany
Shaker CAT RM5	CAT, Staufen, Germany
Sonicator Sonopuls	Bandelin, Berlin, Germany
Sorvall RC-5B refrigerated superspeed centrifuge	DuPont Instruments, Newtown, USA
Steri 250	Keller, Burgdorf, Switzerland
Sucofin milk powder	TSI, Zeven, Germany
Super Frost Plus Microscope slides	Menzel-Gläser, Braunschweig, Germany
Super RX medical X-Ray film	Fujifilm, Düsseldorf, Germany
Thermomixer comfort	Eppendorf, Hamburg, Germany
Thermomixer compact	Eppendorf, Hamburg, Germany
Tongue depressor	NOBA Verbandmittel Danz, Wetter, Germany
Tri-Carb 2100TR Liquid Scintillation Analyzer	Perkin-Elmer, Boston, USA
UV-Cuvette micro	Brand, Wertheim, Germany
UV-light	Bachofer, Reutlingen, Germany
Water bath GFL 1083	GFL, Manchester, UK
Welted glasses	Carl Roth, Karlsruhe, Germany

2.1.2 Chemicals

Chemical	Company
Acrylamide/Bis-Acrylamide 29:1	Biorad, Munich, Germany
Agar	Sigma-Aldrich, Munich, Germany
Agarose	Sigma-Aldrich, Munich, Germany
Ampicillin	Sigma-Aldrich, Munich, Germany
APS	Sigma-Aldrich, Munich, Germany
Boric acid	Sigma-Aldrich, Munich, Germany
Bromophenol blue	Sigma-Aldrich, Munich, Germany
BSA	New England Biolabs, Ipswich, USA
Chloroform	Sigma-Aldrich, Munich, Germany
complete Mini, EDTA-free	Roche, Penzberg, Germany
Cresol red sodium salt	Sigma-Aldrich, Munich, Germany
Developer	Agfa, Mortsel, Belgium
dNTPs	Fermentas, St. Leon-Rot, Germany
di-Potassiumhydrogenphosphate	Applichem, Darmstadt, Germany
di-Sodiumhydrogenphosphate	Applichem, Darmstadt, Germany
Distilled water (DNase/RNAse-free)	Life Technologies, Darmstadt, Germany
EDTA	Sigma-Aldrich, Munich, Germany
EGTA	Sigma-Aldrich, Munich, Germany
Ethanol	Sigma-Aldrich, Munich, Germany
Ethidium bromide	Carl Roth, Karlsruhe, Germany
Glycerol	Sigma-Aldrich, Munich, Germany
Glycine	Sigma-Aldrich, Munich, Germany
H_2O_2	Sigma-Aldrich, Munich, Germany
HCl	Sigma-Aldrich, Munich, Germany
Yeast extract	Carl Roth, Karlsruhe, Germany
Immersol 518N	Carl Zeiss AG, Oberkochen, Germany
IPTG	Carl Roth, Karlsruhe, Germany
Isopropanol	Sigma-Aldrich, Munich, Germany
Methanol	Sigma-Aldrich, Munich, Germany
$MgCl_2$	Sigma-Aldrich, Munich, Germany
NaCl	Sigma-Aldrich, Munich, Germany
NaOH	Sigma-Aldrich, Munich, Germany
Peptone from Casein	Carl Roth, Karlsruhe, Germany
PFA	Merck, Darmstadt, Germany
Potassiumchloride	Applichem, Darmstadt, Germany
Rapid Fixer	Agfa, Mortsel, Belgium
SDS Pellets	Carl Roth, Karlsruhe, Germany

Simply Blue Safe Stain	Life Technologies, Darmstadt, Germany
Sodium acetate	Sigma-Aldrich, Munich, Germany
Sodium vanadate	Sigma-Aldrich, Munich, Germany
Sodiumhydroxide	Sigma-Aldrich, Munich, Germany
ß-Mercaptoethanol	Sigma-Aldrich, Munich, Germany
Sucrose	Sigma-Aldrich, Munich, Germany
Super Signal West Pico Lumino/Enhancer Solution	Thermo Scientific, Schwerte, Germany
Super Signal West Pico Stable Peroxidase Solution	Thermo Scientific, Schwerte, Germany
TEMED	Sigma-Aldrich, Munich, Germany
Tris	Applichem, Darmstadt, Germany
Triton-X	Sigma-Aldrich, Munich, Germany
Tween20	Applichem, Darmstadt, Germany
UltraPure Low Melting Point Agarose	Life Technologies, Darmstadt, Germany
Urea	Biorad, Munich, Germany
X-Gal	Carl Roth, Karlsruhe, Germany
Xylol	Sigma-Aldrich, Munich, Germany

2.1.3 Buffers

Cell fractionation extraction buffer 1
50 mM Tris, pH 7.5, 25 mM KCl, 5 mM $MgCl_2$, 0.25 m sucrose, 1 mM PMSF, 1 mM Na_3VO_4, Protease inhibitors (Sigma, St. Louis, USA), 200 g/ml CHX, 1% Phosphatase Inhibitor Cocktail 1 + 2 (Sigma, St. Louis, USA), 250 U/ml RNAsin (Promega, Mannheim, Germany) and Complete Protease Inhibitor Cocktail (Roche, Penzberg, Germany)

Co-Immunoprecipitation lysis buffer
10 mM HEPES, pH 7-7.5, 10 mM KCl, 5 mM $MgCl_2$, 1% Igepal, 0.5 mM PMSF, 25 µl/ml protease inhibitor cocktail (Sigma), 10 µl/ml phosphatase inhibitor cocktail 1 & 2 (Sigma), 5 µl/ml RNase out (Life Technologies, Darmstadt, Germany), 1 mM NaF

PBS
137 mM NaCl, 2.7 mM KCl, 4.3 mM Na_2HPO_4-$7H_2O$, 1.4 mM KH_2PO_4, pH 7.4

PBST
PBS, 0.05% Tween

Pink Juice
2 mM Cresol, 12.5% 10x PE buffer, 2 mM dNTPs, 15% sucrose

Proteinase K buffer
10 mM Tris-HCl; 100 mM NaCl; 10 mM EDTA, pH 8; 0.5% SDS

RIPA lysis buffer
50 mM Tris-HCl (pH 8.0), 150 mM NaCl, 1 mM EDTA, 1 mM EGTA, 1% Igepal CA-630 (Sigma), 0.5% sodium deoxycholate, 0.1% SDS, 1 mM PMSF and one tablet Complete Protease Inhibitor Cocktail (Roche, Penzberg, Germany)

SDS lysis buffer
68.5 mM Tris-HCl, pH 6.8; 2% SDS; 10% glycerol

Southern Blot Pre-hybridization and hybridization buffer
4 x SSC, 1% SDS, 0.5% skimmed milk, 20 mM EDTA, 100 µg/ml herring sperm

Southern Blot Washing buffer 1
3 x SSC, 1% SDS

Southern Blot Washing buffer 2
0.5 x SSC, 1% SDS

TBE buffer
890 mM Tris, 890 mM Boric acid, 20 mM EDTA

TE buffer
10 mM Tris-HCl, 1mM EDTA, pH 7.5-8

Urea/SDS lysis buffer
8 M Urea, 5% SDS, 1 mM PMSF, Complete protease inhibitor cocktail

Western Blot Running buffer
25 mM Tris, 192 mM glycine, 0.1% SDS

Western Blot Running gel buffer
1.5 M Tris, 0.4% SDS, pH 8.8

Western Blot Stacking gel buffer
0.5 M Tris, 0.4% SDS, pH 6.8

Western Blot Transfer buffer
25 mM Tris, 192 mM glycine, 10% methanol

Western Blot Loading buffer (2x)
25% stacking gel buffer, 20% glycerol, 4% SDS, 5% ß-Mercaptoethanol, 0.05% Bromophenol blue

2.1.4 Oligonucleotide primers

Oligonucleotide primers were purchased from ©Eurofins MWG Operon (Ebersberg, Germany) or Sigma-Aldrich (Munich, Germany).

Primer	**Sequence 5'-3'**
NOW1-A3	CTATCAGGACATAGCGTTGGCTACC
NOW1-B3	CTGGTCTACAAAGTAGATGCTGCC
NOW1-C1	TCCACTTTCCCAAACACAGGTCT
NOW1-D1	GGTCATCTTCACCTTCATATAACT
NOW1-5E-G1	TCCCAAACACAGGTCTGAGTAAGAAGC
NOW1-5E-G2	CTGGGGAATCAAACTCAAAGTCTGC
NOW1-K2	TGAGTTGACTCCACAGGGAGGTGAGC
NOW1-H2	CCATCTCGCCAGCCCGTAAGATTC
M13 reverse	CAGGAAACAGCTATGAC
Sca-In0-F3	TGACCTCTATCTCCCGAATGCT
Sca-In0-R2	GCTCGCTCGGACTTCTTAGTT
Sca-In0-R3	TGCTATCTCAAACATGACGCCT
Sca2Ex1fwd5_m	CCCCGCCCGGCGTGCGAGCCGGTGTAT
Sca2Ex1rev2_m	CGGGCTTGCGGCCAGTGG
T7 forward	TAATACGACTCACTATAGGG

2.1.5 TaqMan® assays

All TaqMan assays were purchased from Life Technologies (Darmstadt, Germany).

Assay ID	Gene symbol	Gene name
Mm00507463_m1	Acat1	Acetyl-Coenzyme A acetyltransferase 1
Mm02581738_s1	Adam1a	A disintegrin and metallopeptidase domain 1a
Mm00503568_m1	Ankrd33b	Aankyrin repeat domain 33B
Mm01199894_m1	Atxn2	Ataxin-2
Mm01198165_m1	Bri3bp	Bri3 binding protein
Mm01163611_m1	Cthrc1	Collagen triple helix repeat containing 1
Mm00619326_m1	Ddx6	DEAD (Asp-Glu-Ala-Asp) box polypeptide 6
Mm00782672_s1	eIF2alpha	Eukaryotic initiation factor 2 alpha
Mm00782672_s1	eIF2s2	Eukaryotic initiation factor 2s2
Mm00725633_s1	eIF4e	Eukaryotic initiation factor 4e
Mm00839121_gH	eIF5a	Eukaryotic initiation factor 5a
Mm00554876_m1	Fbxw8	F-box and WD-40 domain protein 8
Mm00924548_m1	Fmr1	Fragile X mental retardation 1
Mm00836363_g1	Fus	Fused in sarcoma
Mm00519131_s1	Gjc2	Gap junction protein, gamma 2
Mm01325931_g1	Hnrnpa2b1	heterogeneous nuclear ribonucleoprotein A2/B1
Mm00446968_m1	Hprt1	Hypoxanthine phosphoribosyltransferase 1
Mm00835449_g1	Ifi27l1	Interferon, alpha-inducible protein 27 like 1
Mm00839408_g1	Lgals1	Lectin, galactose binding, soluble 1
Mm01250668_g1	Lsm12	Lsm12
Mm01329688_m	Nlrp12	NLR family, pyrin domain containing 12
Mm00849569_s1	Pabpc1	Poly(A)-binding protein 1
Mm00471342_m1	Paip2	Poly(A)-interacting protein 2
Mm01211202_m1	Pls3	Plastin 3
Mm03825096_m1	Smn1	Survival of motor neuron 1
Mm01263699_m1	Tardbp	Tar-DNA-binding protein
Mm00446973_m1	Tbp	TATA-box-binding protein
Mm00441748_m1	Tia-1	T-cell-restricted intracellular antigen-1
Hs00268077_m1	ATXN2	Ataxin-2
Hs00743792_s1	PABPC1	Poly(A)-binding protein cytoplasmic 1
Hs99999910_m1	TBP	TATA-box-binding protein

2.1.6 Primary antibodies

Antibody	Company	Catalogue number	Dilution
Ataxin-2	BD Biosciences	611378	WB 1:500; IHC 1:50, ICC 1:100
BiP/GRP78	BD Biosciences	610979	WB 1:500
Calbindin D-28K	Sigma	C9848	IHC 1:3000
Calnexin	Cell Signaling	2433	IHC 1:100
EEA-1	BD Biosciences	610456	WB 1:500
eIF3B	Santa Cruz	sc-16377	WB 1:400
eIF4E	Cell Signaling	9742	IHC 1:100
GAPDH	Calbiochem	CB1001	WB 1:5,000
GFAP	Dako	M0761	IHC 1:500
HSP90	Santa Cruz	sc-7974	WB 1:1,000
PABP1	Abcam	ab21060	WB 1:1,000
PABP1	Cell Signaling	4992	IHC 1:50
Phospho-TDP-43 (pS409/410)	Cosmo Bio	TIP-PTD-M01	IHC 1:3,000
polyglutamine-1C2	Millipore	MAB1574	WB/IHC 1:1,000
Ribophorin	Santa Cruz	Sc-25559	IHC 1:100
S6	Cell Signaling	2217	IHC 1:100
SQSTM1/p62	Santa Cruz	sc-25575	IHC 1:50
ß-Actin	Sigma	a5441	WB 1:10,000
TDP-43	Proteintech	10782-2-AP	WB 1:1,000, IHC 1:50
TIA-1 (c-20)	Santa Cruz	sc-1751	ICC 1:500

2.1.7 Secondary antibodies

Antibody	Company	Catalogue number	Dilution
ECL anti-mouse HRP linked whole antibody	GE Healthcare, Munich, Germany	NA934V	1:10,000
ECL anti-rabbit HRP linked whole antibody	GE Healthcare, Munich, Germany	NA931V	1:10,000

2.1.8 DNA and protein ladders

Ladder	Company	Catalogue number
TrackIt™ 100 bp DNA Ladder	Life Technologies, Darmstadt, Germany	10488-058
TrackIt™ 1 Kb DNA Ladder	Life Technologies, Darmstadt, Germany	10488-072
Precision Plus Protein Dual Color Standards	Biorad, Munich, Germany	161-0374

2.1.9 Enzymes

Enzyme	Company
Expand HF Polymerase	Roche, Penzberg, Germany
TaKaRa LA Taq-Polymerase	Takara Bio Inc., Japan
Taq DNA-Polymerase	Life Technologies, Darmstadt, Germany

2.1.10 Cell culture reagents

Type	Company
BGS	Thermo Scientific HyClone, Logan, USA
DMEM 21013, methionine-free	Life Technologies, Darmstadt, Germany
DMEM 21969	Life Technologies, Darmstadt, Germany
Dulbecco's PBS	PAA, Pasching, Austria
FCS	PAA, Pasching, Austria
HEPES H0887	Life Technologies, Darmstadt, Germany
HyQtase	Thermo Scientific HyClone, Logan, USA
L-glutamine	Life Technologies, Darmstadt, Germany
MEM 31095	Life Technologies, Darmstadt, Germany
MEM NEAA 11140	Life Technologies, Darmstadt, Germany
Pen/Strep	Life Technologies, Darmstadt, Germany
Sodium Pyruvate 11360	Life Technologies, Darmstadt, Germany
Trypsin	Life Technologies, Darmstadt, Germany

2.1.11 Software and online databases

Software/ Database	Source
Acrobat Reader	Adobe
Allen brain atlas	http://www.brain-map.org/
ApE	http://biologylabs.utah.edu/jorgensen/wayned/ape/
Axio Vision	Carl Zeiss AG
ClustalW	http://www.ebi.ac.uk/Tools/msa/clustalw2/
DNAStar	DNAStar Inc.
Endnote	Thomson Reuters
GeneCards	http://www.genecards.org/
GraphPad Prism	GraphPad Software Inc.
GraphPad Software	http://www.graphpad.com/quickcalcs/)
Grip strength software	TSE Systems
Illustrator	Adobe
ImageJ	http://rsbweb.nih.gov/ij/
MS Office	Microsoft
NCBI tools	http://www.ncbi.nlm.nih.gov/
NetAffx Analysis Center	http://www.affymetrix.com/analysis/index.affx
Peak Scanner Software 1.0	Life Technologies
Photoshop	Adobe
Primer3	http://frodo.wi.mit.edu/primer3/
Spidey	http://www.ncbi.nlm.nih.gov/spidey/
StatView	SAS Institute Inc.
Step One Software 2.1	Life Technologies
TotalLab	Amersham Biosciences
Versamax software	Omnitech/Accu Scan

2.2 Methods

2.2.1 Mouse mutants

2.2.1.1 Generation of *Atxn2*-CAG42-knock-in mouse

The generation of the *Atxn2*-CAG42-knock-in mice was outsourced to Genoway (Lyon, France).

2.2.1.1.1 Vector construct

The sequences necessary for the generation of the *Atxn2*-CAG42-knock-in mouse descended from a publicly available database (NC_000071 and NM_009125, http://www.ncbi.nlm.nih.gov/). The previously described pKO-*Sca2*-vector was the basis for the new vector construct (Figure 7) (Lastres-Becker *et al*. 2008a). *LoxP* sites distal and proximal to the targeted gene were inserted into the vector. An additional NsiI restriction site was introduced to the distal *loxP* site that allowed its detection. The homology arms were isogenic with the used 129/Sv ES cell lines. The positive selection of successfully transfected ES cell clones was done through a Neomycin selection cassette that was flanked by FRT (Flippase recognition target) sites. These sites allow the removal of the selection cassette *in vitro* using the Flp-recombinase or *in vivo* following breeding with Flp-expressing mice. The presence of the Diphtheria Toxin A (DTA) negative selection marker reduces the isolation of non-homologous recombined ES cell clones.

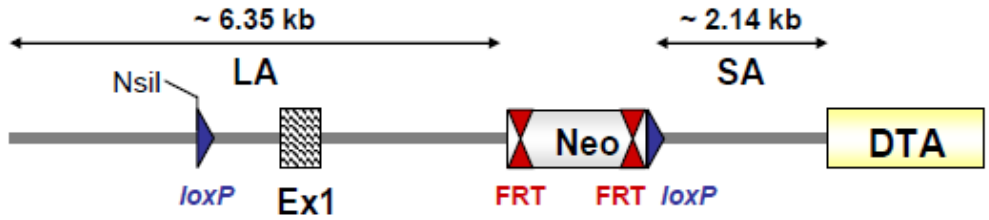

Figure 7. The targeting vector pKO-Sca2. Coding sequences of the targeted gene (hatched rectangle) are flanked by a distal *loxP* and the FRT-Neo-FRT-*loxP* positive selection cassette. A Diphtheria toxin A (DTA) cassette served as negative selection. FRT sites are represented by double red triangles and *loxP* sites by blue triangles. The sizes of the long homology arm (LA) and the short homology arm (SA) are indicated (Genoway).

The first modification of the pKO-Sca2 targeting vector was done by introducing a small oligonucleotide linker which contained the restriction sites SpeI and StuI into the SgfI restriction site located upstream of the 5' FRT recognition site. This resulted in the deletion of the SgfI recognition site and allowed the unequivocal detection of the neomycin recognition cassette deletion by Southern analysis. This vector was named NOW1-LSAmod (Figure 8).

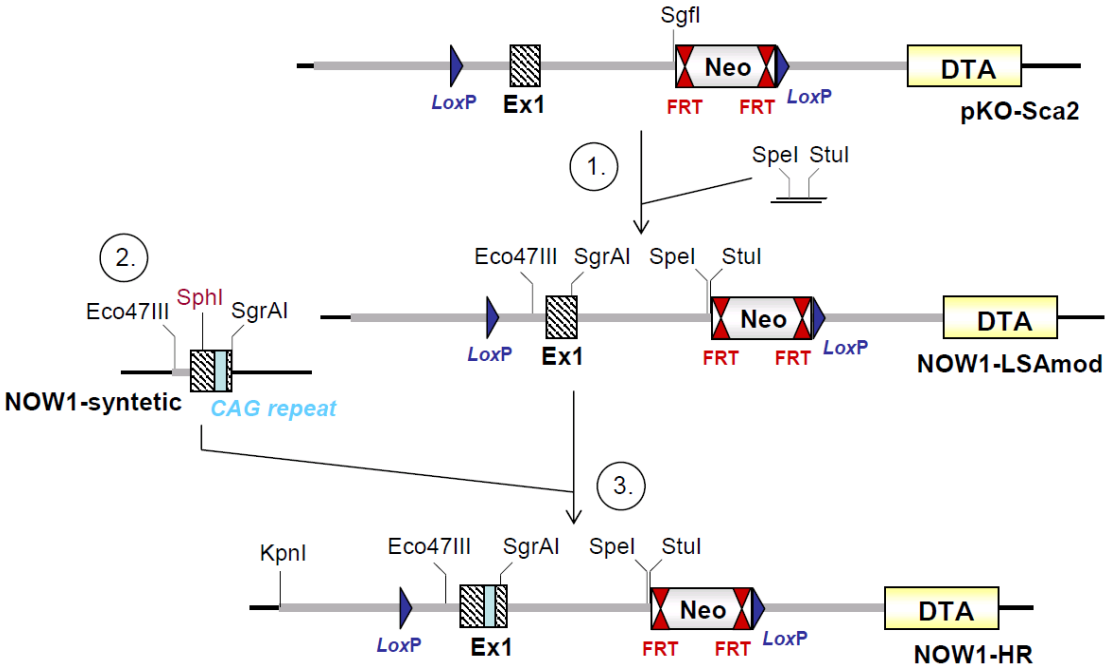

Figure 8. Schematic representation of the targeting vector construction strategy. Cloning steps are represented by circled numbers (Genoway).

As intermediate step, a vector named NOW1-synthetic, was created by introducing a synthesized exon 1 fragment containing a CAG42-repeat (Geneart, Regensburg) at the amino acid position glutamine 156 into the vector backbone via additional 5'-KpnI and 3'-SacI-sites. One nucleotide within exon 1 was modified during its synthesis from G>A to generate an additional SphI restriction site, without changing the amino acid code. The synthesized fragment was sequence verified (J. Nowock, Frankfurt, Germany). Exon 1 was deleted from the NOW1-LSAmod vector via the unique restriction sites SgrAI and Eco47III and replaced by the synthesized exon 1 fragment. The final targeting vector construct was named NOW1-HR (Figure 8).

The *loxP* sites are relics of the conditional targeting vector strategy for the previously generated *Atxn2*-knock-out mouse (Lastres-Becker *et al*. 2008a) and have no relevance for the generation of the *Atxn2*-CAG42-knock-in-mouse.

2.2.1.1.2 ES cell electroporation and integration verification

The sequence verified vector NOW1-HR was linearized with KpnI and 40 µg electroporated into 5 x 10^6 129Sv ES cells (260 V, 500 µF) to allow for homologous recombination at the endogenous *Atxn2* locus. 48 h after electroporation, positive selection started by addition of the antibiotic G418 (200 µg/ml). G418-resistant clones were isolated and amplified and the correct integration verified by PCR. The correct 3' integration was verified using a forward

primer hybridizing in the neomycin selection cassette and a reverse primer downstream of the targeting vector homology sequence. Verification of the correct 5' integration was achieved with a primer pair flanking the *loxP* site. The forward primer was located upstream of the long homology arm of the targeting vector and the reverse primer hybridized upstream of the distal *loxP* site within the 5' homology arm of the targeting vector. Additionally, the integration of the CAG repeat insertion was verified using primers flanking the CAG repeat (Figure 9, Table 4, Table 5).

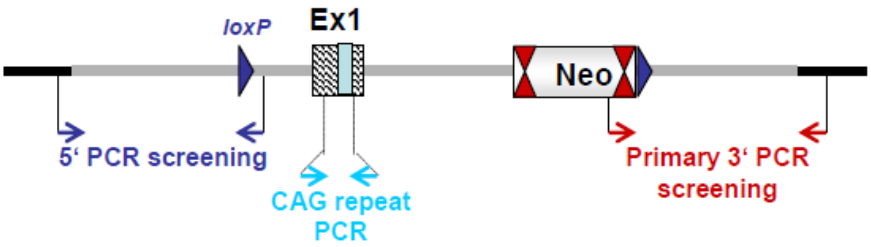

Figure 9. PCR screening strategy for the detection of homologous recombination at the targeted *Atxn2* locus. Exon 1 is symbolized by a hatched rectangle and the CAG repeat by a light blue rectangle. FRT sites are represented by double red triangles and *loxP* sites by blue triangles. The positions of the primer binding sites are indicated (Genoway).

Table 4. Primer for the verification of the correct 3' and 5' integration

	Primer	Sequence 5'-3'	PCR product size
3`-integration	NOW1-A3	CTATCAGGACATAGCGTTGGCTACC	3132 bp
	NOW1-B3	CTGGTCTACAAAGTAGATGCTGCC	
5`-integration	NOW1-C1	TCCACTTTCCCAAACACAGGTCT	2891 bp
	NOW1-D1	GGTCATCTTCACCTTCATATAACT	3132 bp

Table 5. PCR conditions for the verification of the correct 3' and 5' integration

Reaction mix		Conditions			
Genomic DNA	10 ng	**Step**	**Temperature**	**Time**	**Cycles**
Primer	15 pmol each	Denaturing	94 ℃	2'	1x
dNTPs	0.5 mM	Denaturing	94 ℃	30''	35x
Reaction buffer 2 (3`)/ 3 (5')	0.1 vol.	Annealing	65 ℃	30''	
Expand HF Polymerase (Roche)	2.6 U	Extension	68 ℃	3'	
Reaction volume	50 µl	Completion	72 ℃	8'	1x

Further validation of positively screened clones was performed by Southern blot analysis. The standard hybridization conditions used are indicated in Table 6. The genomic DNA was digested with AvrII or SpeI, and to detect the 3' homologous recombination, the DNA was

probed with an internal 3' probe (3I-D), hybridizing within the sequences of the short targeting arm. The verification of the 5' homologous recombination was performed with an external 5' probe (5E-G) hybridizing upstream of the 5' homology sequence (Table 7). The digestion with SphI allowed the specific detection of the genomic integration of the CAG repeat (Figure 10, Table 8).

Table 6. Standard hybridization conditions for Southern blot.

Application	Materials and conditions
Pre-hybridization and hybridization	4 x SSC, 1% SDS, 0.5% skimmed milk, 20 mM EDTA, 100 µg/ml herring sperm, 65 ℃ for 18 h
Washing	2 times 3 x SSC, 1% SDS at 65 ℃ for 15 min, then 2 times 0.5 x SSC, 1% SDS at 65 ℃ for 15 min
Exposure	3 days on BioMax MS films with BioMax intensifying screens

Table 7. Primers for the generation of the internal 3' probe 3I-D and external 5' probe 5E-G.

	Primer	Sequence 5'-3'	Size of probe
3` probe	NOW1-3I-D1	CTTAACTTTGACCTTTTGTGAGGCTGTGC	418 bp
	NOW1-3I-D2	TGAAAGCACATGCCTTGTTGAATGC	
5`probe	NOW1-5E-G1	TCCCAAACACAGGTCTGAGTAAGAAGC	365 bp
	NOW1-5E-G2	CTGGGGAATCAAACTCAAAGTCTGC	

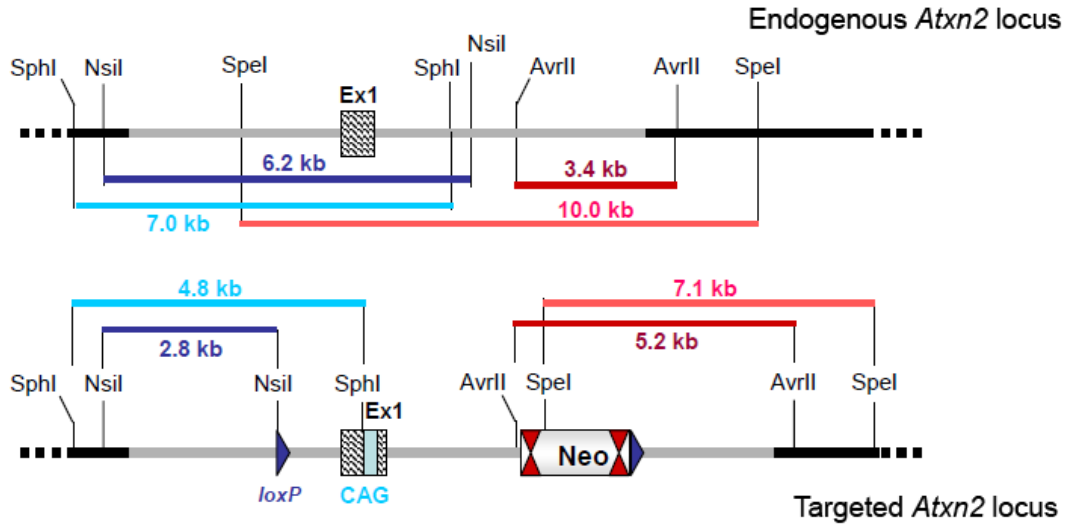

Figure 10. Southern blot strategy detecting homologous recombination at the *Atxn2* locus. Exon 1 is symbolized by a hatched rectangle and the CAG repeat by a light blue rectangle. FRT sites are represented by double red triangles and *loxP* sites by blue triangles. The expected DNA fragment sizes for the 5' Southern analysis are indicated in light and dark blue and for the 3' Southern analysis in light and dark red (Genoway).

Table 8. Expected DNA fragment sizes of the designed Southern blot analysis.

Genomic DNA digestion with enzyme	5' homologous recombination		3' homologous recombination	
	exp. WT fragment size	exp. targeted fragment size	exp. WT fragment size	exp. targeted fragment size
NsiI	6.2 kb	2.8 kb (*loxP insertion*	/	/
SphI	7.0 kb	4.8 kb (CAG repeat insertion)	/	/
AvrII	/	/	3.4 kb	5.2 kb
SpeI	/	/	10.0 kb	7.1 kb

Removal of the FRT flanked neomycin resistance cassette was performed via Flp-mediated excision in ES-cells and its success again verified using PCR and Southern blot analysis. For the PCR a primer pair was used that hybridizes to endogenous, also wild-type, sequences up- and downstream of the integration locus of the FRT-neo-FRT-*loxP* cassette (Figure 11). This resulted in different product sizes for wild-type, targeted Flp-not excised and Flp-excised alleles. The 3' PCR screening, with one primer hybridizing within the Neo-cassette and one primer 7.2 kb further downstream, further confirmed the excision when no product was amplified (Table 9, Table 10).

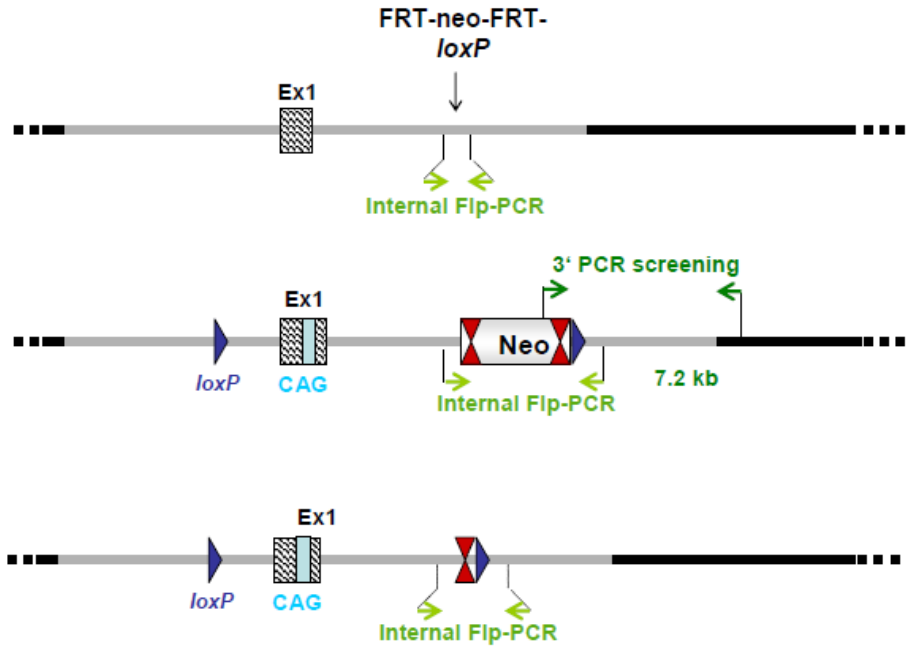

Figure 11. PCR screening strategy for the detection of the Flp-excision event at the targeted *Atxn2* locus. Exon 1 is symbolized by a hatched rectangle and the CAG repeat by a light blue rectangle. FRT sites are represented by double red triangles and *loxP* sites by blue triangles. The positions of the primer binding sites are indicated (Genoway).

Table 9. Primer for the screening PCR detecting the Flp-mediated excision.

Primer	Sequence 5'-3'	PCR product in allele of		
		WT	Targeted	Flp-excised
NOW1-K2	TGAGTTGACTCCACAGGGAGGTGAGC	793 bp	2944 bp	948 bp
NOW1-H2	CCATCTCGCCAGCCCGTAAGATTC			

Table 10. PCR conditions for the screening PCR detecting the Flp-mediated excision.

Reaction mix		Conditions			
		Step	Temperature	Time	Cycles
Genomic DNA	100 ng	Denaturing	94 ℃	2'	1x
Primer	15 pmol each	Denaturing	94 ℃	30''	35x
dNTPs	0.5 mM	Annealing	65 ℃	30''	
Reaction buffer 3	0.1 vol.	Extension	68 ℃	3'	
Expand HF Polymerase (Roche)	2.6 U	Completion	72 ℃	8'	1x
Reaction volume	50 µl				

As this internal PCR screening method is not specific for the targeted locus, and would also be positive in case of a non-homologous integration, Southern blot analysis was performed that also showed the presence of the wild-type allele. This analysis was equal to the verification of the 3' homologous recombination (Figure 12, Table 11).

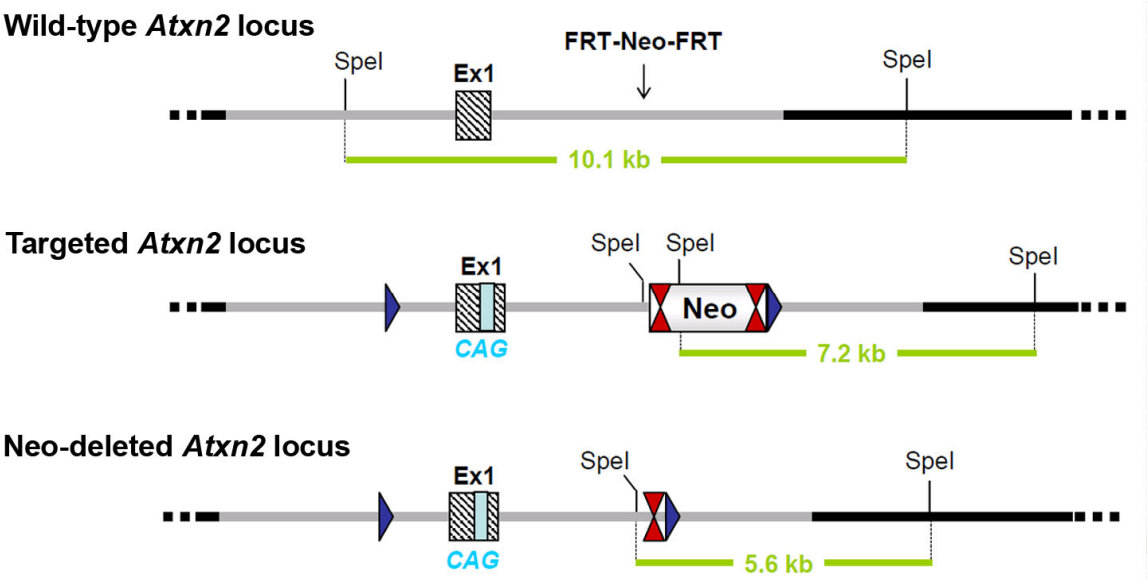

Figure 12. Southern blot strategy detecting Flp-mediated excision of the targeted *Atxn2* locus. Schematic representation of the wild-type, targeted, and Neo-deleted *Atxn2* allele with the relevant restriction sites for the Southern blot analysis (Genoway).

Table 11. Expected fragment sizes for the Flp-excision Southern blot analysis.

Allele	Expected size of SpeI fragment
wild-type	10.1 kb
targeted	7.2 kb
Flp-excised	5.6 kb

2.2.1.1.3 Breeding of chimeras and generation of F1 heterozygous mice

Correctly targeted ES cell clones were injected into C57BL/6 blastocysts leading to the generation of male mice whose chimerism rate was determined. Male mice displaying 50-100% chimerism were mated with C57BL/6 females which led to agouti coloured pups of the F1-generation when ES cells also contributed to the germ layer. Agouti coloured pups were genotyped according to the Flp-excision PCR described in the previous section 2.2.1.1.2 with optimized PCR conditions (Table 12). Further confirmation was achieved by Southern blot analysis. Mice that showed correct recombination were used to establish the mouse line at the ZFE in Frankfurt (Germany).

Table 12. Optimized PCR conditions for the genotyping of agouti pups according to the detection of the Flp-mediated excision.

Reaction mix		Conditions			
Genomic DNA	10 ng	**Step**	**Temperature**	**Time**	**Cycles**
Primer	15 pmol each	Denaturing	94 ℃	2’	1x
dNTPs	0.5 mM	Denaturing	94 ℃	30’’	35x
Reaction buffer 3	0.1 vol.	Annealing	65 ℃	30’’	
Expand HF Polymerase (Roche)	2.6 U	Extension	68 ℃	1’	
Reaction volume	50 µl	Completion	72 ℃	8’	1x

2.2.1.2 Mouse genotyping

At around postnatal day 1 the sex of the mice was determined and each mouse marked with an ear punch. Tail biopsies were taken (approximately 3 mm) and the DNA from the biopsies isolated (described in 2.2.2.2) to determine the genotype.

2.2.1.2.1 Genotyping of *Atxn2*-CAG42-knock-in mouse

TaKaRa LA Taq-Polymerase (Takara Bio Inc., Japan) was used to amplify the neomycin cassette excised locus with the primer pair NOW1-K2 and NOW1-H2 flanking this site. The wild-type (WT) allele is predicted to yield an amplification product of 793 bp and the knock-in (CAG42) allele one of 984 bp, while heterozygous (CAG1/CAG42) mice show products of both sizes (Figure 13, Table 13).

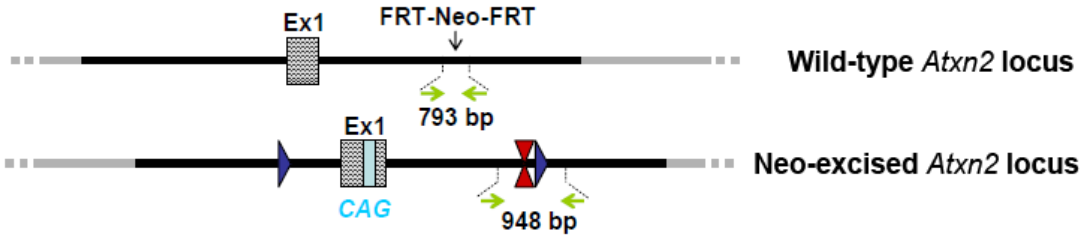

Figure 13. Genotyping strategy by PCR. Exon 1 is symbolized by a hatched rectangle and the CAG repeat by a light blue rectangle. FRT sites are represented by double red triangles and *loxP* sites by blue triangles. The positions of the primer binding sites are indicated (Genoway).

Table 13. PCR conditions for the genotyping of the *Atxn2*-knock-in mice.

Reaction mix		Conditions			
Genomic DNA	~50 ng	**Step**	**Temperature**	**Time**	**Cycles**
Primer	5 pmol each	Denaturing	94 ℃	3’	1x
10x LA PCR Buffer II	0.1 vol.	Denaturing	94 ℃	15’’	30x
dNTPs	2.5 mM each	Annealing	68 ℃	1’	
LA Taq Polymerase	5 U/µl	Extension	68 ℃	3’	
Reaction volume	25 µl	Completion	68 ℃	9’	1x

2.2.1.2.2 Genotyping of *Atxn2*-knock-out mice

For the genotyping PCR of the *Atxn2*-knock-out mice (Lastres-Becker *et al*. 2008a), the excised locus was utilized (Figure 14).

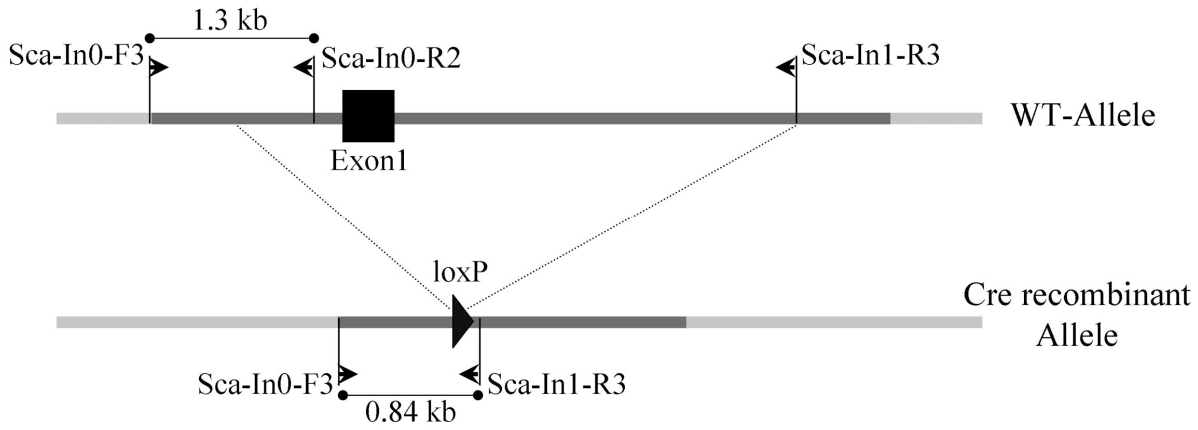

Figure 14. Genotyping strategy for *Atxn2*-knock-out mice. The wild-type PCR is based on a primer pair hybridizing to genomic DNA upstream of exon 1 (product size: 1.3 kb). For the detection of the Cre recombinant allele, the forward-primer remains equal. The reverse primer binds right after the *loxP* site and is therefore specific for the recombinant allele (product size: 0.84 kb) (Lastres-Becker *et al*. 2008a).

Table 14. PCR conditions for the genotyping of *Atxn2*-knock-out mice.

Reaction mix		**Conditions**			
Genomic DNA	~50 ng	**Step**	**Temperature**	**Time**	**Cycles**
Primer 10 µM	1 µl	Denaturing	95 ℃	5’	1x
Pink Juice	17 µl	Denaturing	94 ℃	30’’	35x
Taq Polymerase	1 µl	Annealing	60 ℃	30’’	
(Life Technologies)		Extension	72 ℃	1’20’’	
Reaction volume	20 µl	Completion	72 ℃	3’	1x

2.2.1.3 Animal housing

Mice were housed in accordance with the German Animal Welfare Act, the Council Directive of 24 November 1986 (86/609/EWG) with Annex II and the ETS123 (European Convention for the Protection of Vertebrate Animals) at the FELASA-certified Central Animal Facility (ZFE) of the Frankfurt University Medical School.

Mice were kept at a 12h-light and 12h-dark cycle in individually ventilated cages (IVC) and were supplied with water and food *ad libitum.* Mice were backcrossed from a 129Sv x C57BL/6 mixed background for at least 8 generations into the C57BL/6 strain. Littermates derived from heterozygous matings were used for all experiments.

2.2.1.4 Segregation analysis

To assess whether a normal genotype and sex distribution of the *Atxn2*-CAG42-knock-in line was apparent, litters from 42 matings of heterozygous mice were examined. X^2-analysis was used to compare expected versus observed numbers.

2.2.1.5 Body weight and behavioural observations

Mice were weighed before behavioural testing on a digital kitchen balance (Zeitlos-Vertriebs GmbH, Breisach, Germany).

The motor performance of mice was assessed using an accelerating rota rod apparatus (Ugo Basile, Robert & Jones, model 7650, Comerio VA, Italy). Mice from three founder lines were placed at independent time points on the accelerating rod. Within the 5 minute trial, the rod accelerated from 4-40 rpm and the latency to fall was recorded. For motor learning behaviour, the mice were placed on the rod for four trials per day for 4 consecutive days and their latency to fall recorded. Each trial lasted 5 minutes.

Grip strength was assessed by measuring the peak force of the fore-limbs in 10 trials per mouse on an electronic grip strength meter (TSE, Bad Homburg, Germany).

Footprints were evaluated by painting the hind limbs of mice with a non-toxic ink. The mice were allowed to walk through a paper lined tunnel (height: 6 cm x width: 9 cm x length: 40 cm) and step length, gait width, alternation coefficient and linear movement were analyzed on the basis of the footprints according to Clark *et al.* (Clark *et al*. 1997). The data interpretation was previously excellently described: “Step Length: average distance of forward movement between alternate steps; step length was calculated by measuring the distance of travel through the tunnel divided by the number of steps used to traverse that distance. Gait Width: average lateral distance between opposite left and right steps; the gait width was determined by measuring the perpendicular distance of a given step to a line connecting its opposite preceding and succeeding steps. Alternation Coefficient: calculated value describing the uniformity of step alternation; a perfect tandem alternating gait in which all alternate steps fell exactly equidistant between the preceding and succeeding opposite steps would have a calculated alternation coefficient of zero. Conversely, a shuffle gait in which all alternate steps fell exactly beside the preceding opposite steps would have a calculated value of 0.5. The alternation coefficient was calculated by determining the mean of the absolute values of 0.5 minus the ratio of right–left step distance to right–right step distance for every right–left step pair taken in the tunnel. Linear Movement: average change in angle between consecutive right–right steps; this measurement was calculated by drawing a line perpendicular to the direction of travel, starting at the first right footprint. The angle

between this perpendicular line and each subsequent right footprint was determined, and differences in angle were calculated between each consecutive step pair. The absolute values of all angle differences were summed and divided by the number of steps scored. A large linear movement measurement would be indicative of nonlinear movement, or weaving, through the tunnel" (Clark *et al*. 1997).

The spontaneous motor activity of the mice was recorded by a Versamax animal activity monitor (Accuscan, Columbus, USA). The mouse was placed into the 20 x 20 cm arena and its activity recorded by infrared beams during the 5 minute trial. The infrared emitting photocells are placed in such a way that every movement of the mouse, both horizontally and vertically, will be detected and recorded by software. Parameters measured include horizontal activity, vertical activity, total distance traversed, movement time, total number of movements, centre time (time spent in the centre), centre distance, margin time (time spent in the perimeter), margin distance and number of stereotypy counts.

In the inverted screen test, mice were placed on a 20.5 x 14 cm metal grid that was then rotated 180 degrees so that mice were turned upside down. The latency to fall was recorded during the trial which lasted 1 minute maximum.

2.2.1.6 Tissue preparation

After cervical dislocation the brain tissue was immediately removed and dissected into cerebellum, brainstem, hippocampus and cortex. Furthermore, the liver was extracted and a tail biopsy (approximately 3 mm) was taken to verify the genotype of the mouse. All tissues were immediately frozen in liquid nitrogen and stored at -80 ℃ until used.

2.2.2 Nucleic acid techniques

2.2.2.1 PCR to amplify the CAG repeat in mice

To amplify the CAG repeat in mice, the primer pair Sca2Ex1fwd5_m and Sca2Ex1rev2_m (2.1.4) was used with the following PCR protocol on ~ 50 ng of genomic DNA:

Reaction mix		**Conditions**			
Primer	5 pmol each	**Step**	**Temperature**	**Time**	**Cycles**
10x LA PCR Buffer II	0.1 vol.	Denaturing	98 ℃	3’	1x
dNTPs	2.5 mM each	Denaturing	98 ℃	40’’	39x
BSA (100x)	0.25 µl	Annealing	60 ℃	40’’	
LA Taq Polymerase	5 U/µl	Extension	72 ℃	1’	
Reaction volume	25 µl	Completion	72 ℃	7’	1x

2.2.2.2 DNA extraction from tail biopsy

To extract DNA from a tail biopsy of the mouse, 500 µl of Proteinase K buffer and 25 µl proteinase K (10 mg/ml, Life Technologies, Darmstadt, Germany) were added to the biopsy and incubated at 800 rpm at 55 ℃ overnight. Then, 250 µl of 6 M NaCl were added and mixed vigorously for 1-2 minutes. After centrifugation at 5000 rpm for 10 minutes, 500 µl of the aqueous phase were transferred to a new tube. To precipitate the DNA, 1 ml of 100% ethanol was added and the tube was gently mixed for 5 - 6 times. After centrifugation for 10 minutes at 14,000 rpm, the ethanol was removed and replaced by 70% ethanol to wash the pellet. The pellet was vortexed and precipitated at 14,000 rpm for 5 minutes. After drying the pellet, it was resuspended in 100 µl of TE-buffer and stored overnight at 4 ℃ to dissolve the DNA. The long-term storage occurred at -20 ℃.

2.2.2.3 DNA extraction from agarose gels

To isolate a specific fragment, DNA extraction from low melting agarose gels was performed using the Wizard SV Gel and PCR Clean-up system (Promega, Mannheim, Germany). DNA was dissolved in 30 µl DNase- and RNase-free H_2O.

2.2.2.4 Ligation

Ligation reactions were performed with the pGEM-T Easy Vector System according to manufacturer's protocol.

2.2.2.5 Transformation

Transformation of DH5α (Life Technologies, Darmstadt, Germany) was done according to manufacturer's protocol.

2.2.2.6 Mini- and Midipreparation

Solutions for the minipreparation were taken from the GenElute HP Free Plasmid Maxiprep Kit (Sigma-Aldrich, Munich, Germany). 2 ml of the inoculated overnight bacterial culture was pelleted for 5 minutes at 7000 rpm. Bacteria were resuspended in 200 µl resuspension solution. 200 µl of lysis solution were added and inverted gently for 6 times. After a 5 minute incubation step at RT, 200 µl of neutralization solution were added, again mixed gently by inverting 6 times and incubated for 5 minutes on ice. Before centrifuging the solution at 14,000 rpm for 10 minutes, the tube was mixed again gently. 500 µl of the supernatant were transferred into a new tube and 1000 µl of 100% ethanol added. The tube was vortexed and spun at 14,000 rpm for 10 minutes. After discarding the supernatant, the pellet was washed with 70% ethanol and again spun for 2 minutes. The supernatant was discarded and approximately 50 µl of DNase- and RNase-free H_2O were added to the dried pellet.
For Midipreparations, the Jet Star Plasmid Purification Kit (Genomed, Löhne, Germany) was used according to manufacturer's instructions.

2.2.2.7 Plasmid stocks

900 µl of overnight grown bacterial culture were mixed with 100 µl DMSO and stored at -80 ℃ in cryo tubes.

2.2.2.8 Restriction

DNA digestions were performed as follows in a final volume of 20 µl:

DNA	x µl (~600 ng)
Buffer	2 µl
Enzyme	1 µl
H_2O	y µl

2.2.2.9 Sequencing

Sequencing was outsourced to Seqlab (Göttingen, Germany). The company was provided with the following reaction mix using primer T7 or M13 in a final volume of 7 µl.

DNA	1 µl (~700 ng)
TrisHCl 10 mM	4.7 µl
Primer	1.3 µl

Chromatograms obtained from Seqlab were analyzed with ApE and the DNAStar package.

2.2.2.10 Precipitation of nucleic acids

Precipitation of nucleic acids was done by adding 1/10 vol. of sodium acetate (pH 5.2) and 0.6 vol. 100% isopropanol. After mixing, an incubation step of 10 minutes at room temperature followed. After centrifugation at 4 ℃ for 15 minutes, the supernatant was discarded and the pellet washed twice with 75% ethanol. The nucleic acids were dissolved in DNAse- and RNase- free H_2O.

2.2.2.11 Fragment length analysis

The determination of the CAG repeat length was done by fragment analysis. The CAG repeat was amplified with TaKaRa LA Taq-Polymerase (Takara Bio Inc., Japan) from DNA from tail biopsies using the 5'-FAM-labeled forward primer Sca2Exfwd5_m and the reverse primer Sca2Ex1rev2_m under the following conditions: 96 ℃-4', followed by 38 cycles of 94 ℃-1', 60 ℃-1' and 72 ℃-1' with a final elonga tion step at 72 ℃-7'. The determination of the fragment length was outsourced to GENterprise GENOMICS (Mainz, Germany). Peak Scanner Software 1.0 (Life Technologies, Darmstadt, Germany) was used to determine the exact PCR product size according to the GS500 size standard.

2.2.2.12 RNA isolation and quantification

RNA extraction from tissue was performed with Trizol reagent (Life Technologies, Darmstadt, Germany) and from cells using the RNeasy Mini Kit (Qiagen, Hilden, Germany) according to manufacturers' instructions. Extracted RNAs were quantified and quality-tested by spectrophotometry and stored at -80 ℃.

2.2.2.13 Poly(A)+-isolation

Poly(A)+-mRNA was isolated with the Oligotex Direct mRNA Mini Kit (Qiagen, Hilden, Germany) according to manufacturer's instructions.

2.2.2.14 Quantitative Real-time RT-PCR

For expression studies, 1 µg of total RNA was digested with DNaseI Amplification Grade (Life Technologies, Darmstadt, Germany) and reversely transcribed using SuperScript III Reverse Transcriptase (Life Technologies, Darmstadt, Germany). Expression levels were investigated with a StepOnePlus Real-Time PCR System (Life Technologies, Darmstadt, Germany). 25 ng of cDNA were used in each PCR reaction. The PCR conditions were 50 ℃-2', 95 ℃-10' followed by 40 cycles of 95 ℃- 15'' and 60 ℃-60''. The gene expression data were analyzed according to the $2^{-\Delta\Delta Ct}$ method (Livak & Schmittgen 2001).
Ribosomal RNA contents were measured using the TaqMan Ribosomal RNA Control Reagents (VIC probe) from Life Technologies, Darmstadt, Germany on cDNA that was diluted 1:100 prior to amplification.

2.2.2.15 Microarray analysis

Cerebellum, brainstem and liver from 18 months old wild-type and *Atxn2*-CAG42-knock-in mice were sent to the Microarray Genechip Facility in Tübingen (Germany) for analysis. The RNA was isolated, its quality documented (one young CAG42 liver sample had to be eliminated from analysis) and 100 ng of total RNA amplified with the Affymetrix 3' IVT Express Kit, labeled and hybridized onto the mouse specific MOE430 2.0 Gene Chip (Affymetrix, Santa Clara, CA, USA) that detects 39,000 transcripts and variants corresponding to 34,000 mouse genes. Scanning of the arrays was performed in the Gene Chip Scanner 3000 and the raw data obtained with the AGCC 3.0 software. Further analysis was done using the Bioconductor package (www.bioconductor.org). RMA normalization was

applied and calculation of differentially expressed transcripts was done by compiling a linear model (Irizarry *et al.* 2003, Smyth 2005). F-statistics was applied (empirical Bayes model) and the p-values obtained were further corrected for multiple testing with the “Benjamini-Hochberg” test (Benjamini & Hochberg 1995). P-values < 0.05 were considered significant. Genes that were detected within their exons and that were dysregulated consistently according to more than one spot were prioritized for further analysis. After the determination of differentially expressed transcripts (CAG42 compared to wild-type), the number “1" was added to upregulated and the number “-1” was added to downregulated transcripts and further marked with the colors red and green. Furthermore the fold-change of expression change was added.

2.2.3 Protein biochemistry

2.2.3.1 Western Blot

50 mg of tissue was homogenized with a motor pestle in 10 vol. RIPA buffer followed by 15 minutes incubation on ice. After centrifugation at 14,000 rpm at 4 ℃ for 20 minutes, the supernatant (soluble fraction) was preserved and either 1/2 vol. Urea/SDS-buffer or 1/2 vol. 2 x SDS-lysis buffer was added to the pellet, sonicated and centrifuged at 14,000 rpm for 10 minutes. The supernatant represented the insoluble fraction. Protein concentration was determined using the BCA protein assay kit (Thermo Scientific, Schwerte, Germany). Proteins were separated on 8% polyacrylamide gels and transferred to PVDF membranes (90 minutes, 50 V). The membrane was blocked in 5% skimmed milk to diminish unspecific binding and incubated with primary antibodies. The membrane was washed in PBST for 3 x 5 minutes and incubated with the adjacent secondary antibody. After another washing step of 3 x 5 minutes, antibodies were visualized using ECL method (Thermo Scientific, Schwerte, Germany). Densitometric analysis was carried out using the ImageJ software.

2.2.3.2 Co-immunoprecipitation

2.2.3.2.1 Co-immunoprecipitation of ATXN2 and eIF3

In total, three different conditions for the lysis buffer were tested: 1- pH 7.1, 150 mM NaCl; 2- pH 7.1, 200 mM NaCl; 3- pH 8.0, 200 mM NaCl. HEK293 cells were grown until confluent and washed with ice-cold PBS. Cells were collected with a cell scraper and centrifuged for 3 minutes at 4 ℃ and 200 g. 250 µl of lysis buffer (pH 7.1 or 8.0) was added per 10 cm dish, resuspended and incubated for 10 minutes on ice. After centrifugation for 10 minutes at 4 ℃ and 14,000 rpm, the supernatant was transferred into a falcon tube. Tubes were

supplemented with 400 µl of supernatant and 15 µl of beads (Protein A/G Plus-Agarose, Santa Cruz, California, USA) and 100 µl preserved as the input control. The tubes were supplemented with NaCl, and for each condition one IP and one control reaction was run. 50 µl of SCA2-12B6 antibody was added and incubated under rotation for 1.5 h at 4 ℃ to allow for protein-antibody-bead binding. Then, everything was centrifuged for 1 minute at 5,000 g at 4 ℃ and the supernatant discarded, 1 ml of lysis buffer (without inhibitors) were added and rotated for another 5 minutes. This was repeated 4 times. After discarding the supernatant for the last time, 40 µl of loading dye were added and the proteins together with the beads boiled for 5 minutes at 95 ℃. Proteins were stored at -80 ℃ until used for Western blot.

2.2.3.2.2 Co-immunoprecipitation of ATXN2 and PABPC1

Approximately 50 mg cerebellar tissue from 6 months old wild-type, CAG42 and KO mice were homogenized with a motor pestle in 10x Vol. lysis buffer (10 mM HEPES, 10 mM KCl, 5 mM $MgCl_2$, 0.1% NP-40 and one tablet Complete Protease Inhibitor Cocktail), incubated for 10 minutes at 4 ℃ and subsequently centrifuged for 20 minutes at 16,000 g. 200 µg of soluble proteins derived from the supernatant were incubated o/n under rotation with 40 µl of anti-ATXN2 antibody (SCA2-12B6). Beads (Protein A/G Plus-Agarose, Santa Cruz, California, USA) were pre-treated o/n with buffer W (0.2 M NaCl, 1% gelatine, 0.05% NaN_3, 50 mM Tris, 0.1% Triton) to avoid unspecific protein binding. Antibody-protein complexes were precipitated with 40 µl of beads under rotation for one hour at 4 ℃. Beads were sedimented by centrifugation and washed 4 times in PBS including protease inhibitors, resuspended in 2x loading buffer, boiled for 3 minutes and Western blot was performed with anti-PABP antibody (Abcam).

2.2.3.3 Cell fractionation

Two mouse brains (age 6 months) were rapidly removed after decapitation and washed in cold PBS. The brain was homogenized in 5 vol. extraction buffer 1 by 12 loose and 12 tight strokes using a dounce homogenizer and incubated for 20 minutes on ice. An aliquot of the homogenate of approximately 100 µl was kept as input control and the rest centrifuged for 10 minutes at 4 ℃ and 1,000 g. To the pellet (nuclei) , 2 ml of RIPA buffer were added and the supernatant (post-nuclear SN) was then centrifuged at 10,000 g for 10 minutes at 4 ℃. The pellet (heavy membranes/mitochondrial pellet) was resuspended in 2 ml of RIPA buffer and the supernatant (post-mitochondrial SN) centrifuged at 100,000 g for 1 h at 4 ℃. The supernatant (cytosolic fraction) was preserved and the pellet in 1.5 ml of RIPA buffer

resuspended (light membranes). From each fraction (nuclei, post-nuclear SN, heavy membranes, post-mitochondrial SN, cytosolic fraction and light membranes) an aliquot of 100 µl was preserved. Each aliquot was supplemented with 100 µl 2 x loading buffer and boiled for 5 minutes at 95 ℃ and stored at -20 ℃ for analysis.

2.2.3.4 ELISA

To investigate the S6-phosphorylation status in MEFs, confluent cells were serum-starved for 24 h, and either left untreated or incubated with 100 nM insulin for 10 minutes. The phosphorylation status of S6 was measured with the PathScan Phospho-S6 Ribosomal Protein (Ser235/236) Sandwich ELISA Kit (#7205, Cell Signaling, Danvers, USA) according to manufacturer's protocol. 1 mM PMSF was added to the cell lysis buffer to prevent protein degradation.

2.2.4 Cell culture

The following growth media were used.
HeLa cells: MEM medium supplemented with 10% FCS, 1% NEAA and 1% HEPES
MEF cells: DMEM supplemented with 15% BGS, 1% L-Glutamine and 1% PenStrep
HEK 293 cells: DMEM supplemented with 10% FCS and 1% L-Glutamine
To freeze cells, cells from a confluent 25 mm^2 flask were trypsinized, pelleted and resuspended in 1 ml freezing solution comprised of 10% DMSO, 50% of the adjacent serum (BGS or FCS) and 40% of the adjacent growth medium. Cells were always seeded the day before the experiment.

2.2.4.1 Transfection

HeLa cells were transfected for 48 h with 1 µg of plasmid according to Effectene Transfection Reagent (Qiagen, Hilden, Germany) manufacturer's protocol.

2.2.4.2 Generation of mouse embryonic fibroblasts (MEFs)

Embryos were removed from the uterus at around embryonic day 17. The carcass of each embryo was minced and digested for 30 minutes at 37 ℃ in HyQTase (Thermo Scientific, Schwerte, Germany). HyQTase was removed and tissue fragments were resuspended in

DMEM with 15% BGS, 1% glutamine and 3% Pen/Strep and plated into six 9.6 cm^2 wells. The medium was changed daily for the first three days and the amount of antibody was reduced to 1% on day 3. When cells reached confluence they were transferred into 25 mm^2-flasks.

2.2.4.3 Population doubling levels

To determine the population doubling levels, a defined number of MEF cells were seeded on the first day of the experiment. When passaging cells, the number of MEFs was counted to determine the exact number of cells. Population doubling levels were calculated according to the following equation:

$$PDL = [3.32 \times \log(X) - \log(Y)] + Z$$

X = cell yield when confluent
Y = cell number at seed
Z = PDL at previous passage

2.2.4.4 Induction of ER stress

10 cm dishes of confluent MEF cells were either left untreated or ER stress was induced by adding 5 µg/ml of tunicamycin for 16 h. Cells were collected with a cell scraper and pelleted at 4 °C and 200 x g for 3 minutes. After washing with ice-cold PBS, cells were again centrifuged. The pellet was lyzed in 150 ml RIPA buffer for 15 minutes and centrifuged for 20 minutes at 4 °C and 16,000 x g. The supernatant was preserved.

2.2.5 Immunohistochemistry

The cerebellum of perfused (4% PFA) mouse brains was cut on a microtome into 5 µm-thick sagittal sections. For antibody staining, sections were immersed for 30 minutes in 10% methanol, 3% H_2O_2 and 50 mM Tris (pH 7.6) and subsequently washed for three times in Tris. Sections were blocked for 90 minutes with 0.25% Triton X, 0.1 M D-Lysine and 10% Tris-BSA. Blocking before Ataxin-2 staining was modified using goat-serum in 0.1 M PBS. Incubation with the primary antibodies lasted 18 h at room temperature. The biotinylated secondary antibody (1:200) was applied for 90 minutes followed by incubation of 2 h in the avidin-biotin-peroxidase complex (1:100 in Tris, ABC-Elite, Vector Laboratories, Burlingame,

USA). Finally, the sections were incubated in Tris with 0.07% DAB and 0.001% H_2O_2. For Ataxin-2 staining sections were pretreated for 30 sec at 125 ℃ in bull's eye decloaker solution (Biocare Medical, Concord, CA, USA) in a decloaker chamber (Decloaker, Biocare Medical, Concord, CA, USA); for PABPC1, S6, eIF4E and TDP-43 staining, sections were pretreated with citrate buffer and for 1C2 staining sections were incubated in the microwave 3 times for 10 minutes in Tris (pH 9), followed by a 3 minute incubation step in 98% formic acid. Determination of the molecular layer thickness and Purkinje cell number were done by ImageJ.

2.2.6 Working with radionuclides

2.2.6.1 Determination of protein synthesis rates

2 x 10^5 MEFs were seeded on 6-well plates the day before the experiment. To determine the protein synthesis rates, cells were deprived of methionine and cysteine for 30 minutes and labelled by adding 20 µCi/ml EasyTag [^{35}S] Express Protein Labeling Mix (Perkin Elmer, Waltham, MA, USA) for 40 minutes. For the treatment with inhibitors, cells were supplemented 30 minutes before the labelling with 1 µM cycloheximide (CHX, Sigma-Aldrich, Munich, Germany) or 20 nM Rapamycin (LC Laboratories, Woburn, MA, USA). After washing twice with ice-cold PBS cells were lyzed in RIPA and precipitated with ice-cold 10% TCA on GF/C filters (Whatman, Dassel, Germany). After washing twice with ice-cold 5% TCA and once with methanol, filters were dried and subjected to liquid scintillation counting (Perkin-Elmer, Boston, USA).

2.2.7 Statistical analysis

The GraphPad Prism software version 4.03 (2005) and Excel 2007 (MS Office) were used to perform unpaired Student's t-test. Error bars indicate SEM. Values $p < 0.05$ were considered significant and marked with asterisks $p < 0.05$ *, $p < 0.01$ **, $p < 0.001$ ***.

3 Results

The currently available transgenic SCA2 mouse models can only describe gain-of-function mechanisms involved in SCA2, while possible loss-of-function mechanisms involved are inevitably disregarded. For this purpose, the first knock-in mouse model for SCA2 was to be thoroughly characterized to have a mouse that describes SCA2 as physiological as possible. With the help of the characterized *Atxn2*-CAG42-knock-in mouse, effects were then to be identified which possibly contribute to SCA2. As the role of ATXN2 is still not fully understood, studies using the available *Atxn2*-knock-out mouse should reveal new insights into its function in RNA metabolism.

3.1 The characterization of the *Atxn2*-CAG42-knock-in mouse

3.1.1 Generation of the *Atxn2*-CAG42-knock-in mouse

The sequence verified targeting vector NOW1-HR containing a 42 CAG repeat in the first exon of the *Atxn2* gene was electroporated into 129Sv ES cells and, in a first step, its correct 3' homologous recombination verified by PCR. 43 (1A1, 1A2, 1A4, 1A5, 1A7, 1A8, 1B5, 1B11, 1C7, 1C8, 1C12, 1D5, 1D7, 1D8, 2A7, 2A8, 2A10, 2B3, 2B5, 2B8, 2B9, 2B12, 2C2, 2C11, 2D3, 2D9, 3A3, 3A4, 3A8, 4A3, 4A4, 4A6, 4B4, 4B8, 4B9, 4C2, 4C4, 4C7, 4C10, 4C12, 4D1, 4D2, 4D8) out of 213 G418-resistant clones were positive in the 3'- PCR screen, displaying the 3.1 kb sized PCR product, and therefore likely to be correctly homologously recombined at the 3' side (Figure 15).

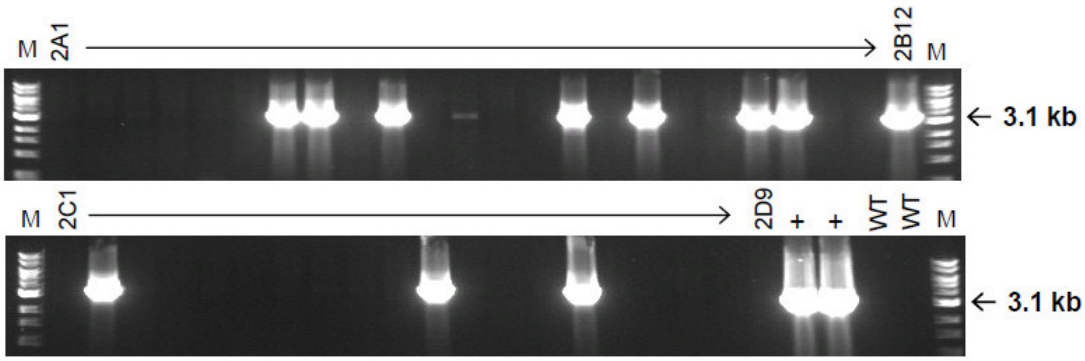

Figure 15. PCR screening for 3' homologous recombination in ES cells. An example of the initial 3' PCR screen result of 42 ES cell clones is shown. 3' homologously recombined clones yielded a PCR product of approximately 3.1 kb. The positive control vector pPC-Sca2 (+) was constructed previously for the generation of the *Atxn2*-knock-out mouse. WT: PCR with wild-type DNA as negative control. M: 1 kb DNA Ladder (NEB) (Genoway).

In a next step, the 43 clones were further validated for their correct 3’ and 5’ integration and the integration of the distal *loxP* site by Southern blot analysis. Non-targeted (wild-type) clones displayed a signal at 10.1 kb, while correctly recombined clones at the 3’ site showed an additional signal at 7.1 kb. Correct 3’ integration was confirmed for 42 out of the 43 clones, while two clones (2B3 and 4B8) contained additional randomly integrated copies of the targeting construct (Figure 16A). Successful 5’ homologous recombination was detectable by a 6.2 kb signal representing the wild-type allele, while an additional 4.8 kb fragment was detected in cells that included the inserted CAG stretch. The existence of the CAG repeat was confirmed in the 2 clones 1B11 and 4B9 (Figure 16B). DNA restriction with NsiI and hybridization with the 5’ probe 5E-G allowed the detection of the distal *loxP* site integration. For the clones 1B11 and 4B9 the *loxP* presence was confirmed as a 6.2 kb signal for wild-type and a 2.8 kb signal for successful integration of the distal *loxP* site (Figure 16C). These results indicate that the 3’ and 5’ homologous recombination in the clones 1B11 and 4B9 occurred properly and that they carry the CAG repeat together with the distal *loxP* site.

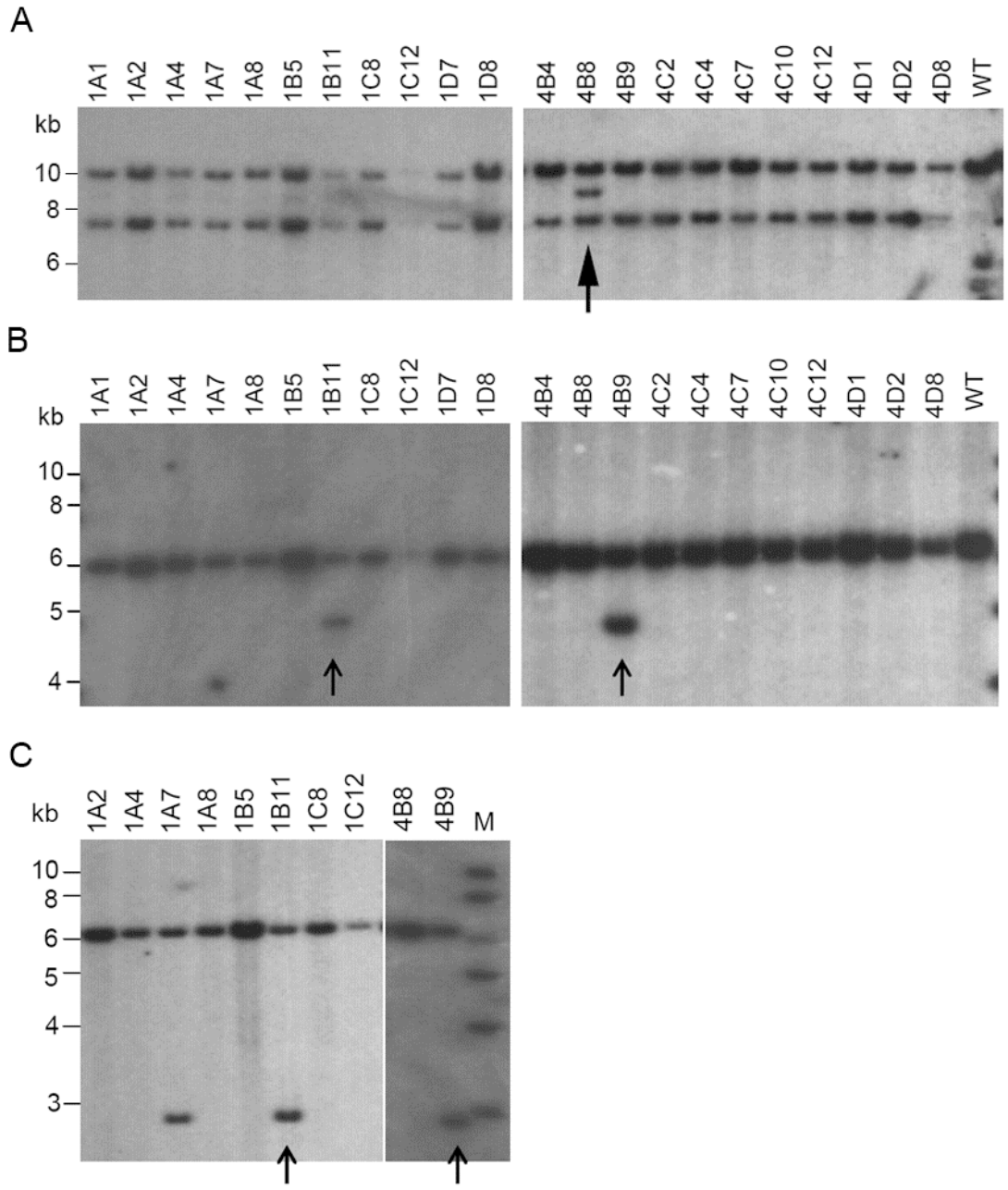

Figure 16. Southern blot analysis verified the successful homologous recombination of the ES cell clones 1B11 and 4B9. Exemplary depiction of recombined clones and their Southern blot validation for their correct integration at the (A) 3' site. The signal at 10.1 kb appeared in wild-type ES cells, while an additional signal at 7.1 kb was detected in targeted clones. Arrow: Clones with randomly integrated copies. (B) the 5' site. The signal at 6.2 kb appeared in wild-type ES cells, while an additional signal at 4.8 kb was detected in clones carrying the CAG repeat (arrow). (C) the distal *loxP* site. The 6.2 kb fragment corresponded to the wild-type signal, while an additional product at 2.8 kb (arrows) confirmed the insertion of the distal *loxP* site (Genoway).

To verify the excision of the Neomycin-cassette by Flp-recombinase, a PCR with primers hybridizing close to the FRT sites of the resistance cassette was performed. Clones after Flp-excision appeared with a PCR product of 984 bp and wild-type cells with a product of 793 bp. Three positive clones, 141A, 141H and 142G, were identified (Figure 17A), and the two clones 141A and 142G were further verified by Southern blot. Both clones were confirmed to be Flp-excised (10.1 kb for wild-type, 7.2 kb for targeted non-excised and 5.6 kb for Flp-

excised; Figure 17B). These results revealed three ES cell clones, 141A, 141H and 142G that showed a correct and complete excision event of the FRT-flanked neomycin selection cassette at the targeted *Atxn2* locus.

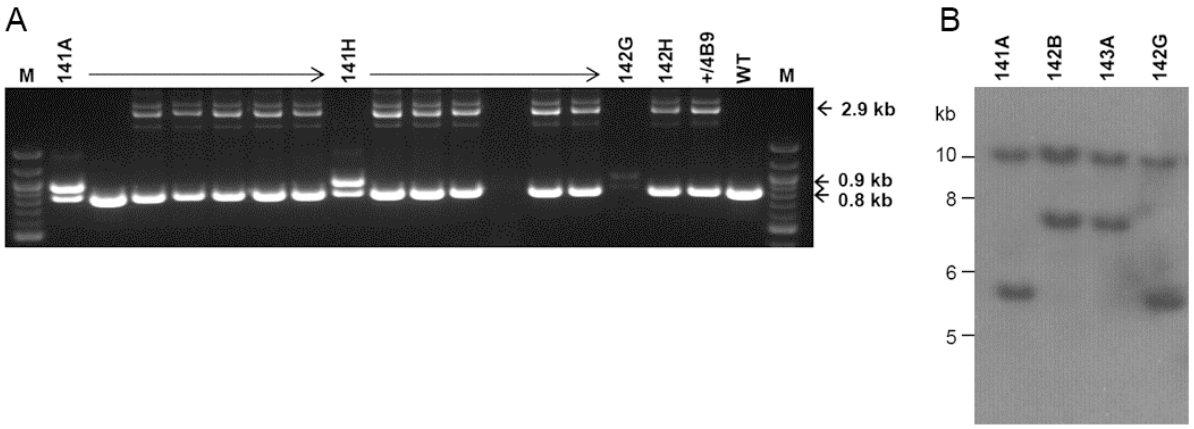

Figure 17. Validation of Flp-mediated Neo-excision by PCR and Southern blot at the targeted *Atxn2* locus. (A) Successful excision of the Neo-cassette yielded a PCR product of 984 bp, in addition to the wild-type (WT) product of 793 bp. M: 100 bp DNA ladder (NEB). (B) Successful Flp-mediated excision verified by Southern blot leads to a 10 kb fragment for wild-type cells, a 7.2 kb fragment for targeted non-excised cells and a fragment of 5.6 kb for Flp-excised cells. Clones 142B and 143A were used as non-excised controls that were negative in the screening PCR (Genoway).

In total, eight clones were identified to be correctly homologously integrated at the 3' and 5' site with a correct Flp-mediated deletion of the neomycin cassette:

- 4B9 derived clones: 141A, 141H and 142G
- 1B11 derived clones: 184A, 191E, 194A, 201B and 202A

The clones 141H, 191E, 194A and 202A carried the CAG repeat and were selected for blastocyst injection which led to the generation of 4 male chimeras displaying a chimerism rate ranging from 50%-100%. The chimera derived from clone 141H displayed a chimerism rate of 80% and produced in total 19 agouti-colored pups (F1-generation). However, the chimera derived from clone 191E died at the age of 10 weeks. The chimera derived from clone 202A seemed to be sterile, since after 7 weeks of breeding still no birth occurred (Table 15).

Table 15. Chimeras breeding with wild-type C57BL/6 mice. Pups screened positive for the recombined allele are highlighted in grey.

Parental chimeras	Clone ID	Nr. Of pups	Nr. Of agouti pups	ID number	Tail biopsy nr.
50% male	194A	cannibalized	-	-	-
80% male	141H	7	6	1	34409
				2	34410
				3	34411
				4	34412
				5	34413
				6	34414
		6	6	7	34574
				8	34575
				9	34576
				10	34577
				11	34578
				12	34579
		7	7	13	34665
				14	34666
				15	34667
				16	34668
				17	34669
				18	34670
				19	34671
100% male	202A	0*		-	-

*seemed to be sterile after 7 weeks breeding without any birth

Among the 19 tested agouti-colored pups, seven mice (34411, 34413, 34575, 34576, 34577, 34578 and 34669) carried the recombined allele as verified by genotyping PCR. To verify again the transmission and the presence of the CAG repeat, the Southern blot strategy was according to the previously described verification of the correct 5' integration after SphI digestion of genomic DNA (Table 8). Overall, two male (34411, 34575) and five female (34413, 34576, 34577, 34578, 34669) heterozygous *Atxn2*-CAG42-knock-in-mice were identified (Figure 18). This indicates that the chimera derived from clone 141H carried the modified allele within its gonads and was able to transmit the mutation successfully to the F1 generation.

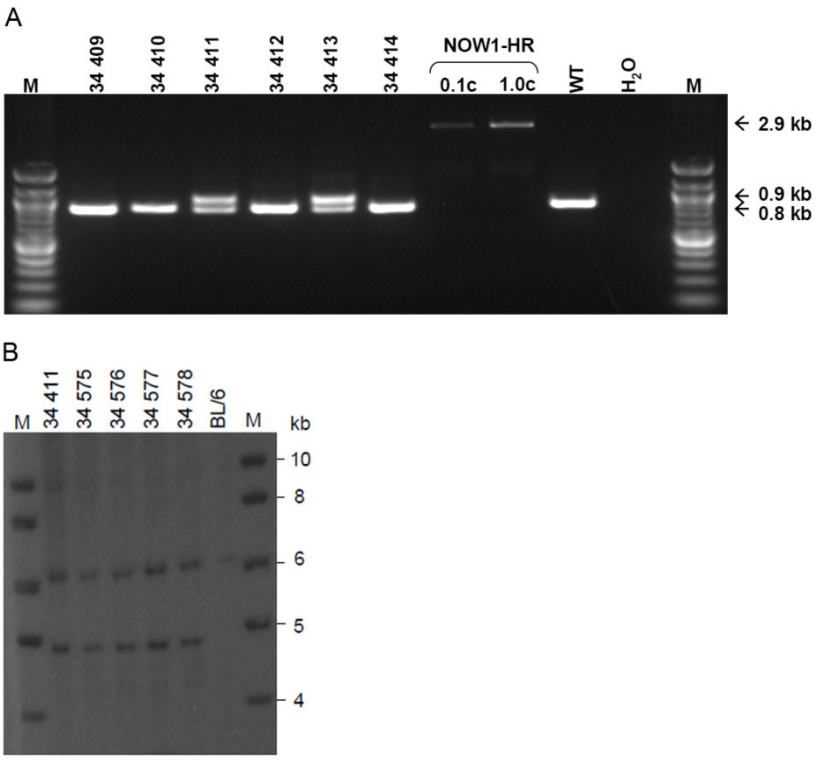

Figure 18. Analysis of successful transmission of the recombined knock-in allele in the F1-generation. (A) All agouti colored pups were genotyped. WT mice displayed a product of 793 bp and the recombined allele of 984 bp. As positive control the targeting vector NOW1-HR and DNA from WT mice was used. A PCR without template served as negative control (H_2O). M: 100bp DNA ladder (NEB). (B) Southern blot analysis of correct 5' and CAG repeat integration was successful showing one product at 6.2 kb for WT and a product of 4.8 kb for the recombined allele (Genoway).

Two male (34411, 34575) and three female (34413, 34576, 34577) heterozygous mice were sent to the ZFE in Frankfurt to establish the knock-in mouse line.

3.1.1.1 Genotyping of the *Atxn2*-CAG42-knock-in mouse

For an unequivocal identification of each mouse from the *Atxn2*-CAG42-knock-in mouse line, the genotyping PCR established from Genoway was further optimized. The forward and the reverse primer remained equal to those from Genoway and thus also the expected product sizes of 793 bp for the wild-type and 984 bp for the knock-in allele (Figure 19).

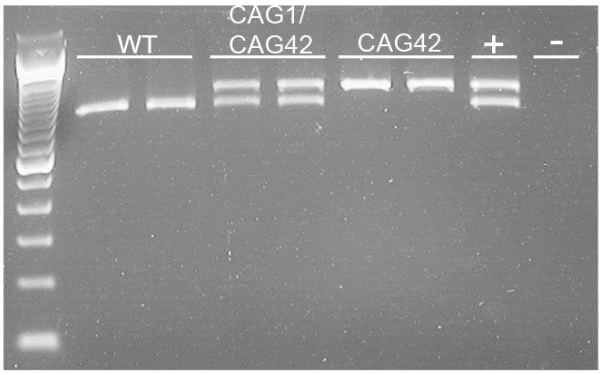

Figure 19. Genotyping PCR. The genotyping strategy is based on the distinction between the homologous recombined Neo-excised knock-in (CAG42) allele (984 bp) and the wild-type (WT) allele (793 bp). Heterozygotes (CAG1/CAG42) displayed both products.

3.1.2 The knock-in mouse has a repeat of 42 CAGs and its paternal and maternal transmission is stable

To confirm the successful homologous recombination, a PCR with CAG repeat flanking primers was performed on DNA from tail biopsies (Figure 20A), the product sequence verified and the introduction of the CAG42-repeat confirmed (Figure 20B). To test how the repeat is transmitted in the mice over successive generations, the PCR products from mice across nine generations from WT, heterozygous (CAG1/CAG42) and homozygous (CAG42) animals were subjected to fragment analysis and their size was determined (Figure 20C). All products had the exact same length. These data indicate that the knock-in mice have a repeat of 42 CAGs that is stably transmitted.

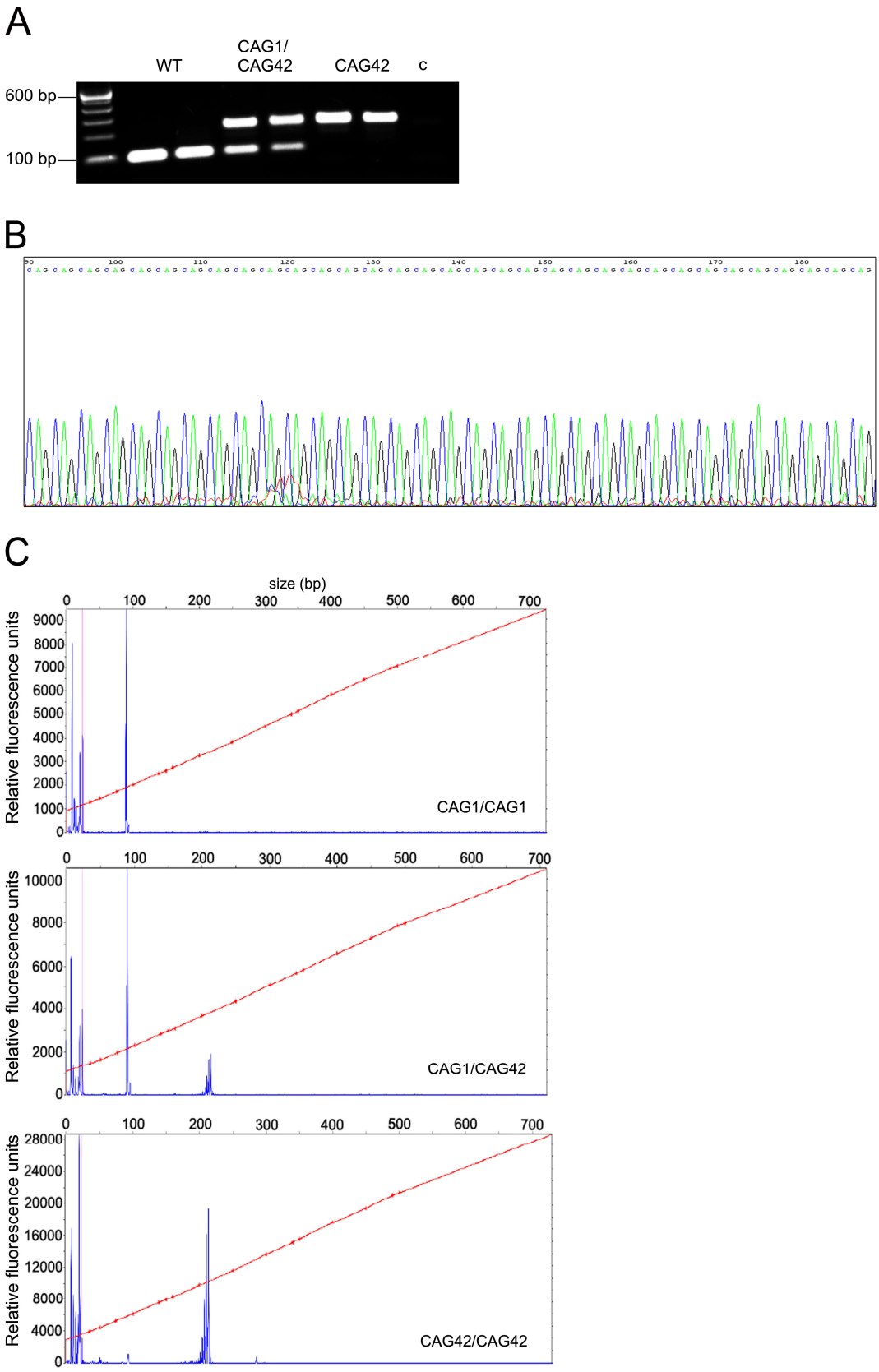

Figure 20. The repeat bears 42 CAGs and its paternal and maternal transmission is stable. (A) A CAG repeat flanking PCR with one FAM-labelled primer was performed. As expected, wild-type (WT) animals showed one product at 94 bp, whereas heterozygotes (CAG1/CAG42) showed an additional larger product at 217 bp. In homozygous mutant mice (CAG42) only the larger product was detected. c: negative control. (B) Sequencing chromatogram of a part of the CAG repeat within the *Atxn2* gene of the knock-in mice. (C) The exact PCR product size was confirmed by fragment length analysis. The peak in the WT sample represents the 94 bp product, while the 217bp-peak appeared in CAG42 animals. Both peaks were detectable in CAG1/CAG42 mice.

3.1.3 The expanded *Atxn2* mRNA is stable and its expression levels elevated in cortex

In order to verify that the homologous recombination event does not interfere with *Atxn2* expression and to assess the stability of the expanded transcript, quantitative real-time RT-PCR (qPCR) was initially performed in cerebral cortex tissue. The *Atxn2* transcript in cortex was apparent. Furthermore, at postnatal day 1, the *Atxn2* mRNA was significantly upregulated to 1.48-fold (p = 0.031) and at 6 weeks to 1.42-fold (p = 0.044) in CAG42 mice. In the cortex, the *Atxn2* transcript in CAG1/CAG42 mice was not altered at both time points measured (Figure 21, Table 22). These data indicate, that the selection marker remaining in the *Atxn2* genomic locus does not impair *Atxn2* transcription and that the presence of a CAG42 repeat in the *Atxn2* transcript does not lead to its instability.

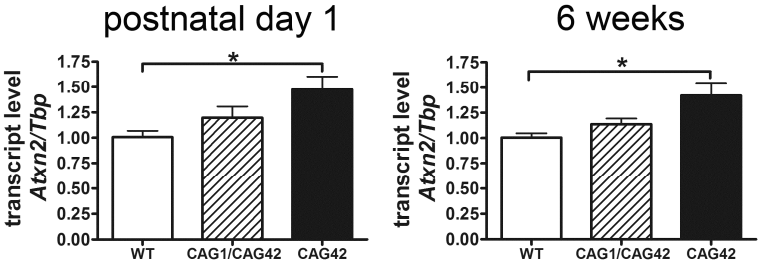

Figure 21. The *Atxn2* mRNA is stable and its expression elevated in the cortex in CAG42 mice. The stability of *Atxn2* mRNA was confirmed in cortex. In addition, a significant upregulation of the *Atxn2* transcript was detected in postnatal day 1 and 6 weeks old cortex (n = 3-7 mice/genotype/tissue in 2 independent technical replicates).

3.1.4 Reduced soluble protein levels of expanded ATXN2 in the young cortex

The investigation of the stability and steady-state levels of expanded ATXN2 protein in the CAG42 mice was done in proteins from tissue soluble in RIPA buffer. Expanded ATXN2 with 42 glutamines displayed slowed electrophoretic mobility in comparison to wild-type ATXN2 (Figure 22). In the cortex of 6 weeks old mice a significant reduction of ATXN2 was detectable in CAG42 mice in comparison to WT (0.58-fold, p = 0.0053) and to CAG1/CAG42 (0.58-fold, p = 0.024) mice. Furthermore, in CAG1/CAG42 mice, displaying both, the non-expanded and the expanded ATXN2, the immunoreactivity of total ATXN2 amounts were equal to WT, while the expanded ATXN2 was reduced in comparison to the WT lane of about 25%, however not significantly (Figure 22). Thus, ATXN2 protein with 42 glutamines is stable. The ATXN2 expression levels are reduced in the cortex of CAG42 and CAG1/CAG42 mice, while the *Atxn2* mRNA transcript levels are elevated.

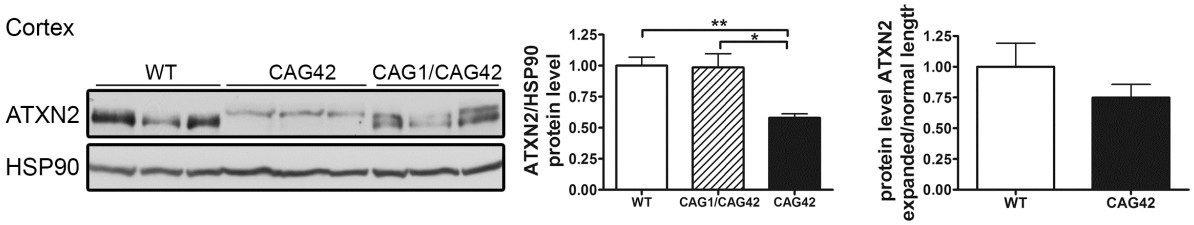

Figure 22. The expanded ATXN2 protein is stable and its expression reduced in cortex tissue of CAG42 and CAG1/CAG42 mice. Western Blot analysis was performed to assess steady-state protein levels in the mice. (M = marker; cortex: n = 3 in one technical replicate)

3.1.5 Phenotype assessment of the *Atxn2*-CAG42-knock-in mice

To obtain a very accurate overview of the phenotype of the mice, the genotype and sex segregation was calculated, the body weight and survival was recorded and several neurological tests were performed in WT, CAG1/CAG42 and CAG42 mice.

3.1.5.1 No aberrant distribution of genotypes or sex

To investigate whether expanded Ataxin-2 leads to an increased lethality *in utero*, segregation analysis was performed. The genotype of 42 litters from matings of heterozygous mice was examined. Both CAG1/CAG42 and CAG42 mice were viable. Out of 338 offspring, 163 were male and 175 were female and thus a deviation from the expected sex ratio of 50% versus 50% was not observed. Furthermore, no aberration from the usual genotype distribution (25% WT versus 50% heterozygous versus 25% homozygous) was observed, neither in males nor females (Table 16). These data indicate that expanded Ataxin-2 has no consequence on either the sex or genotype distribution.

Table 16. Normal distribution of gender and genotypes from heterozygous matings.

Genotype	WT	CAG1/CAG42	CAG42	Total	p-value
Total	87	171	80	338	0.845
Male	46	82	35	163	0.475
Female	41	89	45	175	0.890

3.1.5.2 CAG42 mice have a reduced body weight throughout their lifespan

As changes in body weight frequently accompany neurodegenerative diseases and in particular SCA2 (Abdel-Aleem & Zaki 2008, Auburger 2012), the mice were weighed at regular intervals. Already at the age of 10 days, CAG42 mice had a significant body weight

reduction of 19.27% compared to wild-type littermates (p = 0.0002); a reduction of 13 - 22% remained significant throughout their lifespan up to 21 months (20 days: p = 0.0005; 6 weeks: p = 0.0015; 3 months: p = 0.0025; 6 months: p = 0.0196; 12 months: p = 0.0141; 18 months: p = 0.0265; 21 months: p = 0.0496). Only at the age of 24 months, the body weight between CAG42 and WT was not altered significantly, probably due to the low number of animals remaining alive and available for analyses. Still, the weight gain was similar in CAG42 and WT mice. The body weight of CAG1/CAG42 was consistently, but non-significantly less than that of WT (Figure 23). Thus, CAG42 mice are characterized by a permanent body weight reduction, while CAG1/CAG42 mice appear normal.

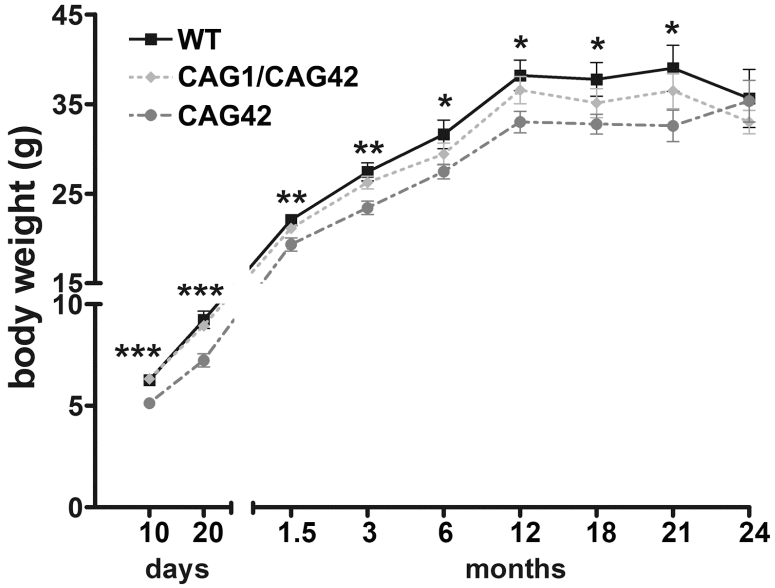

Figure 23. A permanent body weight reduction is apparent in CAG42 mice up to 21 months. Homozygous CAG42 mice had a reduced body weight by birth up to the age of 21 months, while no change was observed at 24 months in comparison to wild-type mice. Heterozygous CAG1/CAG42 mice had a consistent but non-significant body weight reduction (until 21 months: n ≥ 14 per genotype, 24 months: n ≥ 6).

3.1.5.3 CAG42 mice change from excellent motor coordination at young age to a late-onset deficit

The knock-in mice did not show overt ataxic behaviour during cage life. To assess the development of a cerebellar phenotype in more detail, animals were placed on an accelerating rotarod apparatus and their latency to fall was recorded during a one-time 5 minute trial. To maintain balance, this task requires a careful placement of steps and the constant velocity adaptation makes the task more complex (Buitrago *et al.* 2004). At 6 weeks, the first time point tested, the latency to fall was 1.2-fold increased (p = 0.0096) in CAG42 mice in comparison to their wild-type littermates. CAG1/CAG42 mice performed

equally well as wild-types. At 3, 6 and 12 months, both CAG42 and CAG1/CAG42 showed no difference to wild-types in their performance. At the age of 18 months the CAG42 mice showed a significantly shorter latency to fall (0.68-fold, $p = 0.0296$) from the rotarod, while at 21 months a trend was visible (0.65-fold reduction, $p = 0.062$). At 24 months no change was observed, probably due to the low number of animals remaining alive and available for analyses. Thus, CAG42 mice at early adult age performed better than WT, but at old age considerably worse in this cerebellar test paradigm. CAG1/CAG42 mice still performed similarly well as the WT mice (Figure 24).

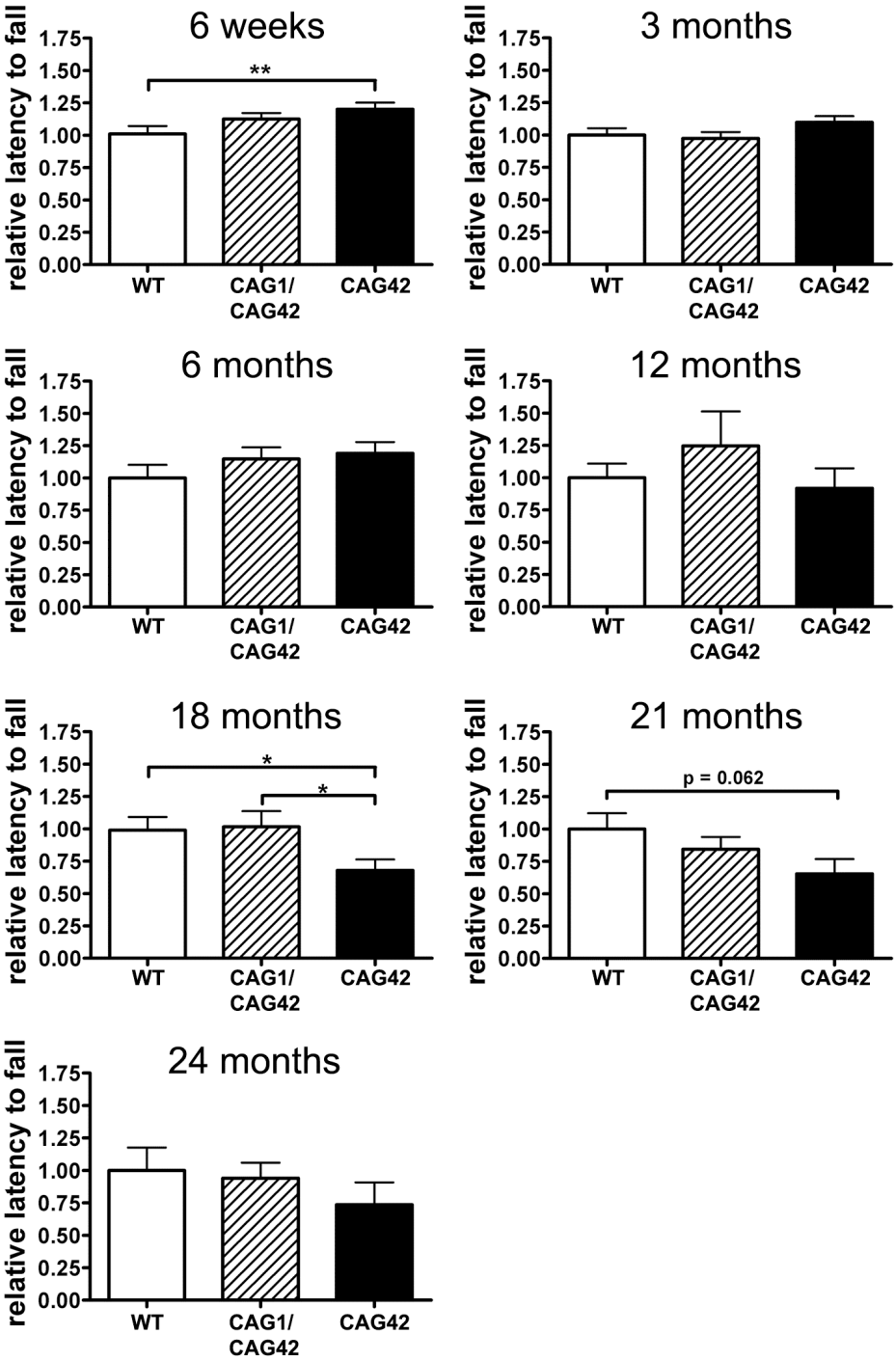

Figure 24. Late-onset deficit in a cerebellar test paradigm. Motor coordination was tested on an accelerating rota rod apparatus. Initial locomotor hyperactivity at 6 weeks of age in the CAG42 mice was replaced by normal activity between 3 and 12 months. At 18 and 21 months age, CAG42 mice performed worse on the rota rod, while at 24 months the change was no longer significant (until 18 months: n ≥ 14 per genotype, 21 months: n ≥ 6 per genotype, 24 months: n ≥ 4 per genotype).

3.1.5.4 Motor skill learning is not impaired

The rota rod test can also be used to study the long-term motor skill learning that develops during training in consecutive days (Buitrago *et al*. 2004). Thus, mice were placed on the rod for 4 trials per day on 4 consecutive days. In all trials, at the age of 6 and 12 months CAG42 and CAG1/CAG42 mice performed similarly well as their wild-type littermates, indicating that motor skill learning is not impaired in adult life. WT, CAG1/CAG42 and CAG42 mice improved their motor skill learning, as their latencies to fall increased constantly during the first trial day. At the age of 18 months, the motor performance was significantly reduced at the first and second day in CAG42 mice, while CAG1/CAG42 mice performed still similar to WT, indicating the cerebellar defect. At the age of 21 and 24 months, the CAG42 mice performed consistently, though not significantly, worse on the rota rod, probably due to the low number of animals remaining alive for analyses - except for the last 6 trials at 21 months where significance was reached (Figure 25, Table 17). Thus, CAG42 mice still improved their motor skills at 18 months age; however, they only caught up with their WT littermates after two days of training, most probably due to their cerebellar deficit that manifests at this age. At the age of 21 months, when only few mice were available and mice behaved very heterogeneously, a significant deficit was not detectable at first. However, after a two day training period, where wild-type animals improved their motor behaviour and CAG42 suffered from their cerebellar deficit, a significantly worse performance was measured during the last two test days. Thus, the motor skill learning of CAG42 and CAG1/CAG42 mice is not impaired, while the late-onset deficit in this cerebellar task starting at 18 months leads to a constantly reduced motor performance up to the age of 24 months during the motor learning task.

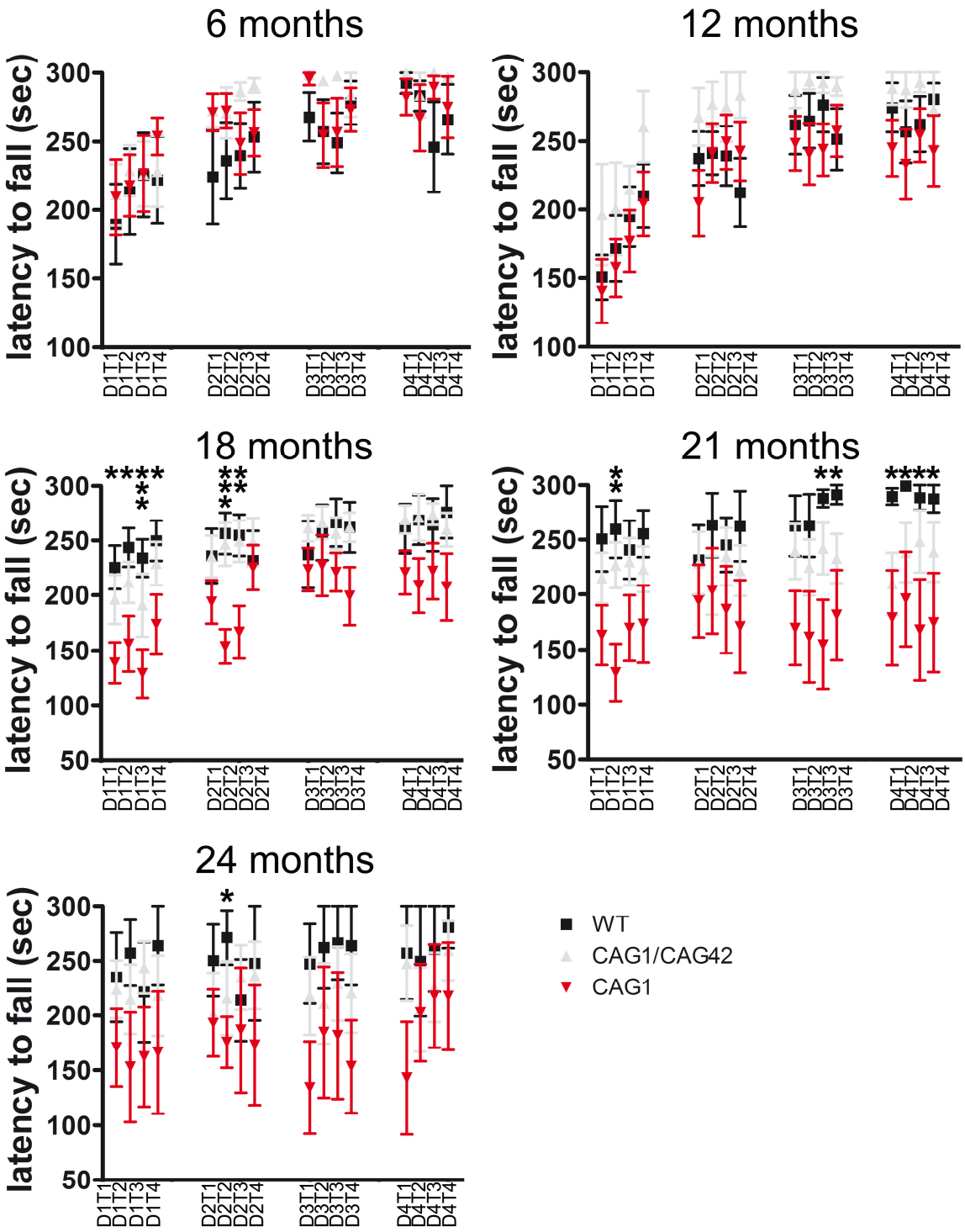

Figure 25. Motor skill learning of CAG42 mice is not impaired. Latencies to fall were recorded on 4 trials per day over 4 consecutive days. CAG42 and CAG1/CAG42 mice learned the motor performance task similarly well as wild-type mice up to the age of 12 months. 18 months old CAG42 showed impaired motor behaviour and learning, while at 21 months, mice are significantly impaired on the last 6 trials. 24 months old CAG42 mice show consistently, but not significantly reduced latencies to fall. P-values are indicated in Table 17 (6 months: n ≥ 8 mice/genotype, 12 months: n ≥ 6 mice/genotype, 18 months: n ≥ 11 mice/genotype, 21 months: n ≥ 6, 24 months: n ≥ 4; D = day, T = trial; asterisks mark significant changes between WT and CAG42 mice).

Table 17. Fold-changes compared to WT mice for trials with a statistical trend or a significant result in the motor learning experiment. Significant results are marked with asterisks, "—" indicates non-significant results.

	Trial 1	Trial 2	Trial 3	Trial 4
6 months day 1	—	—	—	—
6 months day 2	—	—	CAG1/CAG42: 1.19-fold*	—
6 months day 3	CAG1/CAG42: 1.11-fold*	—	CAG1/CAG42: 1.2-fold*	—
6 months day 4	—	—	CAG1/CAG42: 1.22-fold*	—
18 months day 1	CAG42: 0.68-fold*	CAG42: 0.66-fold*	CAG42: 0.56-fold***	CAG42: 0.71-fold*
18 months day 2	—	CAG42: 0.61-fold***	CAG42: 0.66-fold**	—
18 months day 3	—	—	—	—
18 months day 4	—	—	—	—
21 months day 1	CAG42: 0.65-fold	CAG42: 0.5-fold**	—	CAG42: 0.68-fold
21 months day 2	—	—	—	—
21 months day 3	CAG42: 0.64-fold	CAG42: 0.61-fold	CAG42: 0.54-fold*	CAG42: 0.62-fold
21 months day 4	CAG42: 0.62-fold*	CAG42: 0.66-fold*	CAG42: 0.58-fold*	CAG42: 0.61-fold*
24 months day 1	—	—	—	—
24 months day 2	—	CAG42: 0.65-fold*	—	—
24 months day 3	CAG42: 0.58-fold	—	—	CAG42: 0.58-fold
24 months day 4	—	—	—	—

3.1.5.5 No behavioural impairment of CAG42 mice in the grip strength, footprint, open field and inverted screen tests

Grip strength was measured to assess muscle strength of the mice, as an indicator if motor neuron pathology and paralysis occurred. For this purpose the peak force of the fore-limbs in 10 trials per mouse were recorded on an electronic grip strength meter. CAG42 and CAG1/CAG42 mice were as strong as wild-type mice at 18 months of age, a time point where the cerebellar pathology is already apparent. Also, at 21 and 24 months of age, CAG42 and CAG1/CAG42 mice performed equally well as WT mice (Figure 26).

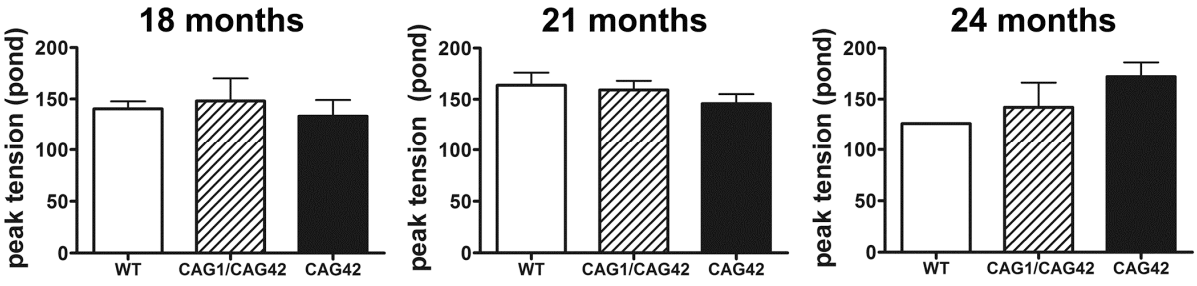

Figure 26. The grip strength is not altered in CAG42 and CAG1/CAG42 mice. Grip strength was assessed on a grip strength meter in 18, 21 and 24 months old mice (18 and 21 months: n ≥ 5 mice/genotype, 24 months: n ≥ 1 mouse/genotype).

In addition, footprint analyses were performed to analyse whether gait abnormalities accompany the motor coordination deficit. The step length, gait width, step alternation and the movement linearity were calculated by analysing the footprints of the hind limbs. No consistent differences between WT and CAG1/CAG42 or CAG42 mice up to 24 months were apparent (Figure 27, Table 18).

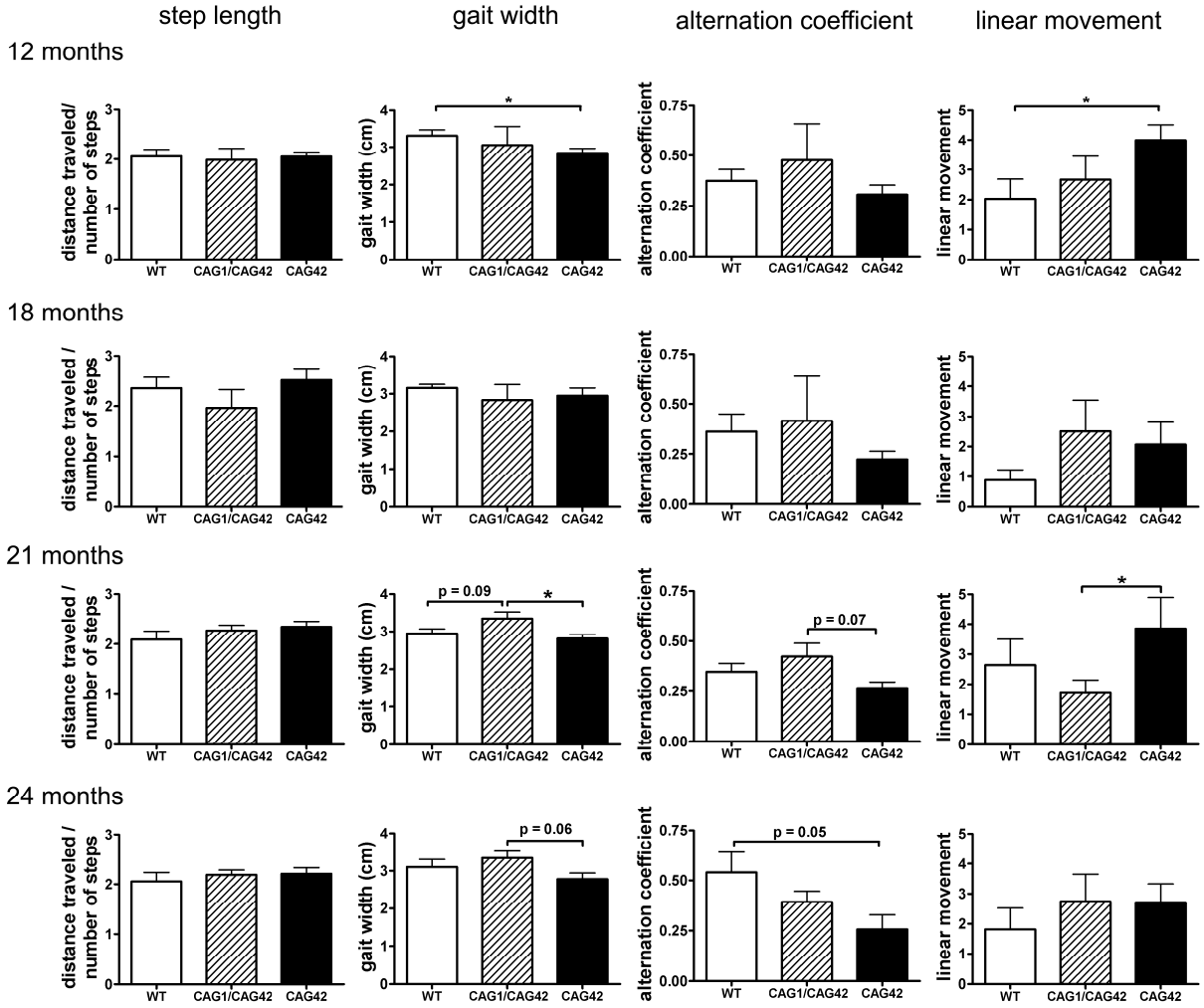

Figure 27. Footprint analysis did not reveal consistent alterations in CAG42 or CAG1/CAG42 mice in comparison to WT littermates up to 24 months. P-values are indicated in Table 18 (n ≥ 3 animals/genotype).

Table 18. Fold-changes for trials with a statistical trend or a significant results in the footprint analysis. Significant results are marked with asterisks. "—" indicates unchanged measurements.

	Step length	Gait width	Alternation coefficient	Linear movement
12 months	—	WT-CAG42: 0.86-fold*	—	WT-CAG42: 1.97-fold*
18 months	—	—	—	—
21 months	—	WT-CAG1/CAG42: 1.14-fold CAG1/CAG42-CAG42: 0.84-fold*	—	CAG1/CAG42-CAG42: 2.24-fold
24 months	—	CAG1/CAG42-CAG42: 0.83-fold	WT-CAG42: 0.48-fold	—

As ATXN2 triplet repeat expansions in human can also lead to Parkinson's syndrome with impaired spontaneous movement (Charles *et al*. 2007, Kim *et al*. 2007, Payami *et al*. 2003, Shan *et al*. 2001), the motor activity of mice in an open field was recorded throughout their lifespan. Neither horizontal/vertical activity, total distance, movement time, number of movements, number of stereotypy counts, margin/centre distance nor margin/centre time were consistently altered (Table 19).

Table 19. The activity during the open field test in CAG42 mice is not altered consistently during their lifespan. Changes between WT and CAG42 mice when manifested as a trend or a significant result are indicated. Significant results are indicated with asterisks (n ≥ 5 animals/genotype).

	HACTV	TOTDIST	MOVNO	MOVTIME	RESTIME	VACTV	VMOVNO	VTIME	STRCNT	STRNO	STRTIME	MRGDIST	MRGTIME	CTRDIST	CTRTIME	Urine	Faeces
6 weeks	—	—	—	—	—	—	—	—	—	—	—	—	—	—	—	—	—
3 months	—	—	—	—	—	—	—	—	—	—	—	—	—	—	—	—	—
6 months	—	—	—	—	—	—	—	—	—	—	—	—	—	—	—	—	—
12 months	—	—	—	—	—	—	—	—	—	—	—	—	—	—	—	—	—
18 months	—	—	—	—	—	—	—	—	—	—	—	—	—	—	—	—	—
21 months	—	—	—	—	—	10-fold	4.6-fold*	9.5-fold*	—	—	—	—	—	—	—	—	—
24 months	—	—	—	—	—	—	—	—	—	—	—	—	—	—	—	—	—

To test motor strength behaviour the inverted screen test was used and the ability to hang from an inverted screen was assessed. Mice were placed at 18 and 21 months on the inverted screen apparatus, that was in turn inverted for 180° and the latency to fall was recorded. No significant changes were observed in CAG42 and CAG1/CAG42 mice in comparison to wild-type littermates.

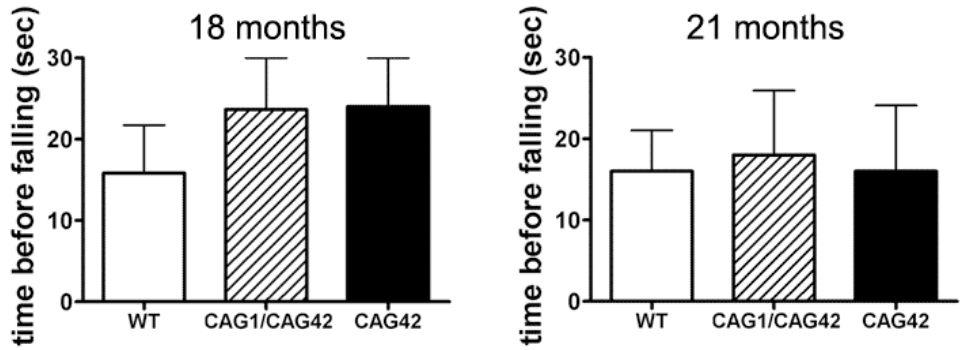

Figure 28. Motor strength is not impaired in CAG42 and CAG1/CAG42 mice. Motor strength was measured with an inverted screen apparatus and the latency to fall was recorded for each mouse. At both time points tested, 18 and 21 months, no impairment was detectable. (18 and 21 months: n ≥ 3).

3.1.5.6 The survival rate is not altered in CAG42 mice

The deletion of a gene or a mutation within a gene might lead to an altered, usually reduced, lifespan. Thus, mice were aged until 24 months and the date of natural death was documented for all mice up to this time point. The survival analysis showed no altered survival rates in CAG42 or CAG1/CAG42 mice up to the age of 24 months.

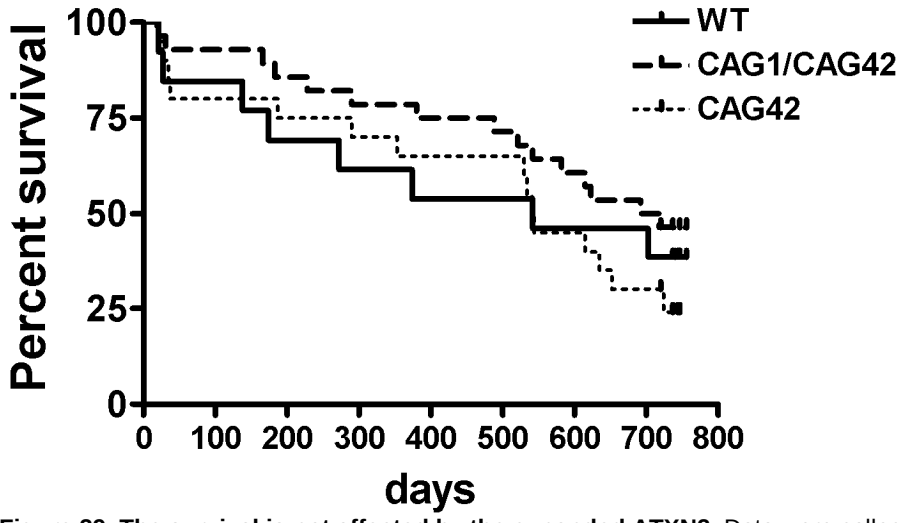

Figure 29. The survival is not affected by the expanded ATXN2. Data were collected of all animals found dead till 24 months of age, when all animals were sacrificed and the survival rates determined (n ≥ 13 mice/genotype).

In summary CAG42 mice are characterized by a permanent body weight reduction and a late-onset motor deficit specifically in a cerebellar test paradigm. Other behavioural abnormalities or apparent motor impairments were not detected up to 24 months of age. CAG1/CAG42 mice showed no behavioural abnormalities in comparison to wild-type mice.

3.1.6 Expanded and wild-type ATXN2 co-sediment with the ER

A previous study documented that wild-type ATXN2 co-sediments with the cytosolic and light/ER membrane fraction and is specifically absent from the heavy membranes/mitochondrial pellet in mouse brain (Nonis *et al*. 2008). In order to examine in which cytosolic fractions expanded ATXN2 is localized, brain homogenates of 6 months old heterozygous animals was fractionated with differential velocity fractionation (Figure 30A). The cytosolic marker EEA1 was detectable in the cytosolic fraction and absent from the heavy and light membrane fraction, indicating that these fractions were free of cytosolic contamination. Calnexin, a marker for light fractions containing the ER membranes was detectable in all but the cytosolic fraction, indicating that it specifically co-sediments with the light membranes. ATXN2 was specifically absent from the heavy membranes. It co-sedimented with the cytosolic fraction and the light membranes, whereas in the latter its immunoreactivity was enhanced (Figure 30B). These data indicate, that wild-type and expanded ATXN2 associate mainly with the ER membranes, but exist also in the cytosol. Wild-type and expanded ATXN2 are specifically absent from the heavy membranes/mitochondrial pellet. These data indicate that the expansion does not alter the subcellular ATXN2 localization within the brain.

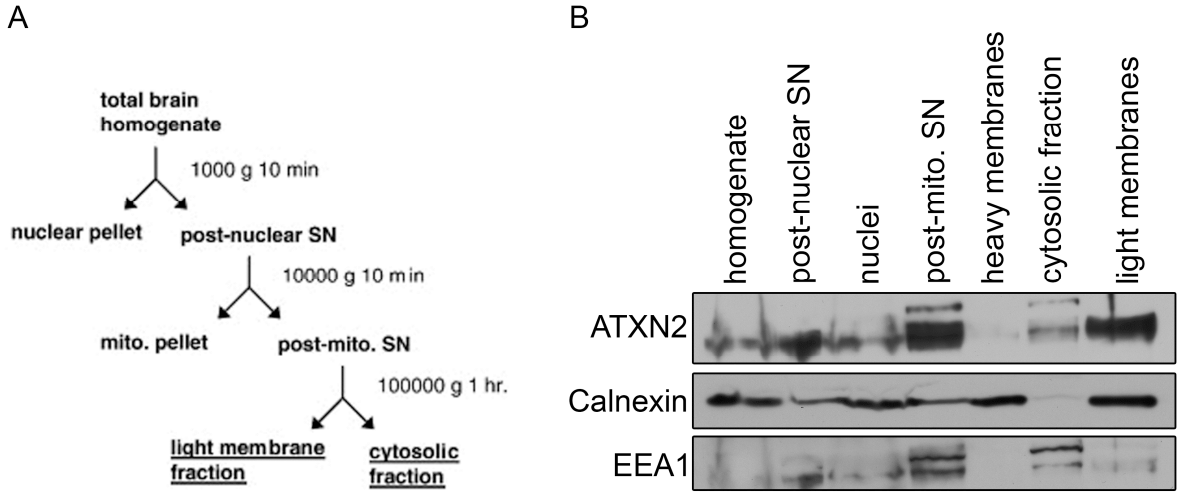

Figure 30. Expanded and wild-type ATXN2 co-sediment with the ER. (A) Differential velocity centrifugation was applied to fractionate brain homogenates (Nonis *et al*. 2008) of heterozygous 6 months old mice. (B) Fractions were separated with Western blot and analyzed for ATXN2 and Calnexin and EEA1 as light membrane and cytosolic subcellular marker, respectively. ATXN2 co-sedimented with light/ER membranes rather than heavy membranes/mitochondria.

3.1.7 Characterization and evaluation of CAG42-MEFs as potential disease model

The use of patient brain material for investigations is problematic because only post-mortem brain is available, where RNAs and proteins have been rapidly degraded. Also, and especially for SCA2, its low abundance makes studies with human brain tissue practically impossible for routine use. A way to obtain material from living patients is the recruitment of skin biopsies that can be cultivated as fibroblast cultures. To have an equivalent in the mouse, fibroblasts are best extracted from embryos at around embryonic day 17. With this tool, mouse and human tissue can relatively easily be investigated and compared; the application of drugs is simplified relative to drug administration throughout a whole mouse organism. Mouse embryonic fibroblasts (MEFs) were generated from the *Atxn2*-CAG-42-knock-in mice to characterize and evaluate them as model system.

3.1.7.1 The *Atxn2* mRNA levels are stable in CAG42-MEFs

The *Atxn2* mRNA was shown before to be stable in cortex tissue (section 3.1.3) of CAG42 mice. As ATXN2 is ubiquitously expressed in mice, the knock-in approach should also guarantee an *Atxn2* expression throughout non-neuronal tissue. For this purpose *Atxn2* transcript levels were assessed with qPCR in MEFs and indeed, the *Atxn2* transcript was detectable (Figure 31). As in brain tissue, the selection marker remaining in the *Atxn2* genomic locus does not impair *Atxn2* transcription and the presence of a CAG42 repeat in

the *Atxn2* transcript does not lead to its instability on mRNA level in the non-neuronal CAG42-MEFs.

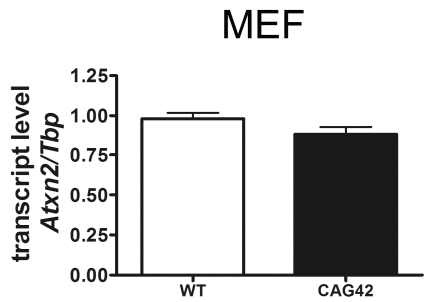

Figure 31. The *Atxn2* mRNA is stable in MEFs. The stability of *Atxn2* mRNA was confirmed in MEFs (n = 3-7 mice/genotype/tissue in 2 independent technical replicates).

3.1.7.2 Soluble ATXN2 is stable and PABPC1 reduced in MEFs

To evaluate the protein expression levels of ATXN2 and its interactor PABPC1 (for further details see 3.2.3) in mouse embryonic fibroblasts (MEFs), proteins were extracted with RIPA buffer. A slight but not significant reduction in ATXN2 expression levels was detected (Figure 32), while the interactor PABPC1 was significantly reduced (0.64-fold, p = 0.019) in comparison to wild-type littermates. Thus, ATXN2 with 42 glutamines is stable in MEFs and, as *Atxn2* mRNA levels, slightly reduced. Despite unaltered *Pabpc1* mRNA levels (Table 22), the PABPC1 protein expression is reduced in CAG42-MEFs.

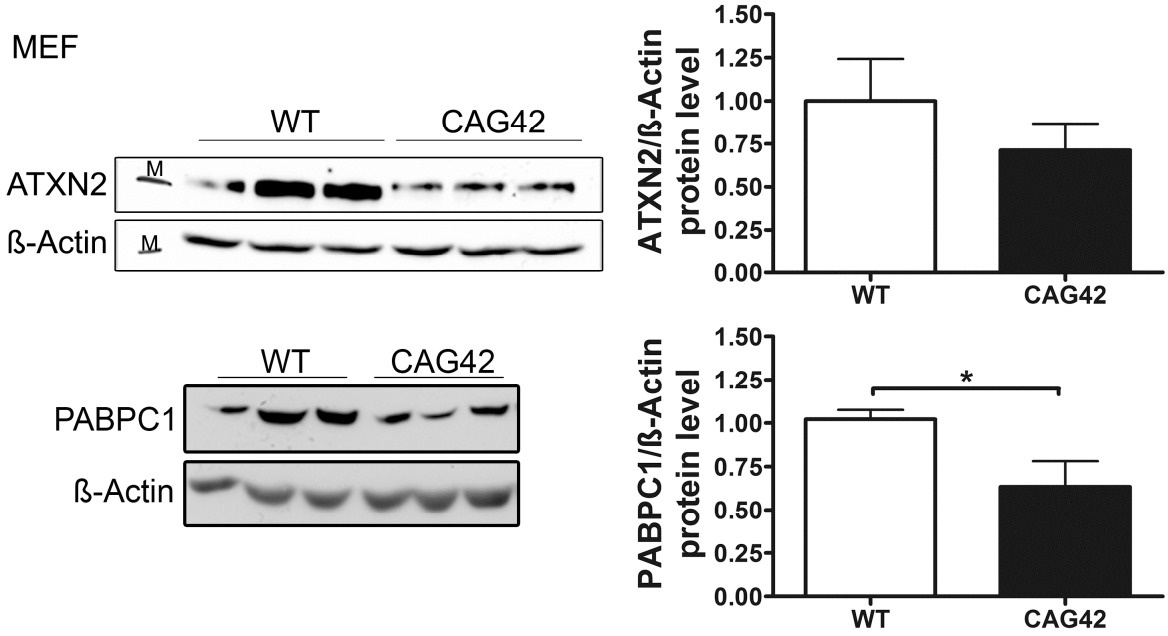

Figure 32. The expanded ATXN2 protein is stable in MEFs. Western Blot analysis was performed to assess steady-state protein levels in the mice. While ATXN2 levels were consistently but non-significantly reduced, PAPBC1 protein expression was significantly reduced (M = marker; n = 5-7 in 3 independent technical replicates).

3.1.7.3 Normal cellular ER stress response in MEFs

Previous data in MEFs from *Atxn2*-knock-out mice indicated that the cellular response to ER stress was impaired by ATXN2 deficiency (Lastres-Becker, in preparation). ER stress was induced through Tunicamycin which blocks the formation of the N-glycosidic linkages of proteins in the ER and thus results in the induction of ER chaperones as e.g. BiP which is one of the best characterized ER chaperones (Li & Lee 2006). The loss of ATXN2 resulted in impaired induction of BiP protein expression, while basal BiP levels were unaffected. In order to elucidate which impact the ATXN2 expansion in CAG42-MEFs has on the ER stress response, BiP induction after 16 h Tunicamycin treatment was determined. BiP levels increased in both, WT and CAG42 mice similarly (Figure 33). The data indicate that the stress response upon the ER stressor Tunicamycin in CAG42-MEFs is comparable to that of WT-MEFs and thus not influenced by the CAG42 expansion.

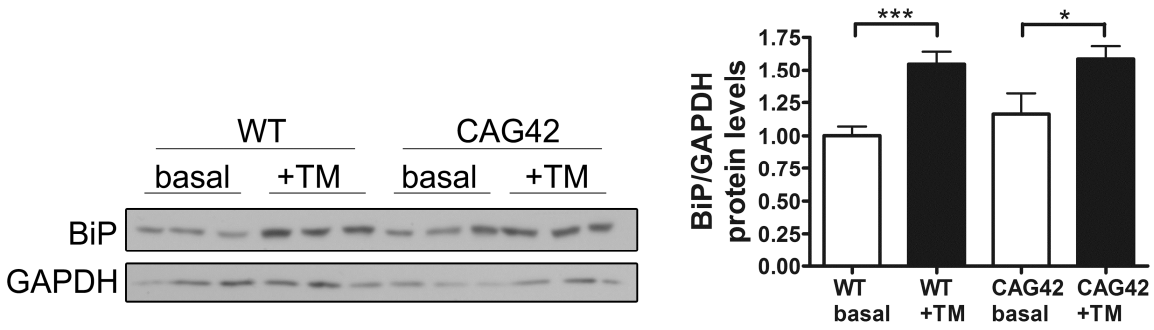

Figure 33. BiP induction after Tunicamycin treatment. MEFs were treated with Tunicamycin (TM), and the BiP protein levels were measured. No difference in ER stress response from CAG42-MEFs in comparison to wild-type MEFs was detectable (n = 7 MEF-lines/genotype in 3 independent technical replicates).

3.1.7.4 Expanded ATXN2 does not influence S6-phosphorylation status

The absence of ATXN2 in MEFs increased the phosphorylation of ribosomal S6, a key regulator of translation initiation (Lastres-Becker, in preparation). The regulation of mRNAs containing an oligopyrimidine tract in their 5' untranslated region (5' TOP-mRNAs) is closely correlated to S6-phosphorylation (Meyuhas & Dreazen 2009). To test whether the reduced ATXN2 and PABPC1 levels have an impact on the phosphorylation of S6 in CAG42-MEFs, its status after 24h starvation at basal level or subsequent insulin treatment for 10 minutes was investigated. Phospho-S6 levels of CAG42-MEFs were equal to those of WT-MEFs at basal conditions. After the insulin induction, a significant elevation of the S6-phosphorylation was observed in both, WT- and CAG42-MEFs; however no difference of phospho-S6 levels

after insulin was observed between the two groups (Figure 34). Thus, the phospho-S6 levels of CAG42-MEFs are induced to similar levels and not altered compared to WT-MEFs.

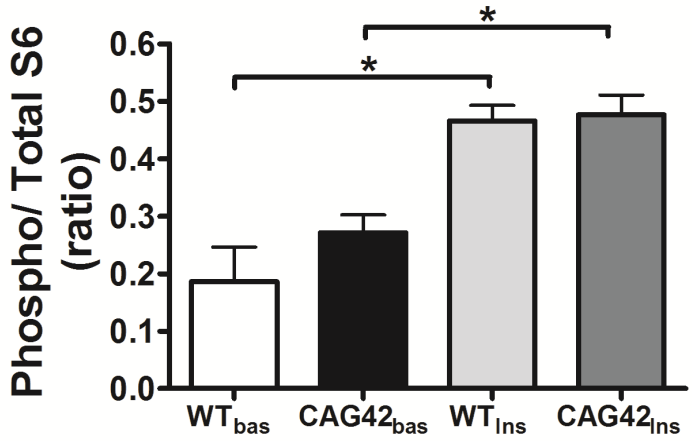

Figure 34. The S6-phosphorylation status after starvation and insulin treatment is similarly elevated in CAG42-MEFs as in WT-MEFs. (n =3 MEF-lines/genotype in one technical replicate).

3.1.7.5 Normal growth behaviour of CAG42-MEFs

MEFs were cultivated up to passage 15 and the cell number calculated at each passage to analyse the population doubling levels. CAG42-MEFs exhibited similar population doubling times than MEFs from wild-type littermates (Figure 35). These data indicate that the polyQ expansion does not influence the growth behaviour of MEFs.

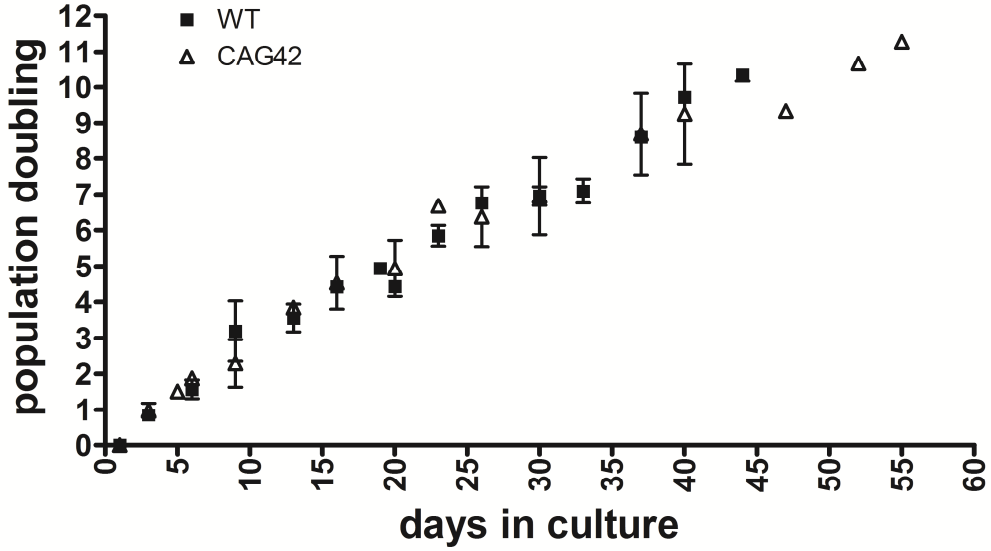

Figure 35. CAG42-MEFs show normal growth behaviour. MEFs were cultivated up to passage 15 and their population doubling (PD) determined (n = 3 MEF-lines/genotype).

3.2 The *Atxn2*-CAG42-knock-in mouse to evaluate disease mechanisms of SCA2

3.2.1 Microarray transcriptome profiling at medium and advanced age documents selective induction of *Fbxw8* in old cerebellum

Attempting a survey of the alterations in mRNA processing underlying this pathology, cerebellum, brainstem and liver tissue from presymptomatic 6 months and symptomatic 18 months old WT and CAG42 mice (3 versus 3 animals per young group, 4 versus 4 per old group) were used to perform Affymetrix microarray transcriptome studies at a genome-wide level. The cerebellum represented the most vulnerable brain region in SCA2 and the brainstem is also involved in SCA2, but to a lesser extent. The reduced body weight of the CAG42 mice and increased body weight of the *Atxn2*-knock-out mouse (Lastres-Becker *et al*. 2008a) indicate that altered Ataxin-2 levels might mediate the liver metabolism. At the age of 6 months, statistical analysis with correction for multiple testing after Benjamini-Hochberg demonstrated that no mRNAs showed dysregulated levels with significance in cerebellum and brainstem, while only one gene was differentially regulated in liver. This gene *Cyp4a14*, is represented only by one oligonucleotide spot on the microarray (1423257_at, p = 0.027). The Cytochrome P-450 enzyme family has a known role in cholesterol biosynthesis and the Cyp4a14 induction is a known response of liver tissue to altered fat content (Fisher *et al.* 2008). Since fatty liver is a feature already documented and molecularly investigated in ATXN2-KO mice (Lastres-Becker *et al*. 2008a), this finding was not studied further. At the age of 18 months, altered regulation was significant after Benjamini-Hochberg correction for 20 genes in cerebellum, 14 in brainstem and 30 in liver (see appendix for complete list). False positives were excluded when oligonucleotides from one spot were unspecific and their target was not found after BLAST search. Only annotated genes were considered for further analyses. Furthermore, only targets that were recognized by oligonucleotides within their exons were chosen. Due to the relatively small number of regulated genes, at least one of the following criteria had to match for the selection of single genes for further validation by qPCR:

- Recognition by more than one spot
- Consistent regulation in all three tissues or in brain tissue into the same direction
- Strongest up- or downregulation in a specific tissue.

Overall ten genes were differentially regulated in CAG42 mice at the age of 18 months in comparison to age-matched wild-type littermates according to these criteria (Table 20). Among those, 5 genes were recognized by more than one spot and only *Fbxw8* matched two

of the selection-criteria: it was recognized by two spots and showed the strongest upregulation in the cerebellum being therefore the most promising target for further analyses. One notable finding was that 3 out of these 10 genes are located in close proximity to the *Atxn2* gene on chromosome 5 F (position 122,162-122,265 kbp, Table 20). One possible explanation might be that the remaining FRT- and *loxP* sites from the targeting vector on the knock-in allele disrupted regulatory sequences for those genes. Also, notions have been discussed that the abnormal DNA structure of a CAG expansion could exert a progressive influence on chromatin structure (Everett & Wood 2004). Finally, it is possible that the genes that surround the *Atxn2* locus are interacting in a common pathway and that feedback-mechanisms regulate their expression in dependence on ATXN2 function.

Table 20. Differentially regulated mRNAs identified by Microarray analysis in CAG42 mice at the age of 18 months in cerebellum, brainstem and liver. Down- and upregulated genes are highlighted in green and red, respectively, ex = exon (n = 4 mice/genotype).

Symbol	Name	Genomic locus	Position (kbp)	Distance to *Atxn2* (kbp)	Spot ID	Oligo-nucleotide binding sites	Cerebellum		Brainstem		Liver	
							fold change	p-value	fold change	p-value	fold change	p-value
Acat1	acetyl-Coenzyme A acetyltransferase 1	9 C-D	53,389-53,418	—	1451271_PM_a_at 1424183_PM_at 1424182_PM_at	Ex 9, 10, 12	—		—		**-1.42** **-1.50** **-1.58**	0.0101 0.0071 0.0052
Adam1a	a disintegrin and metallo-peptidase domain 1a	5 F	121,969-121,972	~ 190	1443378_PM_s_at 1427790_PM_at	Ex 1	**-1.77** **-1.89**	0.0009 0.0071	**-1.47** —	0.0009 —	—	
Ankrd33b	ankyrin repeat domain 33B	15 B	31,221-31,298	—	1453287_PM_at	Ex 2	—		—		**-4.17**	0.0289
Bri3bp	Bri3 binding protein	5 F	125,922-125,941	~ 3657	1438198_PM_at	Ex 3	**1.34**	0.0289	**1.33**	0.0289	—	
Cthrc1	collagen triple helix repeat containing 1	15 C	38,908-38,919	—	1452968_PM_at	Ex 3, 4	—		**-3.68**	0.0480	—	
Fbxw8	F-box and WD-40 domain protein 8	5 F	118,515-118,606	~ 3556	1426944_PM_at 1436732_PM_s_at	Ex 11	**2.55** **2.51**	0.0077 0.0095	—		—	
Gjc2	gap junction protein gamma 2	11 B	58,989-58,997	—	1450483_PM_at	Ex 2	—		**1.93**	0.0250	—	
Ifi27l1	interferon, alpha-inducible protein 27 like 1	12 E	104,672-104,679	—	1452956_PM_a_at 1454757_PM_s_at	Ex 3,6,7	—		—		**3.27** **3.20**	0.0273 0.0213
Lgals1	lectin, galactose binding, soluble 1	15 E	78,757-78,761	—	1419573_PM_a_at 1455439_PM_a_at	Ex 1,2,3,4	—		—		**2.27** **2.14**	0.0165 0.0459
Nlrp12	NLR family, pyrin domain containing 12	7 A	3,222-3,250	—	1440921_PM_at	Ex 10	—		—		**3.86**	0.0131

3.2.1.1 qPCR validation confirms *Fbxw8* as upregulated gene in the cerebellum

Upon independent validation of the Microarray analysis by qPCR, the dysregulation of *Acat1*, *Bri3bp*, *Cthrc1, Gjc2*, *Ifi27l1*, *Lgals1 and Nlrp12* could not be reproduced, while a significant downregulation of *Adam1a* in cerebellum to 0.71-fold (p = 0.0007) and brainstem to 0.73-fold (p = 0.001), *Ankrd33b* in liver (0.49-fold, p = 0.027) as well as a significant upregulation of *Fbxw8* to 2.38-fold (p < 0.0001) in cerebellum were confirmed (Table 21). *Adam1a* encodes a disintegrin/metalloprotease and has an established role for spermatogenesis and fertilization (Nishimura *et al.* 2004). Thus, its dysregulation might correlate to the reduced fertility of ATXN2-KO mice (Lastres-Becker *et al*. 2008a). As indicated in Table 20, *Ankrd33b*, an ankyrin repeat domain carrying protein, was recognized by only one spot and thus not further considered. *Fbxw8* encodes a WD-40 domain containing member of the F-box protein family, which are substrate-recognition mediators within a SCF (SKP1-CUL1-F-box)-type ubiquitin-E3-ligase complex involved in the tagging of phosphorylated target proteins to destine them for degradation (Ho *et al.* 2008).

Table 21. Microarray validation by qPCR. Regulated genes that appeared in the Microarray analysis were validated. (n.s. = not significant," — "= not analyzed. Significant results are marked with asterisks; n = 4 vs. 4 in 1 technical replicate)

Gene	Cerebellum	Brainstem	Liver
Acat1	—	—	n.s.
Adam1a	0.71-fold***	0.73-fold**	—
Ankrd33b	—	—	0.49-fold*
Bri3bp	n.s.	n.s.	—
Cthrc1	—	n.s.	—
Fbxw8	2.38-fold***	—	—
Gjc2	—	n.s.	—
Ifi27l1	—	—	n.s.
Lgals1	—	—	n.s.
Nlrp12	—	—	n.s.

In summary, no transcriptional dysregulation at the age of 6 months was detected in CAG42 mice. At the age of 18 months, two genes, *Adam1a* and *Fbxw8*, were recognized by more than one spot and were also validated with qPCR. Both genes are located in close proximity to *Atxn2*. The function of FBXW8 as ubiquitin-E3-ligase makes it an especially interesting molecule and should be investigated in the future. The questions arise whether the selective upregulation of *Fbxw8* in old CAG42 cerebellum reflects a compensatory response to pathology and whether this is an efficient cellular approach to degrade expanded ATXN2.

3.2.2 Expanded Ataxin-2 has an impact on *Plastin-3* mRNA expression levels

As it was shown that ATXN2 and Plastin-3 associate in mammalian cells and that the overexpression of ATXN2 led to increased Plastin-3 levels (Ralser *et al*. 2005b), the mRNA levels of *Pls3* were analyzed in CAG42 mice. In the cerebellum, only at the age of 18 months, *Pls3* mRNA levels were decreased to 0.94-fold (p = 0.008), while in the other tissues tested, cortex and brainstem, even at old age no altered regulation was observed (Table 22). Thus, *Pls3* mRNA levels decreased in the cerebellum when mice are symptomatic. Also, mice deficient for Ataxin-2 showed decreased *Pls3* levels at medium age specifically in the cerebellum (Table 24), possibly indicating that loss-of-function mechanisms are involved in the cerebellar SCA2 pathogenesis.

Another interesting target is TDP-43. Mutations within the gene, *Tardbp*, can cause ALS and it was recently shown that intermediate expansions in *Atxn2* are a risk factor for ALS. ATXN2 and TDP-43 - usually localized to the nucleus - were found in the same protein complex within the cytoplasm and this colocalization was dependent on RNA (Elden *et al*. 2010). Furthermore, an altered TDP-43 localization from nuclear to cytoplasmic was found in SCA2 patients. Besides, a loss of ATXN2 further resulted in reduced *Tardbp* isoform 3 levels in the brain (TDP-43, see section 3.3.1.1, Table 24). Therefore, *Tardbp* levels were analyzed in CAG42 mice. Only in the cortex and only at the age of 6 months, *Tardbp* was significantly downregulated to 0.94-fold (p = 0.044) in CAG42 mice (Table 22). Altered *Tardbp* mRNA expression was found only in the cortex and not consistently over time, which makes *Tardbp* mRNA expression changes unlikely to be predominantly involved in early stages of the disease.

Table 22. Overview of the measured mRNA gene expression levels in CAG42 mice. Significant changes are marked with asterisks. (Number of animals for each measurement is indicated; "—"= not significant, 3-4 mice/genotype per independent replicate)

		Age				
Gene	**Tissue**	**embryonic**	**postnatal day 1**	**6 weeks**	**6 months**	**18 months**
***Tardbp* isoform 3**	MEF	— 7 vs. 7	/	/	/	/
	Cb	/	/	— 16 vs. 15	— 8 vs. 7	— 11 vs. 10
	Cx	/	/	— 5 vs. 5	0.94-fold* 12 vs. 12	— 11 vs. 10
	Mb	/	/	/	/	— 4 vs. 4
	Lv	/	/	/	/	— 11 vs. 9
Pls3	MEF	— 7 vs. 7	/	/	/	/
	Cb	/	/	— 16 vs. 15	— 4 vs. 3	0.94-fold** 11 vs. 10
	Cx	/	/	— 4 vs. 4	/	— 7 vs. 6
	Mb	/	/	/	/	— 4 vs. 4

Further genes were validated in different tissues and time-points that appeared among others regulated in the Microarray of the *Atxn2*-knock-out mice; however, these genes were not differentially regulated:
MEFs (7 vs. 7): *Bace1*, *Pafah1b3*, *Pink1, Src*.
Cerebellum, 6 weeks (16 vs. 15): *Bace1*, *Fgf11*, *Kitl*, *Pafah1b3*, *Paip2* (4 vs. 4), *Pink1*, *Psenen*, *Src*, *Thap11*, *Tia-1* (7 vs. 8).
Cerebellum, 6 months (4 vs. 3): *Paip2*
Cerebellum, 18 months (4 vs. 4): *Pafah1b3*, *Src*, *Tia-1*
Brainstem, 18 months (4 vs. 4): *Pafah1b3*, *Src*, *Tia-1*
Liver, 18 months (4 vs. 4): *Src*, *Tia-1*

Several other genes that were differentially regulated in Ataxin-2 deficient mice were unaltered or not consistently altered in CAG42 mice up to 18 months of age. Reasons might be that pathways involving those genes are not part of the SCA2 pathology or are involved at a more advanced time point during the disease course.

3.2.3 ATXN2 and PABPC1 in CAG42 mice: from a soluble state to aggregates

The PAM2 domain of ATXN2 gave first hints on its interaction with the poly(A)-binding protein PABPC1 and could further be confirmed in 1998 in yeast (Mangus *et al*. 1998). PABPC1 is a well-characterized molecule that binds to the poly(A)-tails of mRNAs to promote translation initiation by mediating the circularization of the mRNA. The circularization is further important to initiate another round of translation without ribosome run-off, thus making several rounds of translation of one mRNA possible. In addition, PABPC1 binding to mRNAs protects their 3' site from degradation. On the other hand, its interaction with translation termination factors is necessary to maintain a balance between translation initiation and termination rates. Interestingly, it was documented that PABPC1 levels change according to altered ATXN2 levels (Nonhoff *et al*. 2007). These facts made PABPC1 an interesting candidate to study its role in SCA2 pathogenesis further.

3.2.3.1 Altered gene expression patterns of PABPC1 due to expanded *Atxn2*

To evaluate, how the mRNA expression levels in different tissues manifests over time, qPCR analysis from different genes was performed at 6 weeks, 6 months and 18 months of age. While the cerebellar *Atxn2* mRNA levels at 6 weeks of age were unchanged, at 6 months ($p = 0.0146$) and 18 months ($p = 0.0339$) they were significantly elevated to 1.07-fold levels.

In the cortex, the upregulation of *Atxn2* mRNA expression was already significant at postnatal day 1 (Figure 21) and stayed significant at 6 weeks (1.29-fold, p = 0.0101), 6 months (1.16-fold, p = 0.0005) and 18 months (1.16-fold, p = 0.0474). Also in brainstem and liver tissue at 18 months of age, elevated *Atxn2* levels to 1.15-fold (p = 0.012) and 1.28-fold (p = 0.042) were apparent. The transcript levels of the Ataxin-2 interactor *Pabpc1* remained unchanged at all time points in cerebellum as well as brainstem and liver, even at the old age of 18 months. In contrast, in cortex an upregulation of *Pabpc1* mRNA to 1.07-fold (p = 0.0061) and 1.16-fold (p = 0.0028) became apparent at 6 and 18 months, respectively (Figure 36, Table 23). Thus, also in cerebellum the *Atxn2* transcript is stable and significantly elevated during adult life and even earlier in cortex. Abnormally elevated *Pabpc1* mRNA levels appear only in the cortex by 6 months, a noteworthy finding since previous *in vitro* studies found the ATXN2 loss-of-function to increase PABPC1 levels (Nonhoff *et al*. 2007). Further studies were performed on the in SCA2 affected tissue cerebellum and compared to cortex as largely unaffected brain tissue.

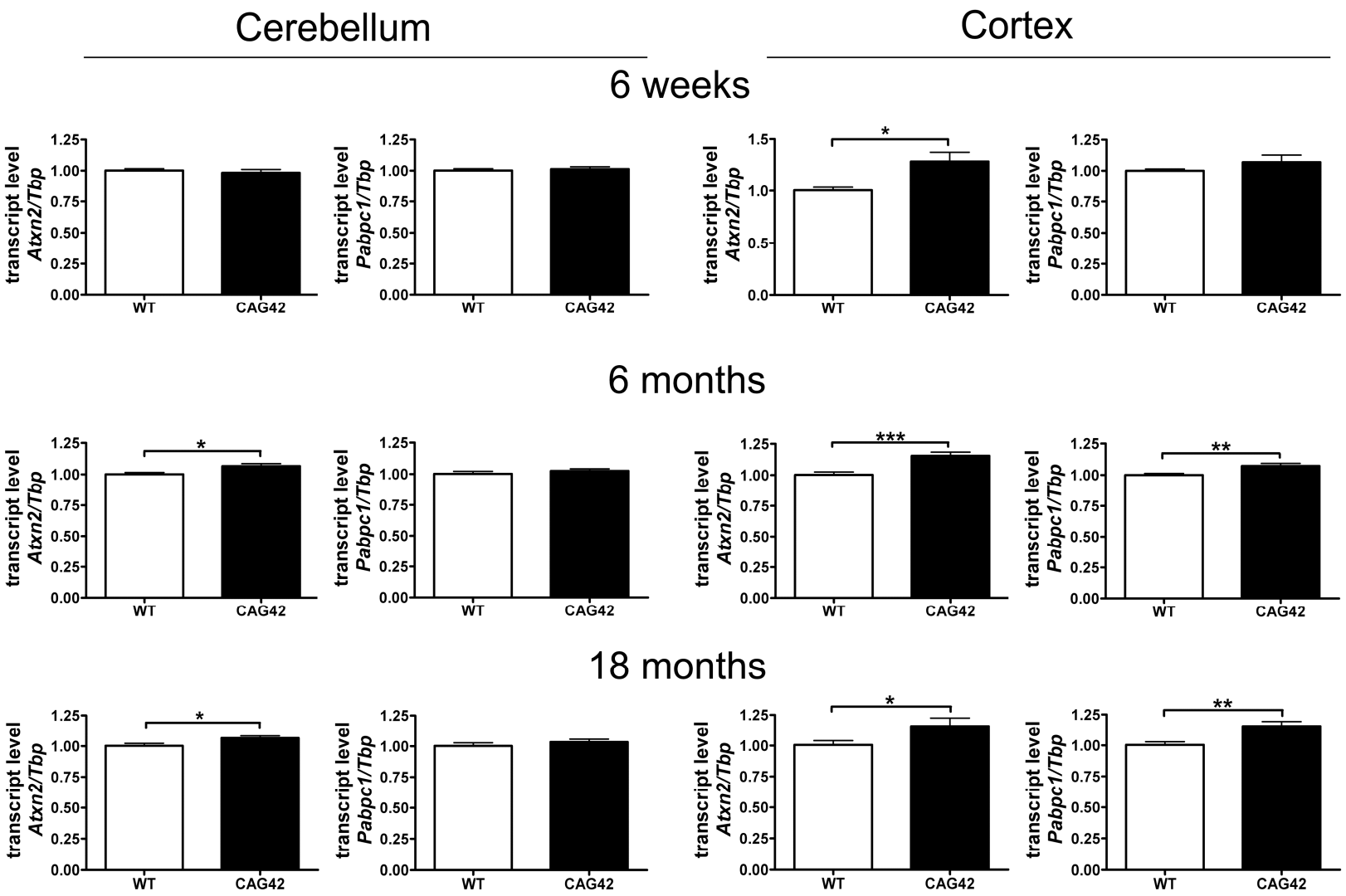

Figure 36. *Atxn2* and *Pabpc1* mRNA levels at 6 weeks, 6 months and 18 months age are elevated in specific ages and areas. In the cerebellum an *Atxn2* mRNA elevation was not detectable until 6 months, whereas the *Pabpc1* transcript levels remained unchanged. In the cortex an *Atxn2* mRNA elevation was already detected by 6 weeks and *Pabpc1* mRNA was upregulated by 6 months. (n = 9-16 animals/genotype/tissue in 4 independent technical replicates).

Table 23. Overview of the mRNA expression levels of *Atxn2* and *Pabpc1* in CAG42 mice throughout their life. Significant changes are marked with asterisks. (Number of animals for each measurement is indicated; "—" = not significant, 3-4 mice/genotype per independent replicate).

		Age				
Gene	**Tissue**	**embryonic**	**postnatal day 1**	**6 weeks**	**6 months**	**18 months**
Atxn2	MEF	— 7 vs. 7	/	/	/	/
	Cb	/	/	— 16 vs. 15	1.07-fold* 12 vs. 10	1.07-fold* 11 vs. 9
	Cx	/	1.48-fold* 3 vs. 3	1.29-fold* 9 vs. 10	1.16-fold*** 12 vs. 12	1.16-fold* 11 vs. 10
	Mb	/	/	/	/	1.15-fold* 4 vs. 4
	Lv	/	/	/	/	1.28-fold* 4 vs. 4
Pabpc1	MEF	— 7 vs. 7	/	/	/	/
	Cb	/	/	— 16 vs. 15	— 12 vs. 10	— 11 vs. 9
	Cx	/	/	— 9 vs. 8	1.07-fold** 12 vs. 12	1.16-fold** 11 vs. 10
	Mb	/	/	/	/	— 4 vs. 4
	Lv	/	/	/	/	— 4 vs. 4

3.2.3.2 The soluble protein levels in old cerebellum and cortex are reduced for ATXN2 and altered for PABPC1

Both in cerebellum and cortex, a reduction of soluble ATXN2 was detectable in the CAG42 mice. The levels were diminished in the cerebellum consistently at 6 weeks (0.75-fold, $p = 0.1008$), 6 months (0.77-fold, $p = 0.0808$) and significantly reduced at 18 months (0.62-fold, $p = 0.0037$). The reduction of levels in the cortex missed significance at 6 weeks (0.86-fold, $p = 0.1553$), but became significant both at 6 months (0.55-fold, $p = 0.0046$) and 18 months (0.75-fold, $p = 0.0344$). As expected by the elevated *Pabpc1* transcript levels, cortical soluble PABPC1 levels were elevated by 18 months (1.28-fold, $p = 0.0293$). Curiously, however, cerebellar soluble PABPC1 was significantly reduced already at 6 weeks (0.82-fold, $p = 0.034$) and again at 18 months (0.75-fold, $p = 0.0235$) (Figure 37). Thus, a reduction of soluble Q42-ATXN2 protein in spite of elevated transcript levels was a consistent finding in both tissues at all ages, in keeping with a partial loss-of-function and explaining the elevated *PABPC1* transcription in the cortex. However, selectively in the cerebellum PABPC1 soluble protein was also reduced in absence of any compensatory mRNA induction.

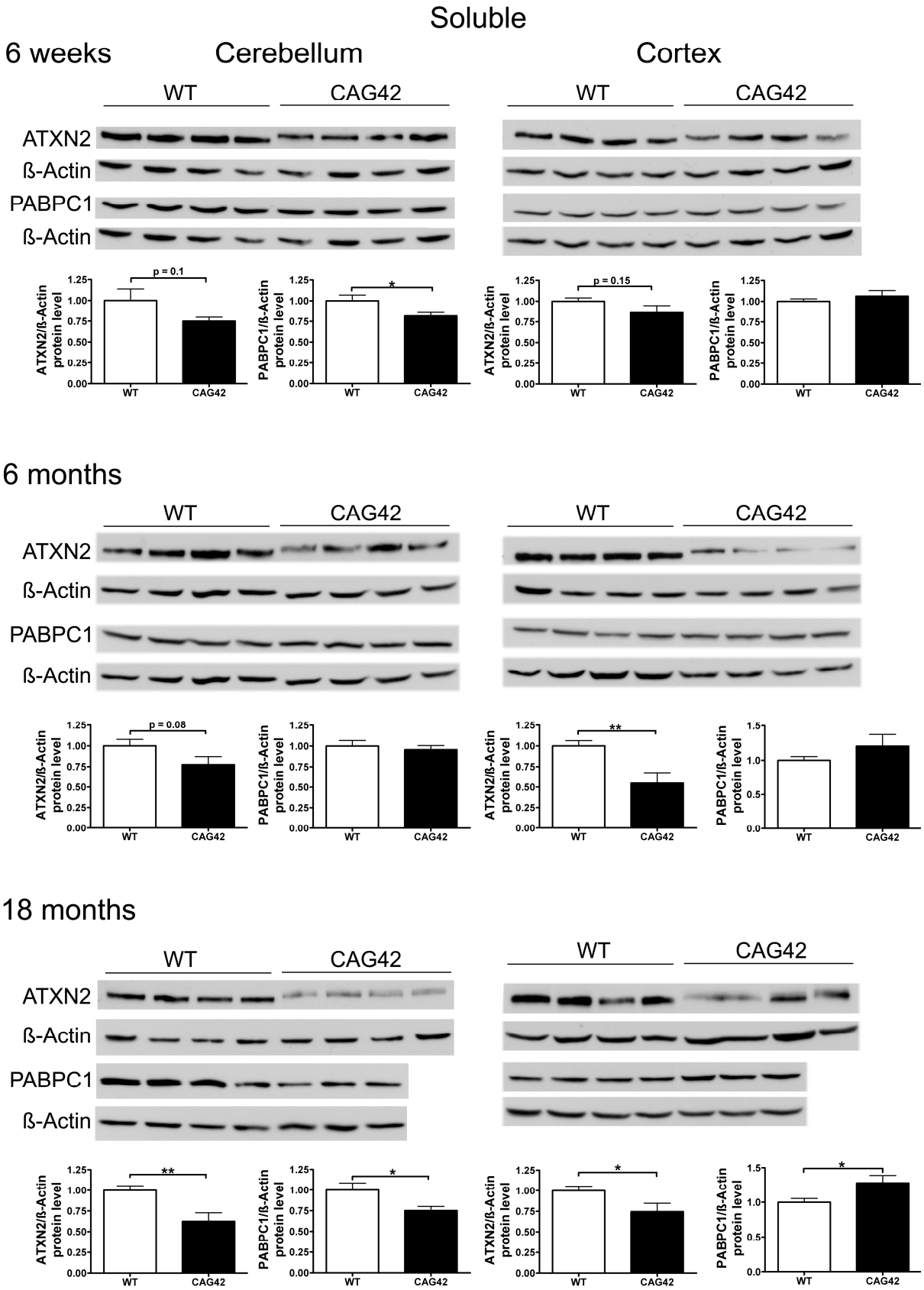

Figure 37. Soluble ATXN2 protein levels are reduced and PABPC1 levels change. In cerebellar tissue, a trend in ATXN2 reduction was observed at 6 weeks and 6 months age, with significance in ATXN2 reduction being reached at 18 months of age. Also, a significant PABPC1 reduction was apparent in 6 weeks and 18 months old CAG42 mice in the cerebellum. In the cortex, a reduction of ATXN2 levels was observed in 6 weeks old animals as a trend and with significance from 6 months onwards. An elevation of PABPC1 levels became significant at 18 months of age. (n = 10-12 mice/genotype/tissue in 3 independent technical replicates).

3.2.3.3 Increased insolubility of ATXN2 and PABPC1 in the old cortex

A possible explanation for the observed effects could be an increased insolubility of ATXN2. Therefore, proteins from the pellet of the RIPA extraction were further extracted with a harsher buffer containing SDS. At the young age of 6 weeks, significantly less ATXN2 (0.54-fold, $p = 0.011$) was also detected under these stronger extraction conditions, while at 6 and 18 months no change of ATXN2 levels was observed in CAG42 mice in the cerebellum. While no change was detected at 6 weeks in the cortex, insoluble ATXN2 levels were elevated with a trend at 6 months (1.78-fold, $p = 0.094$) and were significant at 18 months (1.76-fold, $p = 0.0023$). Significantly increased PABPC1 levels were measurable only at the age of 6 months in the cerebellum (1.61-fold, $p = 0.0028$), while in the cortex PABPC1 levels were elevated at the age of 18 months (1.39-fold, $p = 0.033$, Figure 38). Thus, at young age, less insoluble ATXN2 was detectable in the cerebellum, an effect that diminished at older ages, whereas cortical ATXN2 was insoluble by 6 months. Insoluble cerebellar PABPC1 was only measurable at 6 months, while more insoluble PABPC1 appeared in the cortex at old age.

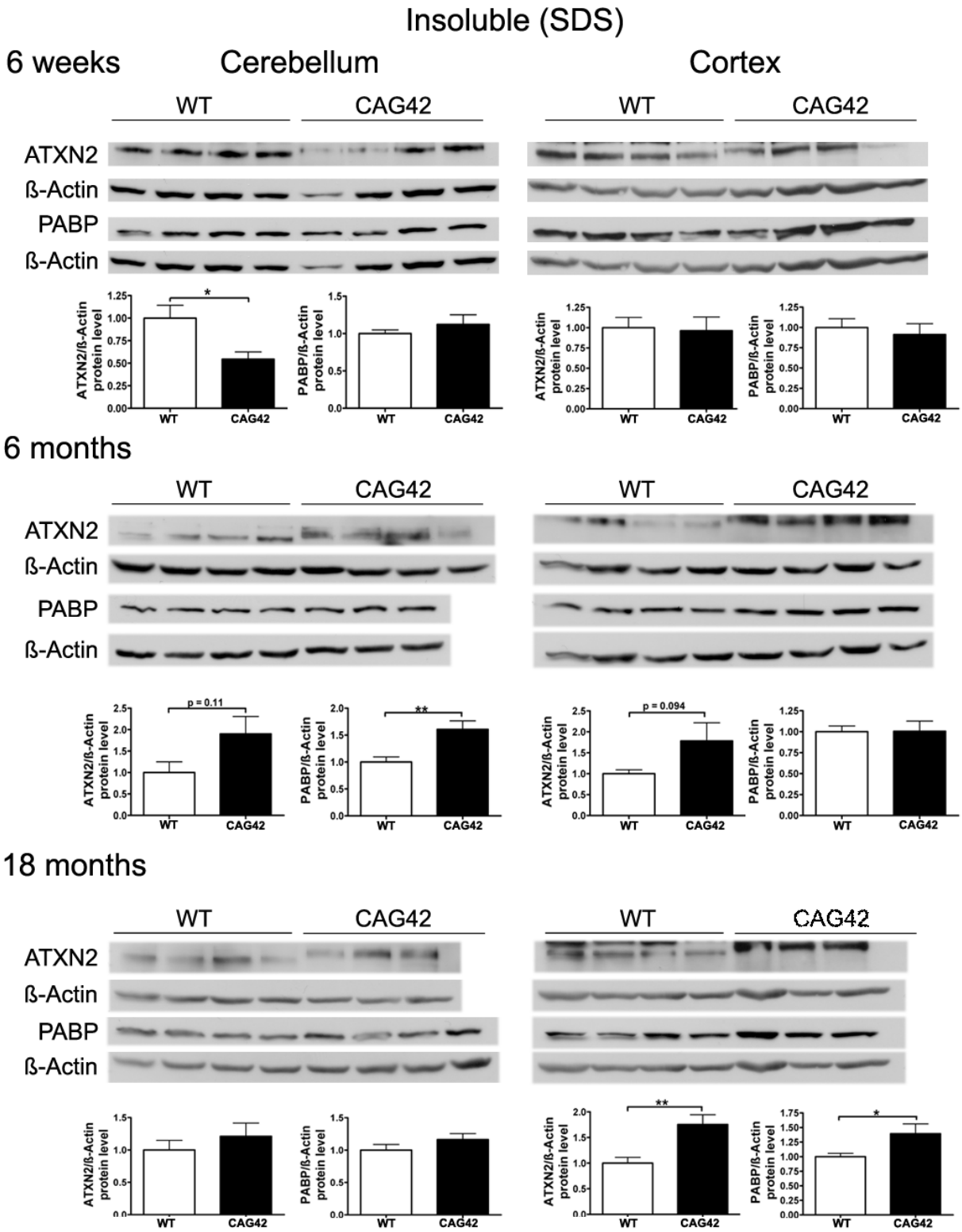

Figure 38. Increased insolubility of ATXN2 and PABPC1 is detectable at old age in the cortex of CAG42 mice. While in the cerebellum at the age of 6 weeks, ATXN2 levels were still decreased, they were not changed at 6 and 18 months. In contrast in the cortex, ATXN2 was elevated at 6 and 18 months. PABPC1 levels were only elevated at the age of 6 months in cerebellum, while in the cortex, significantly more PAPBC1 was detected at 18 months of age (n = 10-12 mice/genotype/tissue in 3 independent technical replicates).

3.2.3.4 Progressive insolubility of Q42-ATXN2 and PABPC1

To extract the maximum of insoluble proteins, a third and even stronger buffer containing urea and SDS was used in the following experiment. Again, the insolubility properties of Q42-ATXN2 and PABPC1 were analyzed. Proteins from the pellet after extraction of the soluble proteins were further extracted with the buffer described above from 6, 12 and 24 months old mice. Detection with the anti-ATXN2 antibody failed, possibly due to epitope masking. Detection with the 1C2 antibody which recognizes polyQ tracts of at least 38 glutamines (Lescure *et al.* 1994) was successful in revealing the expected band of correct size which exclusively appeared in mutant tissue and never in wild-type tissue. In the cerebellum a clear increase of insoluble Q42-ATXN2 was detected, which was significant at 12 (3.14-fold, $p = 0.0096$) and 24 months (4.28-fold, $p = 0.0002$) in comparison to 6 months Q42-ATXN2. In the cortex, however, an increase was not observed. Also, insoluble PABPC1 protein levels in the cerebellum increased over time and were significantly elevated at 24 months both in comparison to 24 months old WT (1.72-fold, $p = 0.0078$) and to 6 months old CAG42 tissue (1.9-fold, $p = 0.0357$). More insoluble PABPC1 was observed in the cortex, a bias which manifested as a trend in 6 months old mice (1.464-fold, $p = 0.0812$) and became significant by 24 months in comparison to the WT of the same age (1.98-fold, $p = 0.02$) and also in comparison to 6 months old CAG42 mice (2.036-fold, $p < 0.0001$). In wild-type animals the levels of insoluble PABPC1 remained similarly low over time (Figure 39). Thus, increased insolubility of Q42-ATXN2, particularly in the old cerebellum, appears to sequester PABPC1 into insolubility and may explain the decreased levels of soluble ATXN2 and PABPC1.

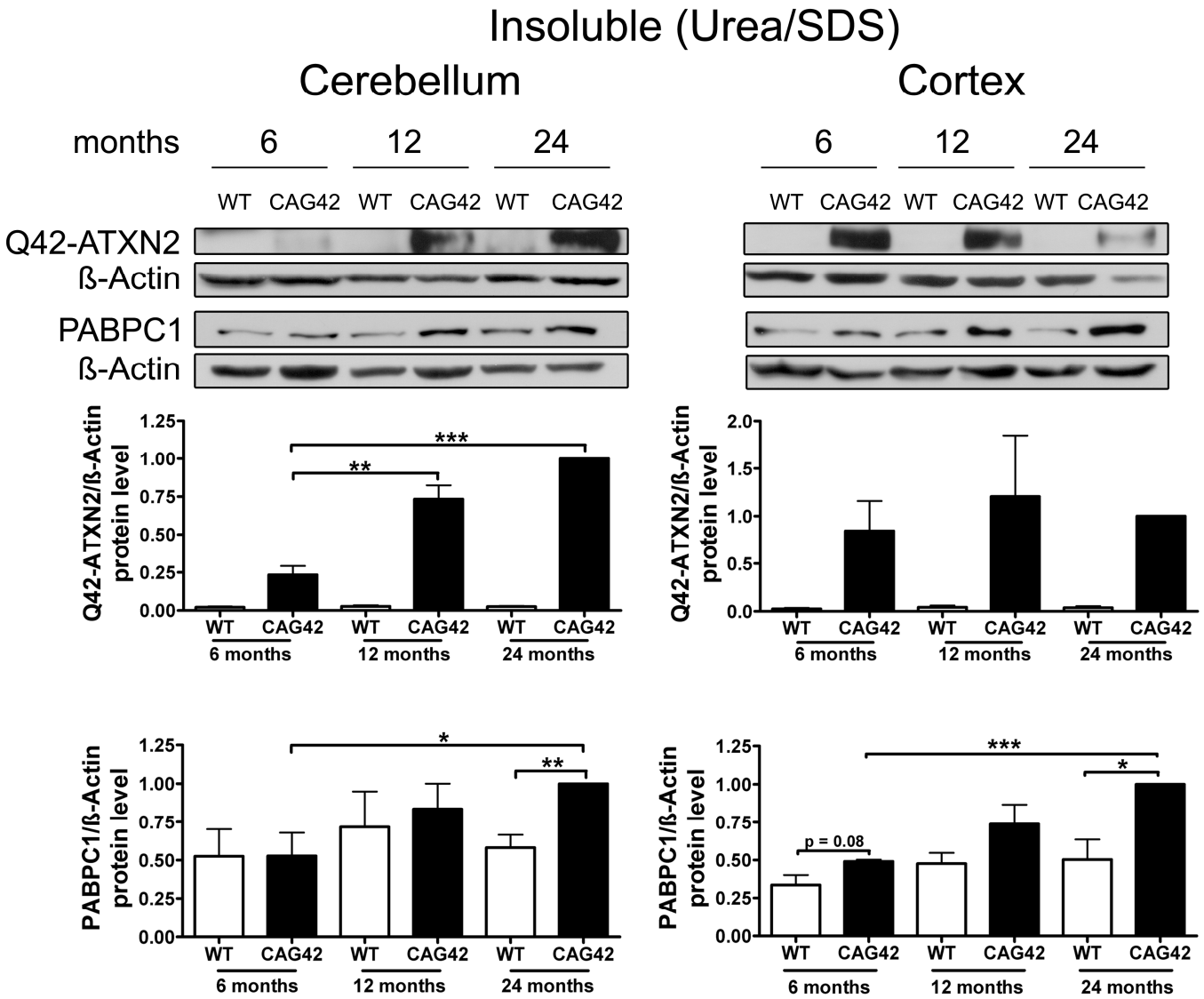

Figure 39. Increased insolubility of Q42-ATXN2 and PABPC1 with age. In the cerebellum, a progressive insolubility of Q42-ATXN2 from 6 to 12 and 24 months was detectable. The solubility of PABPC1 decreased from 6 to 24 months of age. Insoluble Q42-ATXN2 levels did not change in the cortex, however, the insolubility of PABPC1 increased over time in CAG42 mice. Insoluble PABPC1 levels in WT mice remained stably low in both tissues. (n = 3 mice/genotype/tissue in 3 independent technical replicates).

3.2.3.5 ATXN2 and PABPC1 are sequestered into visible aggregates

To investigate whether this insolubility process results in the formation of visible cytoplasmic aggregates containing ATXN2, as described in affected neurons during late stages of SCA2 patients, immunohistochemistry on cerebellar brain sections was performed. At all ages tested, 7, 14 and 24 months, 1C2-immunoreactivity was purely nuclear in wild-type mice, while the presence of Q42-ATXN2 resulted in additional cytoplasmic signals of Purkinje neurons by 14 months age (Figure 40A-F). ATXN2 immunoreactivity could be successfully visualized by an unmasking technique revealing a diffuse cytoplasmic distribution in Purkinje neurons of WT cerebellum, while this cytoplasmic pattern became granular at 14 months in individual Purkinje neurons and at 24 months in most Purkinje neurons of CAG42 mice (Figure 40G-L). In addition, the PABPC1-immunoreactivity was diffusely cytoplasmic in WT mice, but became granular in some Purkinje neurons by 14 months and in most Purkinje neurons by 24 months of age (Figure 40M-R). Nuclear inclusion bodies were never detected. A decrease of the molecular layer thickness or of the Purkinje cell number was not observed even at the age of 24 months (Figure 41) suggesting that a neurodegenerative process is not yet detectable at this age. Thus, the histological analysis supports the concept of progressive insolubility and aggregation of Q42-ATXN2 as well as PABPC1 in the cerebellar Purkinje neurons which are the prominent site of pathology in human SCA2.

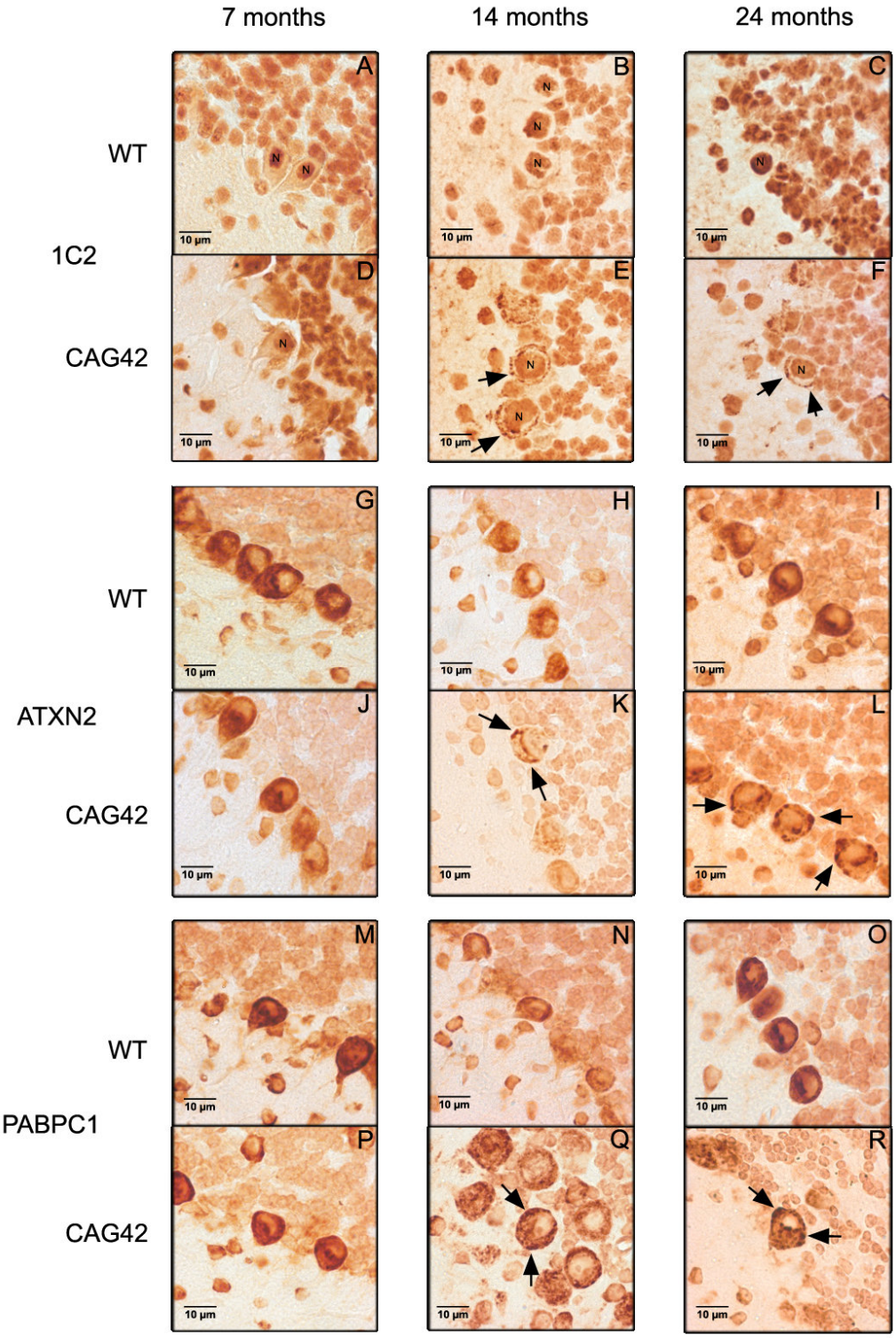

Figure 40. Immunohistochemistry of cerebellar Purkinje cells. At 7, 14 and 24 months age, the Purkinje cells showed a purely nuclear distribution of large polyQ-domains as revealed by 1C2-staining in WT tissue, while an additional granular cytoplasmic staining pattern became apparent at 14 and 24 months in knock-in tissue (A-F). ATXN2 immunoreativity was diffusely distributed throughout the cytoplasm and concentrated in the perinuclear region in WT tissue, while a more granular appearance was detected in CAG42 mice at 14 and 24 months (G-L). The expected diffuse cytoplasmic distribution of PABPC1 was documented in WT mice; whereas again a more granular staining pattern in CAG42 mice appeared by 14 months (M-R).

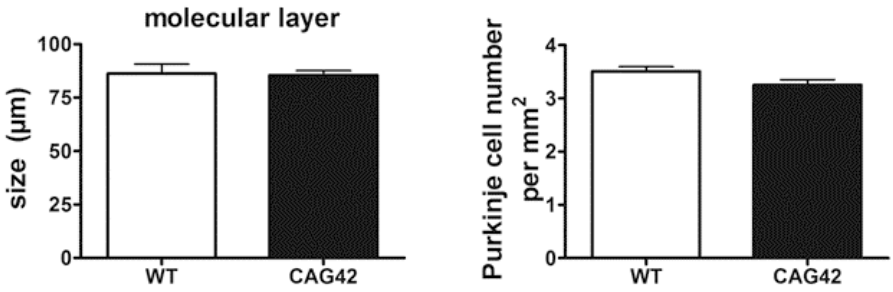

Figure 41. Molecular layer thickness and Purkinje cell number are not changed at the age of 24 months. (n = 2 mice/genotype with at least 3 sections/mouse and at least 10 microscopic fields/section).

3.2.3.6 Insoluble normal and expanded ATXN2 *in vitro* drives endogenous PABPC1 into insolubility

To confirm *in vitro* that insoluble expanded ATXN2 influences the PABPC1 solubility, HeLa cells were transfected transiently with CAG22-ATXN2 and CAG74-ATXN2 constructs. Successful overexpression was verified by qPCR and Western blot. Over 200-fold elevated *CAG22-ATXN2* and *CAG74-ATXN2* mRNA levels were accompanied by reduced *PABPC1* transcript levels (approximately 0.5-fold, $p = 0.0087$ and $p = 0.0041$) (Figure 42), while at the protein level a 7.2-fold ($p = 0.0374$) and 6.7-fold ($p = 0.1667$) excess of soluble Q22-ATXN2 or Q74-ATXN2 was found, accompanied by a reduction of endogenous soluble PABPC1 levels to 0.65-fold ($p = 0.0138$ and $p = 0.002$). To assess the insoluble fractions of both proteins, the pellet after the extraction of soluble proteins was dissolved and re-extracted with more detergents. Overexpressed Q22-ATXN2 and Q74-ATXN2 were strongly detectable, while endogenous ATXN2 in the empty vector control transfection was practically undetectable. Endogenous PABPC1 levels in the insoluble protein fraction were increased to 3.2-fold after both Q22-ATXN2 ($p = 0.0048$) and Q74-ATXN2 ($p = 0.0184$) overexpression. These data corroborate the previous tissue data that insoluble ATXN2 of either normal or expanded size sequesters its interactor protein PABPC1 into insolubility and may thus contribute to the reduction of soluble PABPC1 levels. They are also in keeping with the previous *in vitro* reports that the increase in soluble ATXN2 levels leads to reduced PABPC1 expression levels (Nonhoff *et al*. 2007).

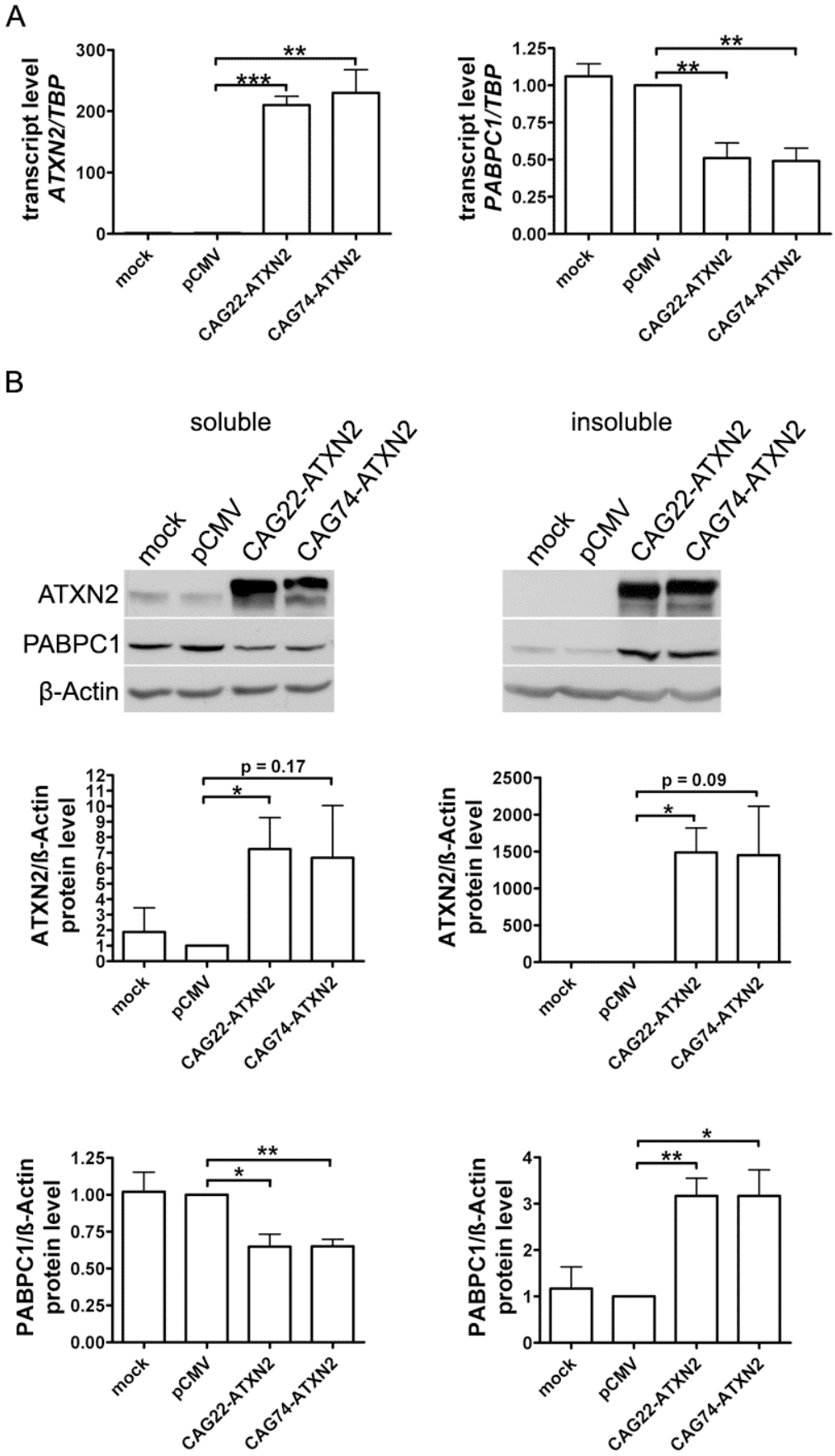

Figure 42. Normal and expanded insoluble ATXN2 drives PABPC1 into insolubility. (A) Overexpression of CAG22-ATXN2 and CAG74-ATXN2 led to significantly decreased *PABPC1* transcript levels. (B) Overexpressed Q22-ATXN2 or Q74-ATXN2 reduced endogenous soluble PABPC1 levels, whereas endogenous insoluble PABPC1 levels were significantly increased in the presence of insoluble ATXN2. (n = 3).

3.2.3.7 Wild-type and expanded ATXN2 interact with PABPC1 in the cerebellum

To confirm that ATXN2 and PABPC1 interact in the mouse cerebellum co-immuoprecipitation in wild-type, CAG42 and KO mice was performed. Both ATXN2 forms, wild-type and expanded, were able to precipitate PABPC1, while no PABPC1 was precipitated when ATXN2 was absent (Figure 43). Additionally, expanded ATXN2 appeared to precipitate more PABPC1 from the cerebellum than wild-type ATXN2. Thus, PABPC1 is likely to be sequestered into aggregates in CAG42 mice through a direct interaction with expanded ATXN2 and not solely via co-aggregation.

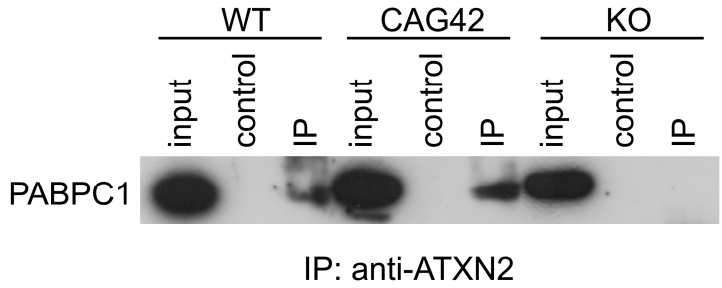

Figure 43. ATXN2 and PABPC1 interact in the cerebellum of WT and CAG42 mice. Co-immunoprecipitation in WT, CAG42 and KO cerebellum was performed. Both wild-type and expanded ATXN2 were able to co-immunoprecipitate PABPC1, while more PABPC1 was precipitated in CAG42 mice.

3.2.4 Is the expression and distribution of other proteins altered?

3.2.4.1 TDP-43 protein expression is not altered at young age

To first assess whether the ATXN2 expansion has an effect on TDP-43 basal levels, its protein levels were measured at the age of 6 weeks in wild-type and CAG42 mice in cerebellum. No protein expression changes were observed at this time point in CAG42 mice (Figure 44). Thus, an expansion of 42 glutamines in the ATXN2 protein does not affect the protein expression of TDP-43 at young age in CAG42 mice.

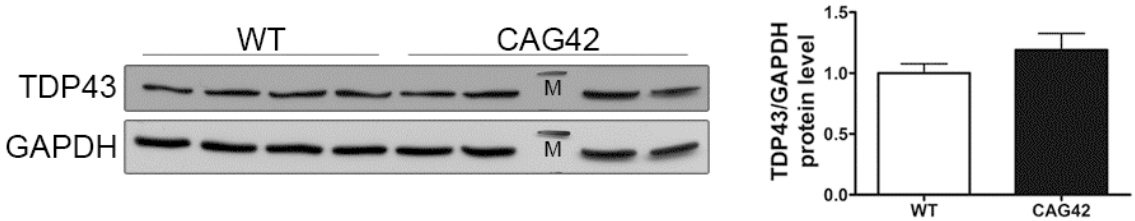

Figure 44. TDP-43 protein expression is not altered in 6 weeks old cerebellum in CAG42 mice. (M: marker, n = 4 mice/genotype in one technical replicate).

3.2.4.2 eIF4E, S6, p62 and TDP-43 do not display an aberrant localization

To assess whether other proteins from the translation machinery, besides PABPC1, are sequestered into aggregates, immunohistochemistry was performed in 24 months old mice of S6 and eIF4E. The S6 ribosomal protein, a component of the 40S ribosomal subunit, is normally localized in the cytoplasm, a pattern that was observed in WT and CAG42 mice, accompanied by a perinuclear aggregation (Figure 45A, B). The translation initiation factor eIF4E was distributed throughout the cytoplasm and showed a slight perinuclear accumulation in both, WT and CAG42 mice (Figure 45C, D). As previous studies showed that p62/SQSTM1 colocalized with neuronal inclusions containing expanded polyglutamine protein (Seidel *et al.* 2011), p62-staining on cerebellar sections was performed. A cytoplasmic localization of p62 was observed in WT and CAG42 mice, while no accumulation was observed in 24 months old mice (Figure 45E, F). TDP-43 localization changes from nuclear to cytoplasmic in ALS, but also in late stages of SCA2 patients (Elden *et al*. 2010). To investigate whether this effect could also be observed in the CAG42 mice at the age of 24 months cerebellar sections were stained with the TDP-43 antibody. TDP-43 staining showed a pure nuclear staining in WT and also CAG42 mice (Figure 45G, H). No altered accumulation or localization of the investigated proteins was found in CAG42 mice. Thus, at the old age of 24 months, none of the investigated proteins S6, eIF4E, p62 and TDP-43, showed an aberrant accumulation or localization in the Purkinje neurons of CAG42 mice.

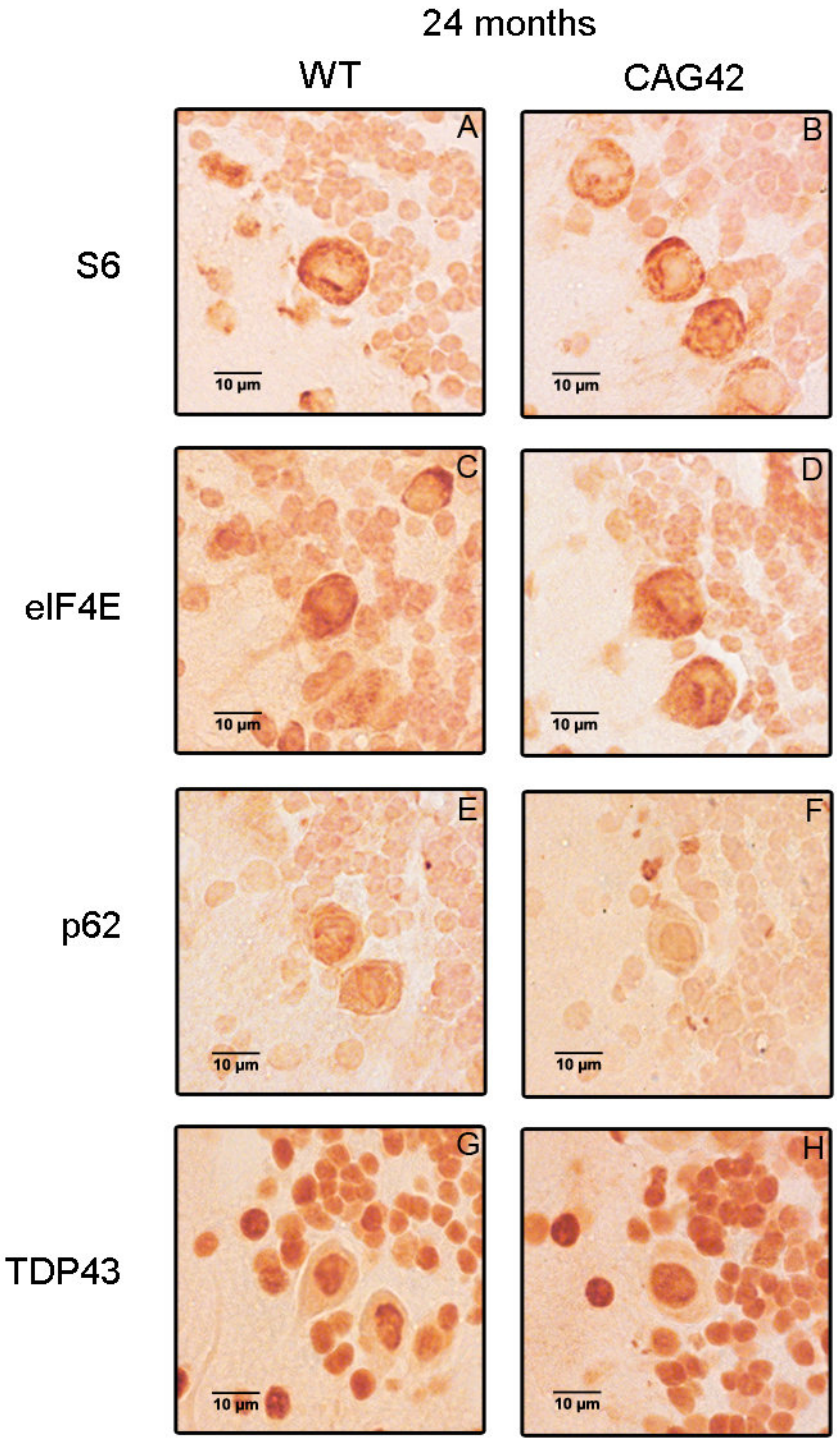

Figure 45. Immunohistochemistry of cerebellar Purkinje cells at the age of 24 months. In the Purkinje cells at the age of 24 months, the S6 ribosomal protein showed a cytoplasmic distribution together with a perinuclear accumulation in WT and CAG42 mice (A, B). The cytoplasmic localization of eIF4E was clearly visible in WT and CAG42 (C, D). p62/SQSTM1 localization to the cytoplasm was apparent in WT and CAG42 mice (E, F). The normal nuclear localization of TDP-43 was observed in WT and also CAG42 mice (G, H). No clear aggregation pattern or aberrant localization of these proteins was observed in CAG42 at the age of 24 months.

3.3 The *Atxn2*-knock-out mouse as a tool to evaluate the function of ATXN2

3.3.1 The role of ATXN2 in the regulation of translation

Even though the function of ATXN2 is still under investigation and not fully understood, several studies attribute ATXN2 a function in RNA metabolism, e.g. by regulating translation initiation. Knock-down cell lines and knock-out mutants/deletion strains were very helpful for this purpose. The interaction of ATXN2 with PABPC1 is well documented and very important in this context and, as described in 3.2.3, PABPC1 possibly also plays an important role in the SCA2 disease mechanism. PABPC1 levels are sensitive to ATXN2 protein expression levels and are consequently altered on transcript and protein level in CAG42 mice where ATXN2 levels are changed. The sequestration into insoluble aggregates of expanded ATXN2 further leads to PABPC1 accumulation. Further studies showed that ATXN2 co-sediments with polysomes and has a RNA-dependent localization at the rER (Satterfield & Pallanck 2006, van de Loo *et al*. 2009). Furthermore, it is a component of stress granules (Nonhoff *et al*. 2007). To further evaluate which function can be ascribed to ATXN2, previously a Microarray analysis of cerebellum, brainstem and liver tissue at the age of 6 weeks, 3 months and 6 months in the *Atxn2*-knock-out mouse, was performed and validated by qPCR (Dissertation M. Fittschen, 2008). And indeed, the ATXN2 involvement in translation was reflected by a consistent upregulation of genes coding for proteins of the small and large ribosomal subunits and dysregulation of other factors involved in translation like the eukaryotic initiation factors and poly(A)-binding-protein-interacting proteins (PAIP1). Further experiments should pursue the current knowledge on ATXN2 function.

3.3.1.1 Genes involved in translation are dysregulated upon ATXN2 loss

To extend the previous Microarray study, further genes that are known to be involved in translation or that were shown before to be differentially regulated when ATXN2 levels change were analyzed in cerebellum and liver with qPCR at the age of 6 months. At this time point the biggest effects were previously found in the *Atxn2*-knock-out mouse (Lastres-Becker *et al*. 2008a) (dissertation M. Fittschen, 2008). *Pabpc1* was significantly upregulated in cerebellum (1.11-fold, $p = 0.014$) and liver (1.15-fold, $p = 0.0174$) at the age of 6 months, in concordance with previous *in vitro* studies where PABPC1 protein levels increased when ATXN2 levels were low (Nonhoff *et al*. 2007). *Pabpc1* was the only gene measured, whose

expression was consistently altered into one direction in both tissues, possibly indicating that it exerts a function independent of the tissue type.

The *Plastin-3* mRNA levels were significantly downregulated only in the cerebellum (0.80-fold, p = 0.013) and unchanged in liver, while the overexpression of ATXN2 leads to increased Plastin-3 levels in mammalian cell lines (Ralser *et al*. 2005b). The specific dysregulation of *Pls3* in cerebellum was also already observed in CAG42 mice. These data might indicate that changes in *Pls3* expression are a cerebellum-specific effect contributing to its vulnerability.

Tardbp expression was not regulated when using an assay that detected all 5 isoforms (0.997-fold, p = 0.912), however, using an assay that specifically detects isoform 3, a significant downregulation in the cerebellum (0.89-fold, $p < 0.0001$) and a significant upregulation in the liver (1.17-fold, p = 0.003) was substantiated. *HnRNPA2/B1* showed a significant upregulation in the cerebellum (1.08-fold, p = 0.015). The eukaryotic initiation factor eIF5a was only significantly increased in the liver (1.12-fold, p = 0.022). However, several other eukaryotic initiation factors or stress granule components were not altered (Table 24). Thus, the differential expression of *eIF5a*, *hnRNPA2B* and *Tardbp* further underlines a role of ATXN2 in RNA metabolism influencing specific proteins. Also, the *Tardbp* expression was elevated in cerebellum and reduced in liver. These tissue-specific differences could indicate that *Tardbp* exerts a tissue-specific function. However, further studies are necessary to solve that question.

Table 24. Differential expression of several genes in the *Atxn2*-knock-out mouse. Significant results are marked with asterisks. "—"= not significant; n.a. = not available. Direction of differential regulation analyzed by Microarray is indicated with arrows. Data were produced in collaboration with J. Drost (dissertation, in preparation).

6 months	Cerebellum 15 vs. 10	Liver 8 vs. 7	Result Microarray Sca2KO
Atxn2	0.0005-fold***	0.08-fold***	↓
Ddx6	—	n.a	n.a
EiF2α	—	n.a	n.a
Eif2s2	—	—	↑
Eif4e	—	n.a	n.a
Eif5a	—	1.12-fold*	n.a
Fmr1	—	n.a	n.a
Fus	—	n.a	n.a
HnRNPA2B1	1.08-fold*	—	↑
Lsm12	—	n.a	n.a
Pabpc1	1.11-fold*	1.15-fold*	↑
Pls3	0.8-fold***	—	↓
Tardbp	0.89-fold***	1.17-fold**	↓
Smn1	—	n.a	n.a

3.3.1.2 18S rRNA levels are not elevated together with the ribosomal proteins in qPCR

The consistent finding of upregulated genes coding for ribosomal proteins, e.g. *Rpl14*, *Rpl18*, *Rps10* and *Rps18* in the Microarray analysis was best validated in liver tissue (dissertation M. Fittschen, 2008). To investigate whether also the rRNA content is increased, qPCR on 6 months old liver tissue with a probe that hybridizes to 18S rRNA was performed. More than 90% of RNA within a cell is comprised of rRNA, therefore the more abundant endogenous control *Gapdh* instead of *Tbp* was used to minimize differences in C_t-values. No difference in 18S rRNA content was detected with this method (Figure 46). Thus, even though an elevated mRNA expression of ribosomal components was identified upon ATXN2 loss, no accompanying effect on the 18S rRNA content was substantiated.

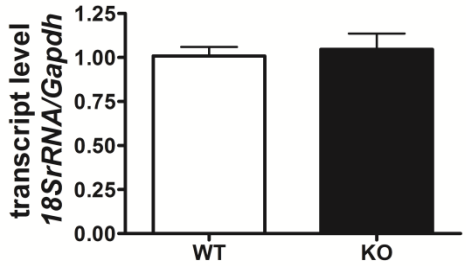

Figure 46. 18S rRNA levels in liver of 6 months old *Atxn2*-knock-out mice are not altered. (n = 7-8 mice/genotype in 2 independent technical replicates)

3.3.1.3 ATXN2 and eIF3 are part of the same protein complex

Co-immunoprecipitation experiments were previously performed that describe ATXN2 to be part of the 48S translation initiation complex (Lastres-Becker, in preparation). To reproduce this finding and to further optimize the lysis buffer used for co-IP experiments in HEK-293 cells, different pH and NaCl concentrations in the lysis buffer (1- pH 7.1, 150 mM NaCl; 2- pH 7.1, 200 mM NaCl and 3- pH 8.0, 200 mM) were tested and the IP performed (Figure 47). All three conditions allowed the detection of ATXN2 and the translation initiation complex component eIF3B, as a part of the same complex. The immunoreactivity increased for both proteins with higher pH and NaCl content in the buffer. Thus, the corroboration that ATXN2 is part of the initiation complex was achieved with all conditions, with 200 mM NaCl and pH 8 being the most suitable concentration for this assay in HEK-293 cells.

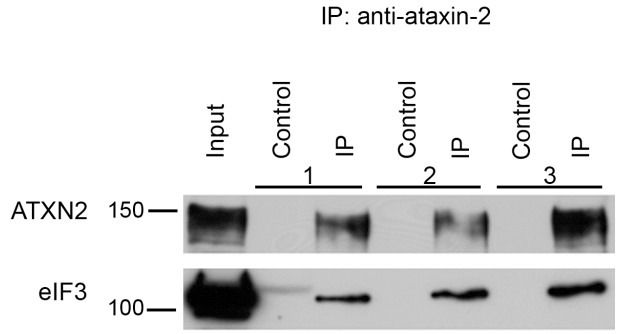

Figure 47. Endogenous Ataxin-2 interacts with eIF3 *in vitro*. Protein extracts of HEK-293 cells were used for immunoprecipitation assay with anti-ataxin-2 antibody and different pH and NaCl concentrations were tested: 1- pH 7.1, 150 mM NaCl; 2- pH 7.1, 200 mM NaCl; 3- pH 8.0, 200 mM NaCl.

3.3.1.4 ATXN2 reduces S6-phosphorylation

What role can be ascribed to ATXN2 in translation initiation? Is it a translational activator or a repressor? In order to describe the role of ATXN2 in translation initiation, the phosphorylation status of one of the key proteins for translation initiation, S6, was studied in MEFs. Translation induction is then reflected by S6-phosphorylation. Cells were serum deprived for 24 h and then either left untreated or incubated for 10 minutes with insulin to induce phosphorylation. At basal levels, increased S6-phosphorylation in KO-MEFs manifested as a trend (2.56-fold, p = 0.072) in comparison to WT-MEFs, while a significant increase of phosphorylated S6 (2.63-fold, p = 0.0097) was detected after serum starvation and insulin induction in KO-MEFs (Figure 48). These data indicate that ATXN2 is necessary to maintain normal S6-phosphorylation levels.

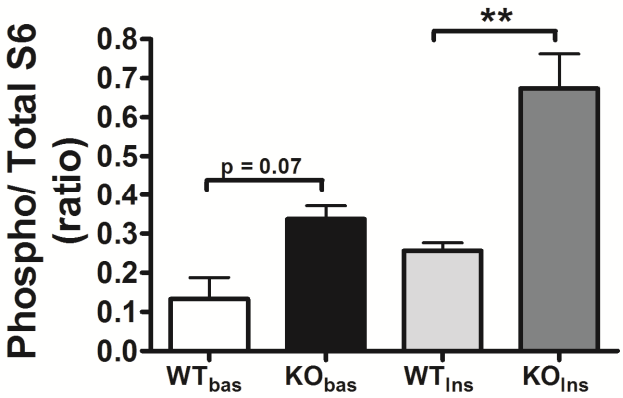

Figure 48. Increased S6-phosphorylation in KO-MEFs. MEFs were serum starved for 24 h and S6-phosphorylation measured at basal conditions (bas) or after a 10 minute incubation step with insulin (Ins). Increased S6-phosphorylation manifested in KO-MEF at basal levels with a trend and after starvation and insulin treatment it was significantly increased. (n = 2-3 MEF-lines in one technical replicate).

3.3.1.5 ATXN2 increases global protein synthesis rates

To further test whether the increased S6-phosphorylation due to ATXN2 loss indeed facilitates global translation initiation, the incorporation rates of radioactively labeled amino acids into global protein content of MEFs were determined in WT and KO cells. The absence of ATXN2 resulted in a moderate reduction of global protein synthesis rates of 34% ($p = 0.029$), an extent comparable to the effect of the mTOR inhibitor rapamycin, while cycloheximide, a repressor of the translational elongation, resulted in a total suppression (Figure 49).

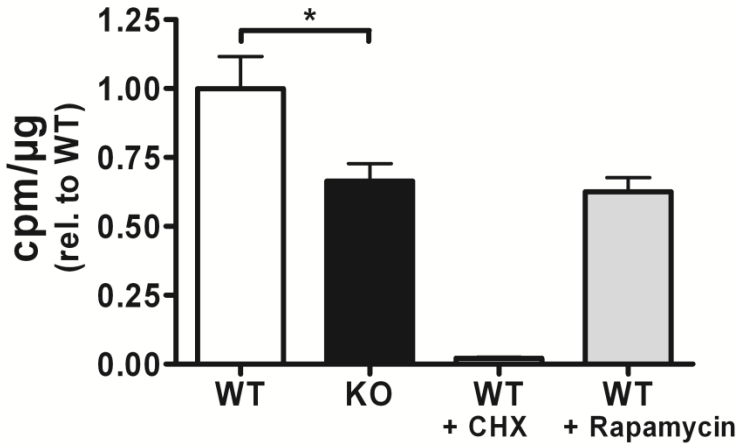

Figure 49. ATXN2 deficiency reduces basal mRNA translational activity. The global protein synthesis rates were determined in MEFs by measuring the incorporation of [S35]-labeled methionine/cysteine. Cycloheximide (CHX) or rapamycin were applied 90 min prior to labeling. KO-MEFs showed a reduction in protein synthesis of 34% in comparison to WT-MEFs (n = 6 MEF-lines in 3 independent technical replicates). In comparison, the translation elongation inhibitor CHX reduced the translation to 2%, the mTOR pathway inhibitor rapamycin to 63% (n = 2).

3.3.1.6 Normal growth behaviour of MEFs

To further analyze whether the decreased protein synthesis rates upon ATXN2 loss have an impact on the growth behaviour of MEFs, population doubling times were calculated. The cells were cultured starting at passage 3 until passage 11 and the cell number counted at each passage. No growth alteration was measured in ATXN2 deficient MEFs. Thus, the absence of ATXN2 does not influence the growth behaviour of MEFs.

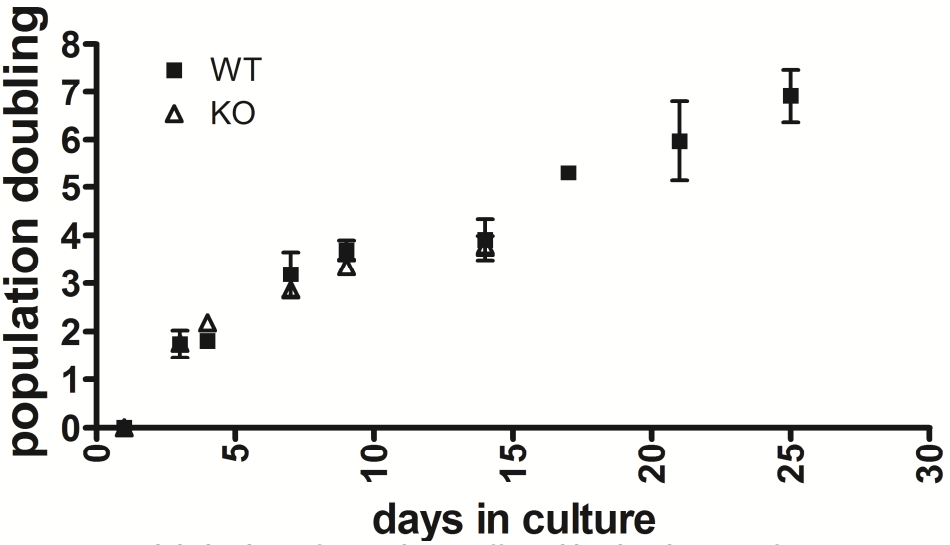

Figure 50. Growth behaviour of MEFs is not affected by the absence of ATXN2. MEFs were cultivated up to passage 11 and their population doubling (PD) was determined (n = 2-3 MEF-lines/genotype).

3.3.2 Late-onset reduction of mRNAs with long poly(A)-tails

ATXN2 is necessary for proper polyadenylation in yeast, leading to pre-mRNAs that lack their full-length poly(A)-tails when ATXN2 is absent. This is a result of increased poly(A)-nuclease activity and therefore increased poly(A)-trimming due to ATXN2 absence (Mangus *et al*. 1998). To investigate whether a similar effect occurs in mammals upon ATXN2 loss, poly(A)+-mRNAs were isolated from MEFs and 3 and 6 months old liver from wild-type and ATXN2-deficient mice. Extracted poly(A)+-mRNA from WT and KO tissue was sent to U. Kühn (University Halle) and the poly(A)-tail lengths analyzed. In MEFs and in liver at the age of 3 months, no alteration in poly(A)-tail length was observed in KO-tissue (Figure 51). While in 6 months old liver the poly(A)-tail length of KO animals was comparable to that of WT, the amount of long poly(A)-tail containing mRNAs (~200 adenines) was reduced as apparent from the densitometry (Figure 52). These data indicate that even though ATXN2 does not influence proper polyadenylation in mammals, its presence possibly stabilizes mRNAs bearing long poly(A)-tails at 6 months age, a time point where the phenotype in ATXN2-KO animals is strongly detectable.

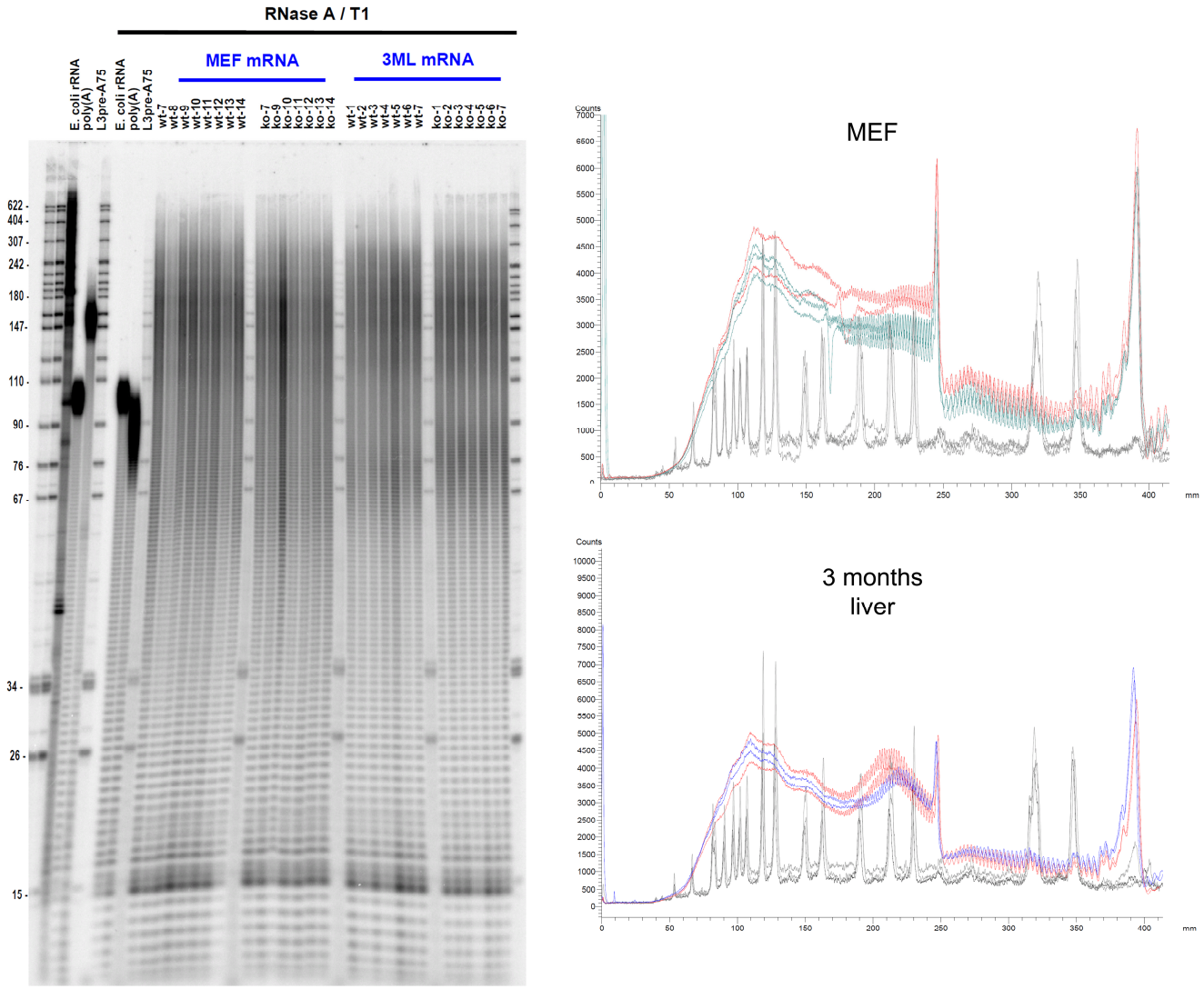

Figure 51. Normal poly(A)-tail length in MEFs and 3 months old liver in absence of ATXN2. The poly(A)-tail length of poly(A)+-mRNA was investigated. Left: Most mRNAs bear poly(A)-tails of around 200 adenines in WT and ATXN2-KO animals. No difference in poly(A)-tail length was observed. In KO-MEF10 more sample was loaded onto the gel (n = 7-8 mice/genotype). Right: The densitogram also indicates equal amounts of long poly(A)-tails in WT (blue) and in KO (red) animals (MEF: n = 2-3 mice/genotype; liver: n = 2 mice/genotype).

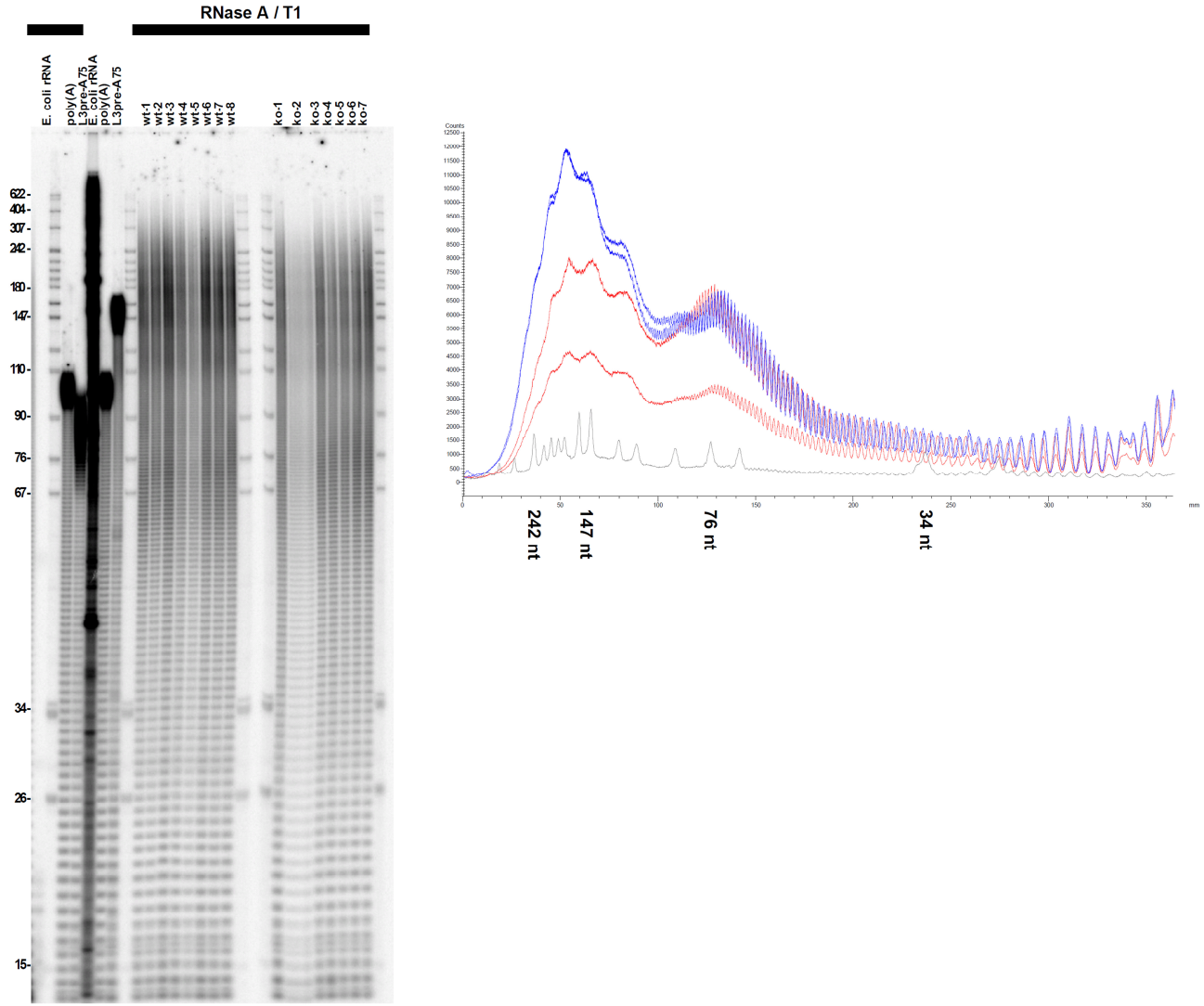

Figure 52. Reduced amount of mRNAs with long poly(A)-tails in 6 months old liver of ATXN2 deficient mice. The poly(A)-tail length of poly(A)+-mRNAs was investigated. Left: Most mRNAs bear poly(A)-tails of around 200 adenines in WT and ATXN2-KO animals. No difference in poly(A)-tail length was observed (n = 7-8 mice/genotype). Right: The densitogram indicates increased amounts of long poly(A)-tails in WT (blue) compared to KO (red) animals (n = 2 mice/genotype).

4 Discussion

SCA2 is a neurodegenerative movement disorder that primarily affects the cerebellum and leads to ataxia and ultimately to death mostly 15-20 years after the first symptoms appeared (Velazquez-Perez *et al*. 2011). The underlying mechanisms are not clarified to date and also the prevailing medical treatment is not sufficient to cure the disease. To elucidate the underlying pathomechanisms of SCA2 and the function of the disease protein ATXN2, several cell and mouse models were generated and applied. However, the currently available SCA2 transgenic mouse lines can only mimic distinct aspects of the disease. The overexpression and the use of heterologous promoters lead to a phenotype that is caused by a gain of protein function, while the loss of normal protein function that also might contribute to the disease is disregarded. To have an established mouse model that covers preferably all aspects of the disease, the *Atxn2*-CAG42-knock-in mouse with a physiological ATXN2 expression was previously generated and characterized in this thesis. In a next step, pathomechanisms that might be involved early on were identified. In particular, the role of PABPC1 was considered here in further detail. The third part included studies on an Ataxin-2 knock-out mouse model to get a deeper understanding of the role of Ataxin-2 in translation initiation.

4.1 Evaluation of the *Atxn2*-CAG42-knock-in mouse as a model for SCA2

This work describes the first *Atxn2*-CAG42-knock-in mouse that expresses expanded Ataxin-2 under the murine *Atxn2* promoter in the same spatial and temporal expression pattern known from human SCA2 patients. But what are the advantages and limitations of this mouse model? To answer this question the mouse was thoroughly characterized.

4.1.1 The *Atxn2*-CAG42-knock-in mouse is a valuable model for SCA2

The characterization of the knock-in mouse as a model for SCA2 covered different aspects. The phenotype was recorded, which included observation of the weight and several motor tests. Brain sections were investigated for aggregate formation and mRNA and protein levels of Ataxin-2 were documented. Furthermore, the transmission pattern of the repeat was analyzed. The main cause for the degeneration of the neurons in polyglutamine disorders is

thought to be mediated by toxic gain-of-function effects of the expanded protein, mechanisms that were found to contribute to the phenotype of the knock-in mice.

Weight

The first symptom detected in the knock-in mice was a change in body weight, which was already reduced at postnatal day 10. The reduction persisted throughout their lifespan (Figure 23). The knock-in mice behaved in the open field test comparable to the wild-type littermates (Table 19). Consequently, there is no motor hyperactivity to explain the reduced body weight of knock-in animals. SCA2 patients also suffer from a loss of body weight and subcutaneous fat, while this effect is preceded by an increased appetite in humans (Abdel-Aleem & Zaki 2008, Auburger 2012). Whether increased food intake is also a symptom in the knock-in mice was not investigated in this thesis. Also patients from other polyglutamine disorders like SCA1 and HD and their adjacent knock-in mouse models were reported to manifest with a body weight reduction (Aziz *et al.* 2008, Genis *et al.* 1995, Lin *et al.* 2001, Trejo *et al.* 2004, Watase *et al.* 2002), which is a common symptom among polyglutamine disorders. Contrary, the loss of ATXN2 in mice causes obesity which is accompanied by insulin resistance (Lastres-Becker *et al*. 2008a). Thus, a gain-of-function in peripheral tissue of expanded ATXN2 might underlie the reduced weight of the knock-in animals.

Locomotor anomalies

Early symptoms of SCA2 include motor incoordination when performing complex motor tasks. This cerebellar dysfunction can easily be assessed in mice on a rota rod apparatus. The first neurological symptom detectable in the knock-in mice was hyperactivity at the young age of 6 weeks, which was followed by late-onset pathology at the age of 18 months in homozygous mice (Figure 24). The hyperactivity possibly reflects an initial overcompensation; however, whether SCA2 patients are hyperactive long before the onset of motor incoordination has never been investigated. A CAG repeat length of around 40 CAGs is common among SCA2 patients whose symptoms mostly start during the 3rd decade of life. The late-onset motor incoordination is well modeled by the knock-in mice, which have a similar repeat size. It was not attributed to muscle wasting or paralysis, as no alteration between wild-type and mutants in the grip strength and inverted screen test was noted (Figure 26, Figure 28). The late-onset phenotype mirrors the human disorder faithfully, and it is marked by a similarly slow progression as in SCA2.

When homozygous mice were already symptomatic, heterozygous mice still performed equally well as WT mice (Figure 24). Similarly, also other studies on SCA mouse models documented that mice homozygous for the expanded allele show a stronger phenotype than heterozygous mice (Aguiar *et al*. 2006, Huynh *et al*. 2000, Yoo *et al.* 2003). Transgenic

SCA2 homozygous mice that express a full-length human CAG58-*ATXN2* cDNA showed motor incoordination already at 16 weeks, while heterozygous animals performed worse only by 26 weeks (Huynh *et al*. 2000). Similar results were obtained for transgenic mice with an *ATXN2* expansion of 75 CAGs (Aguiar *et al*. 2006) and also homozygous Sca7Q266 mice were more severely affected than their heterozygous littermates (Yoo *et al*. 2003). The expression levels of the expanded ATXN2 might thus influence the onset of neurological symptoms, probably not allowing the development of motor incoordination in heterozygous CAG1/CAG42 mice during their limited lifespan. While most SCA2 patients are heterozygous, few reports on homozygous patients shed further light on that issue. Two Indian homozygous SCA2 patients (35/37 and 36/39 CAGs) had the earliest age of onset from all affected family members with similar CAG expansion sizes (Ragothaman *et al.* 2004), and also patients with MJD/SCA3, SCA6 and DRPLA were reported to have an earlier disease onset when being homozygous (Kato *et al.* 2000, Sato *et al.* 1995, Sobue *et al.* 1996). In contrast, the age of onset was not remarkably altered in one Japanese (39/39 CAGs) and two Hungarian (both 33/35 CAGs) SCA2 patients compared to their heterozygous family members (Hoche *et al.* 2011, Sasaki *et al.* 1998). Together with the data obtained in mice, a gene dosage effect, where an additional copy of expanded ATXN2 leads to an earlier disease onset is plausible for these knock-in mice.

Even though the knock-in mice had a cerebellar deficit by 18 months of age, they could still improve their motor performance when they were trained (Figure 25). This is in agreement with the SCA knock-in models Sca1Q154 and Sca7Q266 (Watase *et al*. 2002, Yoo *et al*. 2003). At that time, when the mice present with a cerebellar deficit, training still improves their motor coordination. Interestingly, a recent study shows that training not only improves cerebellar function, but also increases survival rates in Sca1Q154 mice (Fryer *et al.* 2011). This effect could be ascribed to a differential regulation of the ATXN1 interactor Capicua, whose reduced expression alleviates the disease phenotype (Fryer *et al*. 2011).

The gait abnormalities, from which SCA2 patients also suffer, were not detectable in the knock-in mice up to 24 months of age (Figure 27). The stride length of transgenic SCA2 mice was reduced at the same time as first coordination problems occurred (Huynh *et al*. 2000), while in Sca1Q154 and Sca7Q266 knock-in mice, gait abnormalities occurred later than the motor incoordination. Possibly, the SCA2 knock-in mice do not show gait alterations during their short lifespan, potentially reflecting the more physiological disease course in knock-in mice in comparison to transgenic mice. As assessed by the open field test (Table 19), knock-in mice were as active as their wild-type littermates, indicating that Parkinsonism is not a part of the SCA2 pathology up to this time point. This is in agreement with data that show that pure CAG repeats, as in the case of the knock-in mice, lead to a cerebellar phenotype,

while CAA-interrupted CAG repeats in the pathological expansion range manifest as Parkinsonism (Charles *et al*. 2007, Kim *et al*. 2007, Payami *et al*. 2003, Shan *et al*. 2001).
No phenotypic changes were observed regarding the fertility and survival rates in the knock-in mice. In contrast to Ataxin-2 deficient mice that show an increased embryonic lethality *in utero*, the knock-in mice had no genotype or sex ratio aberration due to the Ataxin-2 expansion (Table 16). During the limited lifespan of the knock-in mice, no change in the survival rates was detected (Figure 29). However, as patients die due to respiratory failure during the end stages of SCA2, it is likely that this would be the ultimate cause of death in the knock-in mice if they lived long enough. Similarly, also the Sca1Q154 knock-in mice suffer, as SCA1 patients, from respiratory dysregulation prior to death (Jafar-Nejad *et al.* 2011).

Aggregation

First histopathological changes in the cerebellar Purkinje neurons of the knock-in mice were observed at the age of 14 months when cytoplasmic ATXN2 aggregates formed in individual neurons. This phenomenon preceded the first motor symptoms that appeared at 18 months of age and further progressed over time. Most neurons were affected by an ATXN2 aggregation at 24 months (Figure 40 A-L). Aggregate formation in brain neurons is widely detected in polyglutamine patients and mouse models and is part of the gain-of-function mechanism. While most polyglutamine disorders have nuclear inclusions, a cytoplasmic ATXN2 aggregation is common in SCA2 Purkinje neurons and also the transgenic mouse model manifested that feature (Huynh *et al*. 2000), which is in concordance with the obtained data. Other knock-in mouse models developed nuclear microaggregates and inclusion bodies together with or after the onset of motor symptoms (Lin *et al*. 2001, Menalled *et al.* 2002, Watase *et al*. 2002, Yoo *et al*. 2003), which led to the hypothesis that aggregate formation is unlikely to initiate neuronal dysfunction or to be directly toxic to the neuron but is rather a by-product or even cytoprotective (Arrasate *et al*. 2004, Saudou *et al*. 1998, Slow *et al*. 2005). Despite the fact that aggregate formation in the SCA2 knock-in mice precede the motor symptoms, the data from other knock-in mice argue against the hypothesis that aggregates in polyglutamine disorders are required for neuronal dysfunction. Still, the ATXN2 aggregation in SCA2 appears to be a disease event which mirrors the earliest motor manifestation and correlates with progression.

Molecular characterization

Beside the observed gain-of-function mechanisms, also partial loss-of-function mechanisms might contribute to SCA2 in this mouse model.

The homologous recombination event necessary for the introduction of the CAG repeat can possibly interfere with *Atxn2* expression and therefore lead to a loss of mRNA transcript and/or protein. The apparent Ataxin-2 mRNA and protein expression in cerebellum, cortex and MEF tissue demonstrates their stability, and the reduced electrophoretic mobility of the ATXN2 protein from homozygous and heterozygous mice in Western Blot experiments is attributed to the polyglutamine expansion (Figure 21, Figure 22, Figure 31, Figure 32, Figure 36, Figure 37). While the effect in MEFs was only minor, a partial loss of soluble ATXN2 was observed in spite of elevated mRNA levels, in a quite constant manner in cerebellum and cortex in all ages (6 weeks, 6 months and 18 month). Also in SCA2 patient brain, expanded ATXN2 levels appear slightly reduced in the cortex of a heterozygous patient, even though this effect was not further described in these studies (Huynh *et al.* 1999, Huynh *et al*. 2000) or validated in others. The elevation of *Atxn2* mRNA in the knock-in mice might thus be a brain-specific mechanism to compensate the reduced ATXN2 protein levels. Whether compensation on mRNA level is common in SCA2 patients was not investigated to date. It is conceivable that an enhanced degradation of the expanded ATXN2 occurs to prevent neuronal cell damage. In fact, many polyQ proteins are ubiquitinated and the ubiquitin-proteasome pathway plays a crucial role in the clearance of the misfolded polyQ proteins (Bauer & Nukina 2009). Strikingly, the mRNA and protein expression changes got stronger over time, which might explain or be part of the late-onset appearance of SCA2.

The reduced ATXN2 protein levels are particularly interesting, since in other polyQ neurodegenerative diseases some minor symptoms have clearly been attributed to a partial loss-of-function mechanism. For example, the overexpression of the ATXN1 paralog ATXN1L, which shares several conserved domains and its interaction partners with ATXN1, could partially suppress the phenotype and neuropathology in the Atxn1Q154 mouse model with ATXN1L duplication (Bowman *et al*. 2007). These observations make knock-in models in particular interesting to study loss-of-function mechanisms contributing to polyglutamine diseases.

Repeat stability

While aspects like phenotype and aggregate formation are well reproduced in the knock-in mice, the model has also some limitations. The repeat size was recorded across 9 generations and was found to be stably transmitted (Figure 20). This is conjunction with reports of the other two SCA2 mouse models, where a stable transmission of the repeat over several generations was documented (Aguiar *et al*. 2006, Huynh *et al*. 2000) and is thus likely to be a general feature in SCA2 mouse models. In contrast, the repeat in SCA2 patients is not stably transmitted and shrinks or expands in successive generations with a higher paternal than maternal instability (Giunti *et al.* 1998, Pujana *et al*. 1999). Thus,

although the ATXN2 triplet repeat is transmitted stably across generations in this mouse, in contrast to humans, this may be an advantage for the long term comparability of data from this knock-in model. A possible reason for the observed repeat stability in the mice and instability in humans might be the contribution of *cis*-elements such as the repeat flanking sequence that can determine the levels of instability of identical repeat sequences at different loci (Pearson *et al.* 2005). For instance, the repeat instability seen in myotonic dystrophy can be reproduced in a transgenic mouse model with an insertion of the repeat sequence that is flanked by large human genomic sequences (Seznec *et al.* 2000).
Another limitation is attributed to the fact that the motor symptoms are not detected before 18 months in the mice which makes studies very time-consuming. Thus, the generation of a mouse model with a bigger repeat size and therefore earlier age of disease onset would be advisable. Indeed, our group is currently generating another Ataxin-2 knock-in mouse with an expansion size of approximately 100 CAGs to trigger an earlier disease onset.

In summary, the knock-in mice model in a faithful fashion the gain-of-function mechanism in SCA2 by means of body weight reduction, late-onset motor phenotype and histopathological changes in the cerebellum. The loss-of-function mechanism is represented by the reduced ATXN2 protein levels, a feature that transgenic SCA2 mouse models are not able to represent. However, not all aspects are comparable to humans. The repeat is stable in mice in contrast to humans. This may be seen as an advantage, since studies on the mice will guarantee the long term comparability of the obtained data.

4.1.2 MEFs as model for SCA2

Since patient material from living humans to study neurodegenerative diseases can only be obtained by taking skin biopsies, the use of MEFs as a model system to compare data obtained from human and mouse is particularly attractive. To understand the regulation of mRNA and protein levels in this non-neuronal tissue and whether it is comparable to those of the brain, Ataxin-2 and Pabpc1 mRNA and protein levels were analyzed (Figure 31, Figure 32). Only PABPC1 protein levels were regulated in MEFs, while a marked regulation of Ataxin-2 and Pabpc1 mRNA and protein was detected in the brain. These relatively mild effects might be explained by the robustness of fibroblasts (Auburger *et al.* 2012) and might underline the selective vulnerability of the CNS in SCA2.
Upon ATXN2-deficiency, the ER-stress response was impaired and the phosphorylation levels of the key translation molecule S6 strongly elevated. The corresponding analyses in CAG42-MEFs did not reveal any alterations in these two processes (Figure 33, Figure 34),

indicating that those processes might not be affected early-on in the SCA2 disease course. As no advancing conclusions can be drawn from these investigations, measurable effects could be triggered by applying different stressors (e.g. serum deprivation) or by generating MEFs with a longer CAG repeat tract.

4.2 Insights into pathomechanisms contributing to SCA2

The availability of a good SCA2 mouse model that presents not only with a behavioural phenotype but is also characterized by early molecular changes, allows now the investigation of pathomechanisms contributing to the development of SCA2. First of all, the impact of expanded Ataxin-2 on transcript levels is discussed on the basis of results obtained by genome-wide Microarray analyses and qPCR experiments at different ages. Next, the consequences of aggregate formation and protein insolubility for the cerebellar Purkinje neurons in comparison to the largely unaffected cortex are regarded. Furthermore, gain- and loss-of-function mechanisms contributing to SCA2 are being depicted.

4.2.1 Expanded *Atxn2* mediates gain- and loss-of-function mechanisms

A previous genome-wide transcriptome survey in symptomatic Ataxin-2 knock-out mice demonstrated a strong impact on the transcriptional regulation upon Ataxin-2 loss: a dysregulation of 377 genes (Lastres-Becker, unpublished data). The scarcity of effects due to the ATXN2 expansion for mRNA levels in presymptomatic and symptomatic knock-in mice was thus surprising in view of the ATXN2 role in RNA processing. This could be seen as evidence that rather early-on gain-of-function mechanisms on protein level contribute to the disease course, while transcriptional dysregulation exerts a minor effect during this disease stage. Two *Atxn2* neighbouring genes, however, were highly significant, reproducible and specifically dysregulated in 18 months old mice. Three different hypotheses may explain these transcription effects with specificity to the *Atxn2* locus. Firstly, it is conceivable that the knock-in targeting approach has modified the *Atxn2* locus, but the facts that the selection markers were almost completely removed and that this locus effect was not detectable in the transcriptome data at 6 months age argue against this notion. Secondly, notions have been discussed that the abnormal DNA structure of a CAG expansion could exert a progressive influence on chromatin structure (Everett & Wood 2004); indeed, polyglutamine expansions of the SCA7 disease protein, which is a component of a histone acetyltransferase complex,

was shown to result in aberrant chromatin (McCullough & Grant 2010). However, such effects were not confined to the surrounding locus and represented random toxic side-effects on unrelated proteins rather than an influence on the disease protein and its function. Thirdly, it is possible that the genes that surround the *Atxn2* locus are interacting in a common pathway and that feedback-mechanisms regulate their expression in dependence on ATXN2 function. This is potentially the case for FBXW8 which was found to be upregulated specifically in the cerebellum of old CAG42 mice (Table 20, Table 21). FBXW8 is a member of the F-box protein family which play a role in the ubiquitin-proteasome pathway as part of a SCF (SKP1-CUL1-F-box)-type ubiquitin-E3-ligase complex which attaches ubiquitin onto a substrate to mark it for degradation (Ho *et al*. 2008). *In vitro* experiments indeed demonstrated that an FBXW8 induction might reduce excess ATXN2, an effect that was even stronger for expanded ATXN2 (M. Heck dissertation, in preparation). Another recent study further implicated FBXW8 to act together with Cul7 in the promotion of dendrite growth and arborisation of mammalian neurons. During later developmental time-points, endogenous FBXW8 levels were found to be relatively low, while an additional exogenous FBXW8 expression significantly increased dendrite length (Litterman *et al.* 2011). The FBXW8 upregulation in the knock-in mice might thus be a compensatory cellular effort to degrade the expanded and toxic ATXN2 on the one hand, and to slow or inhibit the degeneration of the dendrites and hence dendritic arborisation loss, which accompany the SCAs, on the other hand. Both mechanisms might thus counteract the gain-of-function of expanded ATXN2 to postpone the onset of pathology. Therefore, FBXW8 represents a promising molecular target for neuroprotective approaches. Further studies are necessary to describe this connection in more detail and to gain further mechanistic insights. Is there a direct interaction between FBXW8 and ATXN2? Is the upregulation specific to expanded Ataxin-2; are other polyglutamine expansion disease proteins like Huntingtin and Ataxin-1 targets of FBXW8? Are also other members of the SCF-complex upregulated, like Cul7; FBXW8 is the only F-box protein known to date to interact with Cul7 (Dias *et al.* 2002, Tsutsumi *et al.* 2008)? Are other F-box protein family members involved in the degradation of ATXN2?

Further functions implicate FBXW8 in growth control in parallel to modulating levels of insulin-like growth factor binding protein 1 and 2 (Tsutsumi *et al*. 2008). It is interesting to note that ATXN2 and the F-box protein FBXW7 (SEL-10) interact with another neuroprotective ubiquitin-E3-ligase, PARKIN (Ho *et al*. 2008, Huynh *et al.* 2007).

An example for a possible loss-of-function mechanism contribution to SCA2 visible on transcript level might be *Plastin-3* (*T-Plastin*). Proper actin cytoskeleton function is in part maintained by the actin-binding proteins to which the Plastins belong. Plastin-3 is the isoform

that is mainly expressed in neurons (Shinomiya 2012). A previous study demonstrated that ATXN2 is relevant in plastin-associated pathways and that the overexpression of ATXN2 results in elevated Plastin-3 levels (Ralser *et al*. 2005b). Correspondingly, the loss of ATXN2 led to diminished *Plastin-3* levels in the cerebellum of *Atxn2*-KO mice (Table 24), while no change was observed in the liver tissue. Also, in the knock-in mice that present with reduced ATXN2 protein levels, a specific and significant reduction in the cerebellum at old age was detected, while neither cortex nor liver *Plastin-3* levels were altered (Table 22). Thus, reduced *Plastin-3* levels might be a specific response of the cerebellum due to absent or reduced ATXN2 levels. However, whether also Plastin-3 protein levels are consequently diminished was not investigated in this thesis. Interestingly, elevated Plastin-3 expression is a protective modifier for the motoneuron disease SMA (spinal muscular atrophy) which is caused by the homozygous deletion of the survival motor neuron 1 gene (*SMN1*). Axon length and outgrowth of motoneurons appear ameliorated by elevated Plastin-3 levels (Oprea *et al.* 2008). It is conceivable that Plastin-3 has also beneficial effects on the cerebellar neurons and its reduction might reflect an early sign of aberrant neuronal processes finally leading to Purkinje cell dysfunction.

4.2.2 Depletion of PABPC1 in Purkinje cells due to aggregation might contribute to the cerebellar vulnerability of SCA2

It was demonstrated in this thesis that cerebellar and cortical ATXN2 and PABPC1, the latter being a key molecule for translation initiation, get progressively insoluble with age, due to aggregate formation. The cellular answer to cope with this stress in the vulnerable cerebellum was different from that of the largely unaffected cortex. In the following, these differences between the cerebellum and cortex are being discussed and further gain- or loss-of-function mechanisms contributing to SCA2 are depicted.

In experiments where cerebellum and cortex tissue were directly compared, the molecular changes observed appeared always earlier in the cortex than in the cerebellum: Elevated *Atxn2* mRNA levels were detected in the cortex already by 6 weeks, those in the cerebellum by 6 months; elevated *Pabpc1* levels were elevated in cortex at 18 months age, those in the cerebellum were unaltered; significantly reduced ATXN2 protein levels were detectable in the cortex by 6 months, in the cerebellum by 18 months (Figure 36, Figure 37). Within the cerebellum, ATXN2 is mainly expressed in the Purkinje neurons which comprise only a small minority of cerebellar cells (Huynh *et al*. 1999) and the experiments were performed in whole cerebellar extracts. This might have masked the effects at first. In contrast, ATXN2

expression is widespread through neuron populations of several layers in the cortex (compare Allen brain atlas).

As described in section 4.1.1, progressive ATXN2 aggregate formation was observed in the knock-in cerebellum which is common in SCA2. For the first time, also the ATXN2 interaction partner PABPC1 was documented to be sequestered into them with a similar pattern as ATXN2: the PABPC1-containing aggregates were cytoplasmic, appeared before the first motor symptoms and progressed over time (Figure 40 M-R). However, it is unlikely that the whole translation initiation machinery is recruited to the aggregates during the early disease course, as the ribosomal protein S6 and eIF4E were not found to relocalize until 24 months (Figure 45 A-D). An increase in insolubility of ATXN2 and PABPC1 was observed with temporal dynamics similar to that of the aggregate formation (Figure 39). These results were further corroborated in a human cell line and demonstrated that excess ATXN2 becomes insoluble and subsequently recruits PABPC1 into insolubility (Figure 42). The recruitment of PABPC1 is probably mediated by its direct interaction with ATXN2 and not solely via co-aggregation with ATXN2 (Figure 43). This progressive insolubility and aggregate formation probably corresponds to the toxic gain-of-function which was shown to drive disease progression in other polyQ disorders (see also section 4.1.1).

What might be the consequences for the Purkinje neuron when ATXN2 and PABPC1 are sequestered into aggregates? The cerebellar and cortical soluble ATXN2 levels are diminished already early on and this effect persists until old age. Thus, the insolubility and sequestration into aggregates of ATXN2 is not the primary cause for the reduced ATXN2 levels at young age, but might reinforce that effect at old age. The *Atxn2* mRNA elevation might thus be a general compensatory effort of the cerebellar and cortical cells to the reduced ATXN2 levels. At old age however, when ATXN2 and PABPC1 aggregates are already widespread, cerebellar and cortical neurons seem to cope with the unavailability of soluble ATXN2 and PABPC1 differently. While cerebellar soluble PABPC1 is reduced at this time point, cortical PABPC1 levels are elevated. Nonhoff *et al*. demonstrated that reduced ATXN2 levels lead to elevated PABPC1 levels and vice versa within a cell (Nonhoff *et al*. 2007), a cellular effort that was also reproduced in this thesis on mRNA and protein level (Figure 42). This probably normal compensatory cellular effort was thus observed in the cortex, where Pabpc1 mRNA and protein were significantly upregulated at old age. However, in the cerebellum, no change on mRNA level and even a reduction of soluble PABPC1 was observed, possibly indicating that the cerebellum fails to activate mechanisms necessary to counteract the reduced PABPC1 levels within its neurons at this early time point during the disease course. This may possibly be due to a maximal PABPC1 expression in cerebellar cells that cannot be enhanced further. The reduced PABPC1 levels in the cerebellum could

thus indicate why the cerebellum is particularly vulnerable and further reflect another loss-of-function mechanism contributing to SCA2.

As the reduction of ATXN2 normally leads to the elevation of PABPC1 and vice versa, and because the Purkinje cells possibly fail to activate this mechanism, they have to cope with both, reduced ATXN2 and reduced PABPC1 levels. Several scenarios are conceivable how this depletion might influence the cellular metabolic balance – especially that of the mRNA metabolism – finally leading to dysfunctional Purkinje neurons and ultimately motor incoordination. First scenario: as key molecule for translation initiation, the reduced amounts of PABPC1 might disrupt proper translation as mRNA circularization is no longer warranted. Additionally, PABPC1 binding to the 3' poly(A)-tail usually protects it from nucleases thus leading to enhanced mRNA degradation upon PABPC1 reduction. Both facts are likely to be critical for the Purkinje cells with their large ribosomal machinery. Furthermore, PABPC1 depletion was shown to result in mammalian cell death (Thangima Zannat *et al.* 2011). How ATXN2 acts on translation is not clear to date, however, if it acts as a translational enhancer and stabilizes mRNAs with long poly(A)-tails (see section 4.3.1 and 4.3.2), its lack might further contribute to a translational dysregulation. Second scenario: Stress granules (SGs) are distinct sites in the cytoplasm that form during conditions of cell stress to stall temporarily translationally active mRNP-ribosome complexes so that the cells' resources are free to translate proteins necessary to counteract that stress (Anderson & Kedersha 2008). ATXN2 is also part of the SGs and its reduction impairs SG assembly (Nonhoff *et al*. 2007). This possibly leads to an unbalanced stress response in Purkinje cells due to the ATXN2 reduction. Third scenario: the Lsm-domains in ATXN2 are generally found in proteins that function in mRNA-splicing (Albrecht *et al*. 2004) and the Ataxin-2-binding protein 1 (A2BP1/FOX1) is a well-established splicing modulator (Gehman *et al.* 2011, Underwood *et al*. 2005). ATXN2 reduction potentially leads to aberrant splicing of the target mRNAs. Forth scenario: ATXN2 might modulate transcription itself, since it was shown to relocalize to the nucleus and control its own expression (Hallen *et al*. 2011). Fifth scenario: As ATXN2 was implicated in the miRNA-mediated translational repression of several miRNA-target mRNAs in *Drosophila* to influence long-term memory (McCann *et al*. 2011) its lack might lead to aberrant synaptic function.

Additionally, intermediate expansions in ATXN2 are a risk factor for ALS, which can be caused by mutations in the RNA-binding protein TDP-43 (Elden *et al*. 2010). Both proteins interact with each other dependent on RNA, further indicating this to be a crucial aspect of ATXN2 effects.

The way the different brain regions cope with the pathogenic effect of expanded glutamine-tracts is indeed crucial and contributes to their vulnerability. The reduction of the ATXN1 interactor and stabilizer 14-3-3 ameliorated cerebellar pathology and the motor phenotype,

but not the brainstem pathology (e.g. weight loss and respiratory dysfunction) in Sca1Q154 mice. This was attributed to the fact that the 14-3-3 reduction diminished the ATXN1 levels and its incorporation into large toxic complexes only in the cerebellum but not in the brainstem (Jafar-Nejad *et al*. 2011).

Were other proteins, known to colocalize to aggregates, redistributed in the Purkinje neurons? P62 is a protein that plays a role in protein degradation and aggresome formation and was found to colocalize to cytoplasmic or nuclear neuronal inclusions in SCA6 and SCA3 patients, respectively (Seidel *et al.* 2009, Seidel *et al*. 2011). A colocalization of p62 to aggregates in the cerebellum of old knock-in mice was not observed (Figure 45 E-F). This could indicate that a p62 relocalization is a rather late disease event. Also, in R6/2 Huntington transgenic mice, p62 localized to aggregates and was apparent at the end stages of the disease (Nagaoka *et al.* 2004). On the other hand, p62 abundance in aggregates in SCA2 might be a rare event, like the abundance of ubiquitin that was found only in a few pontine neurons and never in Purkinje cells (Koyano *et al.* 1999).

In summary, possible gain- and loss-of function mechanisms contributing to SCA2 could be described in this thesis which gave first insights on the specific vulnerability of the cerebellum. The ATXN2 and PABPC1 aggregate formation/insolubility lead specifically in the cerebellum to soluble PABPC1 depletion at old age, possibly resulting in aberrant mRNA translation/decay which might lead to Purkinje cell dysfunction. The upregulation of FBXW8 specifically in the cerebellum might then be a compensatory effort to reduce the toxic expanded ATXN2 and mediate a neuroprotective role.

4.3 Functional analyses to gain insight into the role of ATXN2

4.3.1 ATXN2 might act as a translational enhancer

To get a better understanding of the SCA2 underlying disease mechanisms, it is indispensable to broaden the current knowledge about the physiological function of ATXN2. It is well-established that ATXN2 exerts a role in translation as it directly interacts with PABPC1 and assembles with polyribosomes via its Lsm-domains (Mangus *et al*. 1998, Satterfield & Pallanck 2006). Furthermore, it is part of a complex comprising the 48S-preinitiation complex members eIF4G, eIF3B, eIFA1 and RPS6 (Figure 47, Lastres-Becker in preparation and Figure 53) and migrates together with them into stress granules (Nonhoff *et al*. 2007), which emphasizes its function in translation initiation. However, the

question arises which exact role it exerts in translation initiation; does ATXN2 act as a translational enhancer or repressor?

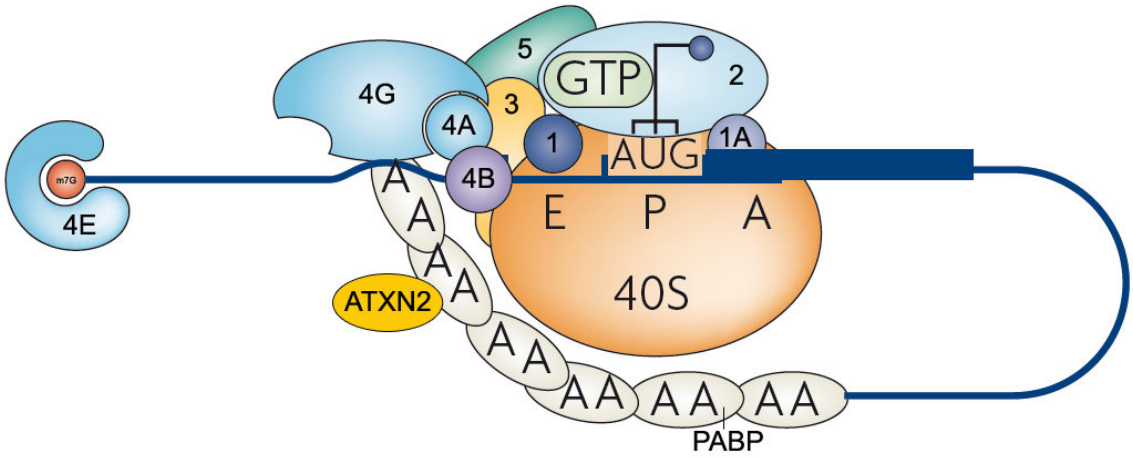

Figure 53. The putative ATXN2 interaction at the 48S preinitiation complex. (according to Lastres-Becker *et al.*, in preparation; adapted from (Jackson *et al*. 2010).

This thesis and previous data showed that the ATXN2 absence leads to an abnormally high phosphorylation of the ribosomal protein S6 (RPS6) and 4E-BP1 in *Atxn2*-KO MEFs (Lastres-Becker in preparation and Figure 48). Both proteins are key-molecules for the rate-limiting initiation step and are phosphorylated in response to mitogens, growth factors and tyrosine kinases to induce translation (Figure 54) (Frederickson & Sonenberg 1992, Richter & Sonenberg 2005).

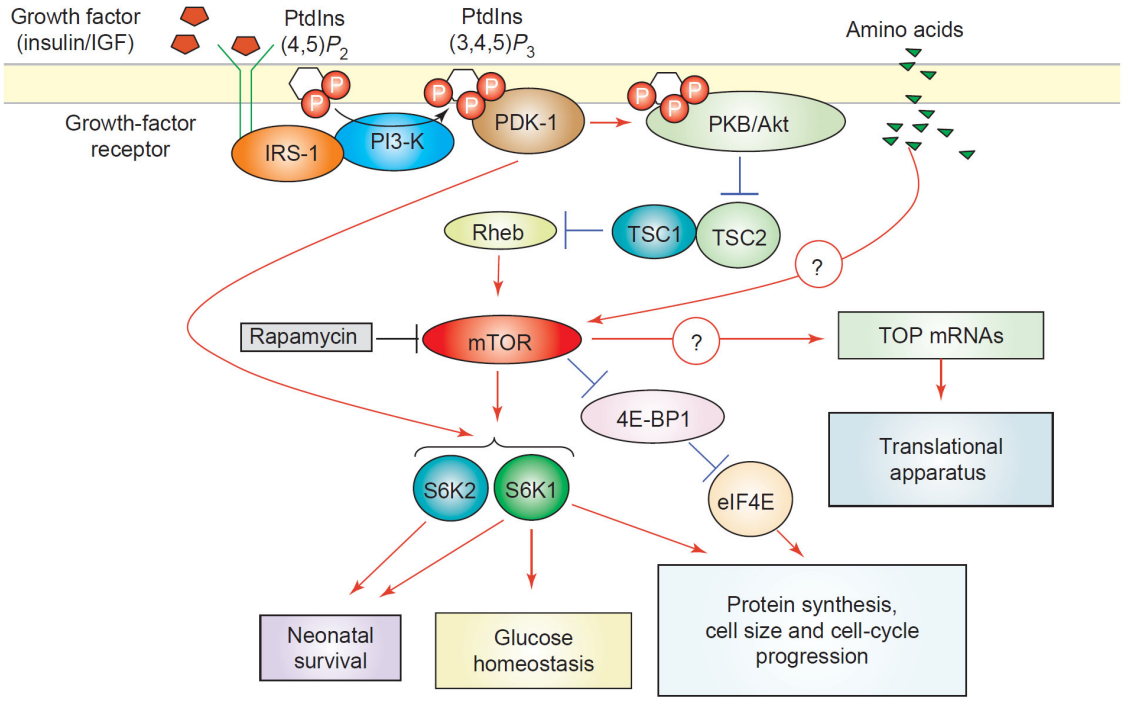

Figure 54. The mTOR/PI3K pathway plays a central role in the regulation of cell growth and cell division. (Ruvinsky & Meyuhas 2006).

The phosphorylation of RPS6 determines the cell size, which was assessed in S6-kinase-deficient mice (S6K$^{-/-}$) and RPS6$^{-/-}$ mice, whose RPS6-phosphorylation sites are mutated and thus no longer phosphorylable. Both mutants manifest with a reduced cell size of the pancreatic ß-cells and MEFs, whereas the population doubling levels of primary MEFs were comparable to those of WT animals (Meyuhas & Dreazen 2009, Pende *et al.* 2000, Ruvinsky *et al.* 2005, Shima *et al.* 1998). Additionally, S6K$^{-/-}$ mice were smaller at birth due to a reduced size of all organs (Shima *et al*. 1998). Even though the cell size was not determined in *Atxn2*-KO MEFs, the elevated S6-phosphorylation did not alter population doubling (Figure 50), which is in agreement with the data of S6K$^{-/-}$ and RPS6$^{-/-}$ mice. However, even with elevated S6-phosphorylation, *Atxn2*-KO MEFs had reduced global protein synthesis rates (Figure 49) and their polysome assembly was reduced in comparison to WT-MEFs (Lastres, in preparation) which indicate an impairment of active protein translation. Contrarily, protein synthesis rates in RPS6$^{-/-}$ MEFs are increased possibly compensating enhanced protein degradation (Ruvinsky *et al*. 2005). The elevated phosphorylation of S6 might be a compensatory mechanism to overcome the reduced global protein synthesis rates in *Atxn2*-KO MEFs.

The elevated S6-phosphorylation can further be linked to the increased insulin levels in the pancreas, hyperinsulinaemia and insulin resistance of *Atxn2*-KO mice (Lastres-Becker *et al*. 2008a), as the reduced size of the pancreatic ß-cells in RPS6$^{-/-}$ and S6K$^{-/-}$ mice leads to an insufficient insulin secretion and thus to an impaired glucose homeostasis and

hypoinsulinaemia (Pende *et al*. 2000, Ruvinsky *et al*. 2005). Furthermore, S6K$^{-/-}$ mice are characterized by a reduced body weight when maintained on a high fat diet due to an increased metabolic rate, while WT littermates rapidly gain weight with a concomitantly increase in S6K activity (Um *et al.* 2004). Similarly, *Atxn2*-KO mice are obese, which might arise from a lower basal metabolic rate (Lastres-Becker *et al*. 2008a). Additionally, the increased phosphorylation of 4E-BP in the *Atxn2*-KO MEFs (Lastres, in preparation) might further account for the metabolic changes in the mice. In contrast to the *Atxn2*-KO phenotype, mice deficient for 4E-BP present with an increase in the metabolic rate, reduced adipose tissue and hypoglycemia (Tsukiyama-Kohara *et al.* 2001).

Even though RPS6 does not regulate the translation of 5' TOP mRNAs directly, their translation and S6K activity/RPS6-phosphorylation correlate closely with each other (Meyuhas & Dreazen 2009). 5' TOP mRNAs bear an oligopyrimidine tract at their 5'-terminus (5' TOP motif) which builds their *cis*-regulatory element for translation. The family is comprised of proteins necessary to build up the translation machinery, including ribosomal proteins, initiation factors and PABPC1 among others (Meyuhas & Dreazen 2009). Indeed, a loss of ATXN2 in mice results in a consistent elevation of the transcript levels of ribosomal proteins and initiation factors (Fittschen dissertation 2008) as well as an elevation of *Pabpc1* mRNA expression in liver and cerebellum (Table 24) and an increased protein expression in the liver (Fittschen dissertation 2008). Whether PABPC1 is also elevated in *Atxn2*-KO cerebellum was not investigated to date, but conceivable as its transcript levels are elevated. The translational elevation of 5' TOP mRNAs is usually further accompanied by an elevation of the rRNA content. An elevation of ribosomal 18S RNA expression could not be corroborated using a commercially available TaqMan assay (Figure 46). In mammalian cells, more than 90% of the total RNA is ribosomal RNA and its content was compared to an endogenous control mRNA which in total account for only up to 5%. This might have led to an inaccurate result. Alternatively, the measurement of the ribosomal RNA-polymerase I activity could provide a more accurate result and clarify whether ribosomal protein elevation is accompanied by an increase of rRNA content in Ataxin-2 deficient mice.

Overall, these data support the concept that ATXN2 regulates translation initiation by acting as a translational enhancer, resulting in decreased global protein synthesis rates when ATXN2 is absent.

However, previous studies in *S. cerevisiae* described ATXN2 rather as a translational inhibitor, as the deletion of its yeast homologue Pbp1 suppresses the effects of Pab1-deletion. An alteration of the global protein synthesis rates was, however, not present (Mangus *et al*. 2004). Furthermore, the overexpression of Pbp1 mimics the effects of the translation elongation inhibitor CHX in strains deficient of the mitochondrial inner membrane protein TIM18 (Dunn & Jensen 2003). On the other hand, a specific positive regulation on

distinct mRNAs was described for *S. cerevisiae* and *C. elegans* (Ciosk *et al.* 2004, Tadauchi *et al.* 2004). Thus, further work will be required to depict the exact role of ATXN2 in translation.

4.3.2 ATXN2 might control proper poly(A)-tail length maturation

Studies in *S. cerevisiae* described a role of Pbp1 to control the extent of mRNA polyadenylation in the nucleus (Mangus *et al*. 1998). This process involves site-specific cleavage of the adjacent mRNA, polymerization of a poly(A)-tail and finally trimming of the newly synthesized tail to its mature length (Mangus *et al*. 2004). To deepen the understanding of ATXN2 function in mammalian poly(A)-tail maturation, mRNAs from MEFs and liver tissue (3 and 6 months) were investigated for their poly(A)-tail lengths (Figure 51, Figure 52). While in 6 months old KO animals the maximum length of poly(A)-tails was not altered, the amount of long poly(A)-tail containing mRNAs (~ 170 nt) from liver was reduced. This is in conjunction with the yeast data, where Pbp1 was described as a negative regulator of the poly(A)-nuclease PAN and its deletion thus leads to a reduced amount of long poly(A)-tails (Mangus *et al*. 2004). Hence, similar to yeast Pbp1, ATXN2 seems to be a factor necessary for proper poly(A)-maturation and thus proper translation by stabilizing mRNAs with long poly(A)-tails. As Pab1 was also described to negatively regulate polyadenylation, the upregulation of PABPC1, translation factors, ribosomal proteins and the accompanying downregulation of the translational repressors Tacc1, Tia-1 and TDP-43 (Lastres-Becker unpublished, Table 24) might reflect a compensatory cellular effort for the reduced translation efficiency.

Overall, these data describe ATXN2 as a translational enhancer, in part by stabilizing mRNAs with long poly(A)-tails.

5 Perspectives

The availability of a valuable *Atxn2*-CAG42-knock-in mouse model allows us to further investigate the early molecular changes leading to SCA2.

The promising target and neuroprotective protein FBXW8 was identified and found to be upregulated specifically in the old cerebellum of CAG42 mice as described in this thesis. Its role in ubiquitination of target proteins might thus play a crucial role in the early disease course of SCA2. These preliminary data should further be extended to confirm the hypothesis that this overexpression is a mechanism to degrade expanded ATXN2 and thus to diminish neuronal damage. The failure of this mechanism in aged SCA2 patients might thus contribute to the clinical picture of SCA2.

Furthermore, the investigation of neuroprotective therapies against SCA2 with the help of the *Atxn2*-CAG42-knock-in mouse, by testing different drugs and their side effects that showed already beneficial effects for other polyQ diseases (e.g. lithium, riluzole) is necessary. However, due to the late manifestation of a cerebellar phenotype at the old age of 18 months, those analyses, would be time-consuming. Therefore, our laboratory is currently generating another *Atxn2*-knock-in mouse containing a repeat of 100 CAGs to trigger an earlier appearance of the phenotype which would facilitate the analyses of neuroprotective therapies.

Additionally, the role of RNA as a driver of toxicity, as was already shown for SCA3, could also be investigated for SCA2 by generating knock-in mice with a CAA-interrupted CAG repeat which presumably results in a milder phenotype. Additionally, a possible phenotypic manifestation of the Parkinson's syndrome in this mouse would allow the investigation of this altered phenotype and its underlying mechanisms.

Even though a function of ATXN2 in translation initiation is plausible, it is currently unknown what its exact function is. It should be clarified whether the ATXN2 association with the 48S-preinitiation complex is mediated through its direct binding to PABPC1 or possibly through RNA. Moreover, it should be determined if ATXN2 is a general initiation factor or only necessary for distinct mRNAs or under distinct conditions like stress.

6 Summary

An expanded polyglutamine tract coded by the first exon of the SCA2 disease protein ATXN2 is responsible for the autosomal dominantly inherited neurodegenerative disease Spinocerebellar Ataxia Type 2 (SCA2). Correspondingly, the human *ATXN2* gene contains a trinucleotide repeat of usually 22 units, whereas affected patients have an expanded repeat beyond 32 units. This is thought to mediate toxic gain-of-functions by protein aggregation, and affect RNA processing, resulting in degenerative processes affecting preferentially the cerebellar neurons. The C-terminal PAM2 domain of ATXN2 mediates a direct interaction to the poly(A)-binding protein (PABPC1). Predominantly, PABPC1 facilitates translation by circularizing the mRNA at initiation, thus allowing ribosomes to run along the transcript for several rounds.

As a faithful animal model, a knock-in mouse was generated by replacing the single CAG of murine *Atxn2* with 42 CAGs, a frequent patient genotype. The first aim was to thoroughly characterize this mouse model. The expansion size was inherited stably and the mice showed a phenotype with reduced body weight and, importantly, late-onset motor incoordination. While Ataxin-2 mRNA levels were increased in the young brain in knock-in animals, protein levels were decreased. Overall, the knock-in mice modelled the phenotype known from SCA2 patients in a faithful manner.

The second aim was to exploit this mouse to evaluate possible disease mechanisms of SCA2. To understand the consequences on mRNA processing, transcriptome profiles at medium and old age in cerebellum, brainstem and liver were studied and demonstrated a selective induction of *Fbxw8* in the old cerebellum. As a component of a ubiquitin-E3-ligase complex, FBXW8 aids in the degradation of target proteins and might thus reduce the toxicity of the expanded ATXN2. Furthermore, it was described to exert a neuroprotective role and could thus exert a beneficial effect for the Purkinje neurons.

It was further found that the solubility of ATXN2 progressively decreases over time and finally results in cytoplasmic aggregate formation in Purkinje neurons: As described above, the *Atxn2* mRNA levels were elevated early in cortex and then later in cerebellum, whereas the protein levels became diminished over time. This observation might explain partial loss-of-function effects in this polyQ disease. The deficit in soluble ATXN2 protein correlated with the appearance of insoluble ATXN2 protein, a progressive feature in cerebellum that might reflect the toxic gain-of-function. In these studies, a special focus was put on the interaction partner and translational activator PABPC1. Since *in vitro* ATXN2 overexpression is known to reduce the levels of PABPC1, its mRNA and protein levels were also documented. In cortex, the levels of PABPC1 transcript, soluble and insoluble protein levels were increased. In contrast, in the more vulnerable cerebellum the progressive insolubility of PABPC1 was

accompanied by decreased levels of soluble protein, while PABPC1 mRNA levels showed no compensatory response. The sequestration of PABPC1 into insolubility by expanded ATXN2 could also be validated in human cell culture. Together with ATXN2, PABPC1 was sequestered into aggregates. Overall, the ATXN2 and PABPC1 insolubility and hence aggregate formation led specifically in the cerebellum to soluble PABPC1 depletion at old age, possibly resulting in aberrant mRNA translation/decay which might lead to Purkinje cell dysfunction.

The third aim was to further describe the physiological function of ATXN2. For this purpose an Ataxin-2 knock-out mouse model was exploited. Previous studies and studies from this thesis demonstrated an increased phosphorylation of the ribosomal protein S6 upon ATXN2 loss. This signal correlates with an increased translation of 5'TOP mRNAs, mRNAs that build up the translational machinery. However, the global protein synthesis levels were diminished. Thus, the net-effect of ATXN2 is possibly the induction of global protein synthesis, while increased S6-phosphorylation in Ataxin-2 deficient mice might be a compensatory effort.

7 References

Abdel-Aleem, A. and Zaki, M. S. (2008) Spinocerebellar ataxia type 2 (SCA2) in an Egyptian family presenting with polyphagia and marked CAG expansion in infancy. *Journal of neurology,* 255, 413-419.

Affaitati, A., de Cristofaro, T., Feliciello, A. and Varrone, S. (2001) Identification of alternative splicing of spinocerebellar ataxia type 2 gene. *Gene,* 267, 89-93.

Aguiar, J., Fernandez, J., Aguilar, A. et al. (2006) Ubiquitous expression of human SCA2 gene under the regulation of the SCA2 self promoter cause specific Purkinje cell degeneration in transgenic mice. *Neuroscience letters,* 392, 202-206.

Al-Ramahi, I., Perez, A. M., Lim, J. et al. (2007) dAtaxin-2 mediates expanded Ataxin-1-induced neurodegeneration in a Drosophila model of SCA1. *PLoS genetics,* 3, e234.

Albrecht, M., Golatta, M., Wullner, U. and Lengauer, T. (2004) Structural and functional analysis of ataxin-2 and ataxin-3. *European journal of biochemistry / FEBS,* 271, 3155-3170.

Anderson, P. and Kedersha, N. (2008) Stress granules: the Tao of RNA triage. *Trends in biochemical sciences,* 33, 141-150.

Arrasate, M., Mitra, S., Schweitzer, E. S., Segal, M. R. and Finkbeiner, S. (2004) Inclusion body formation reduces levels of mutant huntingtin and the risk of neuronal death. *Nature,* 431, 805-810.

Auburger, G., Klinkenberg, M., Drost, J. et al. (2012) Primary Skin Fibroblasts as a Model of Parkinson's Disease. *Molecular neurobiology*.

Auburger, G. W. (2012) Spinocerebellar ataxia type 2. *Handbook of clinical neurology / edited by P.J. Vinken and G.W,* 103, 423-436.

Aziz, N. A., van der Marck, M. A., Pijl, H., Olde Rikkert, M. G., Bloem, B. R. and Roos, R. A. (2008) Weight loss in neurodegenerative disorders. *Journal of neurology,* 255, 1872-1880.

Babovic-Vuksanovic, D., Snow, K., Patterson, M. C. and Michels, V. V. (1998) Spinocerebellar ataxia type 2 (SCA 2) in an infant with extreme CAG repeat expansion. *American journal of medical genetics,* 79, 383-387.

Bauer, P. O. and Nukina, N. (2009) The pathogenic mechanisms of polyglutamine diseases and current therapeutic strategies. *Journal of neurochemistry,* 110, 1737-1765.

Benjamini, Y. and Hochberg, Y. (1995) Controlling the false discovery rate: a practical and powerful approach to multiple testing. *Journal of the Royal Statistical Society Series B,* 57, 289–300.

Bowman, A. B., Lam, Y. C., Jafar-Nejad, P. et al. (2007) Duplication of Atxn1l suppresses SCA1 neuropathology by decreasing incorporation of polyglutamine-expanded ataxin-1 into native complexes. *Nature genetics,* 39, 373-379.

Brook, J. D., McCurrach, M. E., Harley, H. G. et al. (1992) Molecular basis of myotonic dystrophy: expansion of a trinucleotide (CTG) repeat at the 3' end of a transcript encoding a protein kinase family member. *Cell,* 69, 385.

Buitrago, M. M., Schulz, J. B., Dichgans, J. and Luft, A. R. (2004) Short and long-term motor skill learning in an accelerated rotarod training paradigm. *Neurobiology of learning and memory,* 81, 211-216.

Burk, K., Globas, C., Bosch, S., Klockgether, T., Zuhlke, C., Daum, I. and Dichgans, J. (2003) Cognitive deficits in spinocerebellar ataxia type 1, 2, and 3. *Journal of neurology,* 250, 207-211.

Charles, P., Camuzat, A., Benammar, N. et al. (2007) Are interrupted SCA2 CAG repeat expansions responsible for parkinsonism? *Neurology,* 69, 1970-1975.

Ciosk, R., DePalma, M. and Priess, J. R. (2004) ATX-2, the C. elegans ortholog of ataxin 2, functions in translational regulation in the germline. *Development (Cambridge, England),* 131, 4831-4841.

Clark, H. B., Burright, E. N., Yunis, W. S., Larson, S., Wilcox, C., Hartman, B., Matilla, A., Zoghbi, H. Y. and Orr, H. T. (1997) Purkinje cell expression of a mutant allele of SCA1 in transgenic mice leads to disparate effects on motor behaviors, followed by a progressive cerebellar dysfunction and histological alterations. *J Neurosci,* 17, 7385-7395.

Coffee, B., Zhang, F., Warren, S. T. and Reines, D. (1999) Acetylated histones are associated with FMR1 in normal but not fragile X-syndrome cells. *Nature genetics,* 22, 98-101.

Corrado, L., Mazzini, L., Oggioni, G. D., Luciano, B., Godi, M., Brusco, A. and D'Alfonso, S. (2011) ATXN-2 CAG repeat expansions are interrupted in ALS patients. *Human genetics,* 130, 575-580.

Crespo-Barreto, J., Fryer, J. D., Shaw, C. A., Orr, H. T. and Zoghbi, H. Y. (2010) Partial loss of ataxin-1 function contributes to transcriptional dysregulation in spinocerebellar ataxia type 1 pathogenesis. *PLoS genetics,* 6, e1001021.

Cummings, C. J., Mancini, M. A., Antalffy, B., DeFranco, D. B., Orr, H. T. and Zoghbi, H. Y. (1998) Chaperone suppression of aggregation and altered subcellular proteasome localization imply protein misfolding in SCA1. *Nature genetics,* 19, 148-154.

David, G., Abbas, N., Stevanin, G. et al. (1997) Cloning of the SCA7 gene reveals a highly unstable CAG repeat expansion. *Nature genetics,* 17, 65-70.

Derry, M. C., Yanagiya, A., Martineau, Y. and Sonenberg, N. (2006) Regulation of poly(A)-binding protein through PABP-interacting proteins. *Cold Spring Harbor symposia on quantitative biology,* 71, 537-543.

Dias, D. C., Dolios, G., Wang, R. and Pan, Z. Q. (2002) CUL7: A DOC domain-containing cullin selectively binds Skp1.Fbx29 to form an SCF-like complex. *Proceedings of the National Academy of Sciences of the United States of America,* 99, 16601-16606.

Duenas, A. M., Goold, R. and Giunti, P. (2006) Molecular pathogenesis of spinocerebellar ataxias. *Brain,* 129, 1357-1370.

Dunn, C. D. and Jensen, R. E. (2003) Suppression of a defect in mitochondrial protein import identifies cytosolic proteins required for viability of yeast cells lacking mitochondrial DNA. *Genetics,* 165, 35-45.

Elden, A. C., Kim, H. J., Hart, M. P. et al. (2010) Ataxin-2 intermediate-length polyglutamine expansions are associated with increased risk for ALS. *Nature,* 466, 1069-1075.

Emamian, E. S., Kaytor, M. D., Duvick, L. A., Zu, T., Tousey, S. K., Zoghbi, H. Y., Clark, H. B. and Orr, H. T. (2003) Serine 776 of ataxin-1 is critical for polyglutamine-induced disease in SCA1 transgenic mice. *Neuron,* 38, 375-387.

Estrada, R., Galarraga, J., Orozco, G., Nodarse, A. and Auburger, G. (1999) Spinocerebellar ataxia 2 (SCA2): morphometric analyses in 11 autopsies. *Acta neuropathologica,* 97, 306-310.

Everett, C. M. and Wood, N. W. (2004) Trinucleotide repeats and neurodegenerative disease. *Brain,* 127, 2385-2405.

Fisher, C. D., Jackson, J. P., Lickteig, A. J., Augustine, L. M. and Cherrington, N. J. (2008) Drug metabolizing enzyme induction pathways in experimental non-alcoholic steatohepatitis. *Archives of toxicology,* 82, 959-964.

Frederickson, R. M. and Sonenberg, N. (1992) Signal transduction and regulation of translation initiation. *Seminars in cell biology,* 3, 107-115.

Freund, H. J., Barnikol, U. B., Nolte, D., Treuer, H., Auburger, G., Tass, P. A., Samii, M. and Sturm, V. (2007) Subthalamic-thalamic DBS in a case with spinocerebellar ataxia type 2 and severe tremor-A unusual clinical benefit. *Mov Disord,* 22, 732-735.

Fryer, J. D., Yu, P., Kang, H. et al. (2011) Exercise and genetic rescue of SCA1 via the transcriptional repressor Capicua. *Science (New York, N.Y,* 334, 690-693.

Fu, Y. H., Pizzuti, A., Fenwick, R. G., Jr. et al. (1992) An unstable triplet repeat in a gene related to myotonic muscular dystrophy. *Science (New York, N.Y,* 255, 1256-1258.

Gallie, D. R. (1998) A tale of two termini: a functional interaction between the termini of an mRNA is a prerequisite for efficient translation initiation. *Gene,* 216, 1-11.

Gehman, L. T., Stoilov, P., Maguire, J., Damianov, A., Lin, C. H., Shiue, L., Ares, M., Jr., Mody, I. and Black, D. L. (2011) The splicing regulator Rbfox1 (A2BP1) controls neuronal excitation in the mammalian brain. *Nature genetics,* 43, 706-711.

Genis, D., Matilla, T., Volpini, V., Rosell, J., Davalos, A., Ferrer, I., Molins, A. and Estivill, X. (1995) Clinical, neuropathologic, and genetic studies of a large spinocerebellar ataxia type 1 (SCA1) kindred: (CAG)n expansion and early premonitory signs and symptoms. *Neurology,* 45, 24-30.

Ghosh, S. and Feany, M. B. (2004) Comparison of pathways controlling toxicity in the eye and brain in Drosophila models of human neurodegenerative diseases. *Human molecular genetics,* 13, 2011-2018.

Gierga, K., Burk, K., Bauer, M. et al. (2005) Involvement of the cranial nerves and their nuclei in spinocerebellar ataxia type 2 (SCA2). *Acta neuropathologica,* 109, 617-631.

Gispert, S., Kurz, A., Waibel, S. et al. (2012) The modulation of Amyotrophic Lateral Sclerosis risk by ataxin-2 intermediate polyglutamine expansions is a specific effect. *Neurobiology of disease,* 45, 356-361.

Giunti, P., Sabbadini, G., Sweeney, M. G. et al. (1998) The role of the SCA2 trinucleotide repeat expansion in 89 autosomal dominant cerebellar ataxia families. Frequency, clinical and genetic correlates. *Brain,* 121 (Pt 3), 459-467.

Gorgoni, B. and Gray, N. K. (2004) The roles of cytoplasmic poly(A)-binding proteins in regulating gene expression: a developmental perspective. *Briefings in functional genomics & proteomics,* 3, 125-141.

Gwinn-Hardy, K., Chen, J. Y., Liu, H. C. et al. (2000) Spinocerebellar ataxia type 2 with parkinsonism in ethnic Chinese. *Neurology,* 55, 800-805.

Haghighat, A. and Sonenberg, N. (1997) eIF4G dramatically enhances the binding of eIF4E to the mRNA 5'-cap structure. *The Journal of biological chemistry,* 272, 21677-21680.

Hallen, L., Klein, H., Stoschek, C. et al. (2011) The KRAB-containing zinc-finger transcriptional regulator ZBRK1 activates SCA2 gene transcription through direct interaction with its gene product, ataxin-2. *Human molecular genetics,* 20, 104-114.

Harding, A. E. (1993) Clinical features and classification of inherited ataxias. *Advances in neurology,* 61, 1-14.

Heng, M. Y., Detloff, P. J., Paulson, H. L. and Albin, R. L. (2010a) Early alterations of autophagy in Huntington disease-like mice. *Autophagy,* 6, 1206-1208.

Heng, M. Y., Duong, D. K., Albin, R. L., Tallaksen-Greene, S. J., Hunter, J. M., Lesort, M. J., Osmand, A., Paulson, H. L. and Detloff, P. J. (2010b) Early autophagic response in a novel knock-in model of Huntington disease. *Human molecular genetics,* 19, 3702-3720.

Ho, M. S., Ou, C., Chan, Y. R., Chien, C. T. and Pi, H. (2008) The utility F-box for protein destruction. *Cell Mol Life Sci,* 65, 1977-2000.

Hoche, F., Baliko, L., den Dunnen, W. et al. (2011) Spinocerebellar ataxia type 2 (SCA2): identification of early brain degeneration in one monozygous twin in the initial disease stage. *Cerebellum (London, England),* 10, 245-253.

Hornstein, E., Git, A., Braunstein, I., Avni, D. and Meyuhas, O. (1999) The expression of poly(A)-binding protein gene is translationally regulated in a growth-dependent fashion through a 5'-terminal oligopyrimidine tract motif. *The Journal of biological chemistry,* 274, 1708-1714.

Hoshino, S., Imai, M., Kobayashi, T., Uchida, N. and Katada, T. (1999) The eukaryotic polypeptide chain releasing factor (eRF3/GSPT) carrying the translation termination signal to the 3'-Poly(A) tail of mRNA. Direct association of erf3/GSPT with polyadenylate-binding protein. *The Journal of biological chemistry,* 274, 16677-16680.

Huynh, D. P., Del Bigio, M. R., Ho, D. H. and Pulst, S. M. (1999) Expression of ataxin-2 in brains from normal individuals and patients with Alzheimer's disease and spinocerebellar ataxia 2. *Annals of neurology,* 45, 232-241.

Huynh, D. P., Figueroa, K., Hoang, N. and Pulst, S. M. (2000) Nuclear localization or inclusion body formation of ataxin-2 are not necessary for SCA2 pathogenesis in mouse or human. *Nature genetics,* 26, 44-50.

Huynh, D. P., Nguyen, D. T., Pulst-Korenberg, J. B., Brice, A. and Pulst, S. M. (2007) Parkin is an E3 ubiquitin-ligase for normal and mutant ataxin-2 and prevents ataxin-2-induced cell death. *Experimental neurology,* 203, 531-541.

Imataka, H., Gradi, A. and Sonenberg, N. (1998) A newly identified N-terminal amino acid sequence of human eIF4G binds poly(A)-binding protein and functions in poly(A)-dependent translation. *The EMBO journal,* 17, 7480-7489.

Imbert, G., Saudou, F., Yvert, G. et al. (1996) Cloning of the gene for spinocerebellar ataxia 2 reveals a locus with high sensitivity to expanded CAG/glutamine repeats. *Nature genetics,* 14, 285-291.

Irizarry, R. A., Bolstad, B. M., Collin, F., Cope, L. M., Hobbs, B. and Speed, T. P. (2003) Summaries of Affymetrix GeneChip probe level data. *Nucleic acids research,* 31, e15.

Jackson, R. J., Hellen, C. U. and Pestova, T. V. (2010) The mechanism of eukaryotic translation initiation and principles of its regulation. *Nat Rev Mol Cell Biol,* 11, 113-127.

Jafar-Nejad, P., Ward, C. S., Richman, R., Orr, H. T. and Zoghbi, H. Y. (2011) Regional rescue of spinocerebellar ataxia type 1 phenotypes by 14-3-3epsilon haploinsufficiency in mice underscores complex pathogenicity in neurodegeneration. *Proceedings of the National Academy of Sciences of the United States of America,* 108, 2142-2147.

Kato, T., Tanaka, F., Yamamoto, M., Yosida, E., Indo, T., Watanabe, H., Yoshiwara, T., Doyu, M. and Sobue, G. (2000) Sisters homozygous for the spinocerebellar ataxia type 6 (SCA6)/CACNA1A gene associated with different clinical phenotypes. *Clinical genetics,* 58, 69-73.

Kawaguchi, Y., Okamoto, T., Taniwaki, M. et al. (1994) CAG expansions in a novel gene for Machado-Joseph disease at chromosome 14q32.1. *Nature genetics,* 8, 221-228.

Kedersha, N. and Anderson, P. (2009) Regulation of translation by stress granules and processing bodies. *Progress in molecular biology and translational science,* 90, 155-185.

Kiehl, T. R., Nechiporuk, A., Figueroa, K. P., Keating, M. T., Huynh, D. P. and Pulst, S. M. (2006) Generation and characterization of Sca2 (ataxin-2) knockout mice. *Biochemical and biophysical research communications,* 339, 17-24.

Kiehl, T. R., Shibata, H. and Pulst, S. M. (2000) The ortholog of human ataxin-2 is essential for early embryonic patterning in C. elegans. *J Mol Neurosci,* 15, 231-241.

Kim, J. M., Hong, S., Kim, G. P., Choi, Y. J., Kim, Y. K., Park, S. S., Kim, S. E. and Jeon, B. S. (2007) Importance of low-range CAG expansion and CAA interruption in SCA2 Parkinsonism. *Archives of neurology,* 64, 1510-1518.

Koch, P., Breuer, P., Peitz, M. et al. (2011) Excitation-induced ataxin-3 aggregation in neurons from patients with Machado-Joseph disease. *Nature,* 480, 543-546.

Koide, R., Ikeuchi, T., Onodera, O. et al. (1994) Unstable expansion of CAG repeat in hereditary dentatorubral-pallidoluysian atrophy (DRPLA). *Nature genetics,* 6, 9-13.

Koyano, S., Iwabuchi, K., Yagishita, S., Kuroiwa, Y. and Uchihara, T. (2002) Paradoxical absence of nuclear inclusion in cerebellar Purkinje cells of hereditary ataxias linked to CAG expansion. *Journal of neurology, neurosurgery, and psychiatry,* 73, 450-452.

Koyano, S., Uchihara, T., Fujigasaki, H., Nakamura, A., Yagishita, S. and Iwabuchi, K. (1999) Neuronal intranuclear inclusions in spinocerebellar ataxia type 2: triple-labeling immunofluorescent study. *Neuroscience letters,* 273, 117-120.

La Spada, A. R. and Taylor, J. P. (2010) Repeat expansion disease: progress and puzzles in disease pathogenesis. *Nat Rev Genet,* 11, 247-258.

Lagier-Tourenne, C. and Cleveland, D. W. (2010) Neurodegeneration: An expansion in ALS genetics. *Nature,* 466, 1052-1053.

Lastres-Becker, I., Brodesser, S., Lutjohann, D. et al. (2008a) Insulin receptor and lipid metabolism pathology in ataxin-2 knock-out mice. *Human molecular genetics,* 17, 1465-1481.

Lastres-Becker, I., Rub, U. and Auburger, G. (2008b) Spinocerebellar ataxia 2 (SCA2). *Cerebellum (London, England),* 7, 115-124.

Lescure, A., Lutz, Y., Eberhard, D., Jacq, X., Krol, A., Grummt, I., Davidson, I., Chambon, P. and Tora, L. (1994) The N-terminal domain of the human TATA-binding protein plays a role in transcription from TATA-containing RNA polymerase II and III promoters. *The EMBO journal,* 13, 1166-1175.

Lessing, D. and Bonini, N. M. (2008) Polyglutamine genes interact to modulate the severity and progression of neurodegeneration in Drosophila. *PLoS biology,* 6, e29.

Li, J. and Lee, A. S. (2006) Stress induction of GRP78/BiP and its role in cancer. *Current molecular medicine,* 6, 45-54.

Li, L. B., Yu, Z., Teng, X. and Bonini, N. M. (2008) RNA toxicity is a component of ataxin-3 degeneration in Drosophila. *Nature,* 453, 1107-1111.

Lim, J., Crespo-Barreto, J., Jafar-Nejad, P., Bowman, A. B., Richman, R., Hill, D. E., Orr, H. T. and Zoghbi, H. Y. (2008) Opposing effects of polyglutamine expansion on native protein complexes contribute to SCA1. *Nature,* 452, 713-718.

Lin, C. H., Tallaksen-Greene, S., Chien, W. M. et al. (2001) Neurological abnormalities in a knock-in mouse model of Huntington's disease. *Human molecular genetics,* 10, 137-144.

Lin, X., Antalffy, B., Kang, D., Orr, H. T. and Zoghbi, H. Y. (2000) Polyglutamine expansion down-regulates specific neuronal genes before pathologic changes in SCA1. *Nature neuroscience,* 3, 157-163.

Litterman, N., Ikeuchi, Y., Gallardo, G., O'Connell, B. C., Sowa, M. E., Gygi, S. P., Harper, J. W. and Bonni, A. (2011) An OBSL1-Cul7Fbxw8 ubiquitin ligase signaling mechanism regulates Golgi morphology and dendrite patterning. *PLoS biology,* 9, e1001060.

Liu-Yesucevitz, L., Bassell, G. J., Gitler, A. D., Hart, A. C., Klann, E., Richter, J. D., Warren, S. T. and Wolozin, B. (2011) Local RNA translation at the synapse and in disease. *J Neurosci,* 31, 16086-16093.

Livak, K. J. and Schmittgen, T. D. (2001) Analysis of relative gene expression data using real-time quantitative PCR and the 2(-Delta Delta C(T)) Method. *Methods (San Diego, Calif,* 25, 402-408.

Luo, Y. and Goss, D. J. (2001) Homeostasis in mRNA initiation: wheat germ poly(A)-binding protein lowers the activation energy barrier to initiation complex formation. *The Journal of biological chemistry,* 276, 43083-43086.

Mahadevan, M., Tsilfidis, C., Sabourin, L. et al. (1992) Myotonic dystrophy mutation: an unstable CTG repeat in the 3' untranslated region of the gene. *Science (New York, N.Y,* 255, 1253-1255.

Mangus, D. A., Amrani, N. and Jacobson, A. (1998) Pbp1p, a factor interacting with Saccharomyces cerevisiae poly(A)-binding protein, regulates polyadenylation. *Molecular and cellular biology,* 18, 7383-7396.

Mangus, D. A., Smith, M. M., McSweeney, J. M. and Jacobson, A. (2004) Identification of factors regulating poly(A) tail synthesis and maturation. *Molecular and cellular biology,* 24, 4196-4206.

Manto, M. and Marmolino, D. (2009) Cerebellar ataxias. *Current opinion in neurology,* 22, 419-429.

Mao, R., Aylsworth, A. S., Potter, N. et al. (2002) Childhood-onset ataxia: testing for large CAG repeats in SCA2 and SCA7. *American journal of medical genetics,* 110, 338-345.

Matilla, A., Roberson, E. D., Banfi, S. et al. (1998) Mice lacking ataxin-1 display learning deficits and decreased hippocampal paired-pulse facilitation. *J Neurosci,* 18, 5508-5516.

McCann, C., Holohan, E. E., Das, S., Dervan, A., Larkin, A., Lee, J. A., Rodrigues, V., Parker, R. and Ramaswami, M. (2011) The Ataxin-2 protein is required for microRNA function and synapse-specific long-term olfactory habituation. *Proceedings of the National Academy of Sciences of the United States of America,* 108, E655-662.

McCullough, S. D. and Grant, P. A. (2010) Histone acetylation, acetyltransferases, and ataxia--alteration of histone acetylation and chromatin dynamics is implicated in the pathogenesis of polyglutamine-expansion disorders. *Advances in protein chemistry and structural biology,* 79, 165-203.

McMurray, C. T. (1999) DNA secondary structure: a common and causative factor for expansion in human disease. *Proceedings of the National Academy of Sciences of the United States of America,* 96, 1823-1825.
Menalled, L. B., Sison, J. D., Wu, Y., Olivieri, M., Li, X. J., Li, H., Zeitlin, S. and Chesselet, M. F. (2002) Early motor dysfunction and striosomal distribution of huntingtin microaggregates in Huntington's disease knock-in mice. *J Neurosci,* 22, 8266-8276.
Meyuhas, O. and Dreazen, A. (2009) Ribosomal protein S6 kinase from TOP mRNAs to cell size. *Progress in molecular biology and translational science,* 90, 109-153.
Muchowski, P. J. and Wacker, J. L. (2005) Modulation of neurodegeneration by molecular chaperones. *Nature reviews,* 6, 11-22.
Nagafuchi, S., Yanagisawa, H., Sato, K. et al. (1994) Dentatorubral and pallidoluysian atrophy expansion of an unstable CAG trinucleotide on chromosome 12p. *Nature genetics,* 6, 14-18.
Nagaoka, U., Kim, K., Jana, N. R., Doi, H., Maruyama, M., Mitsui, K., Oyama, F. and Nukina, N. (2004) Increased expression of p62 in expanded polyglutamine-expressing cells and its association with polyglutamine inclusions. *Journal of neurochemistry,* 91, 57-68.
Nakamura, K., Jeong, S. Y., Uchihara, T., Anno, M., Nagashima, K., Nagashima, T., Ikeda, S., Tsuji, S. and Kanazawa, I. (2001) SCA17, a novel autosomal dominant cerebellar ataxia caused by an expanded polyglutamine in TATA-binding protein. *Human molecular genetics,* 10, 1441-1448.
Nechiporuk, T., Huynh, D. P., Figueroa, K., Sahba, S., Nechiporuk, A. and Pulst, S. M. (1998) The mouse SCA2 gene: cDNA sequence, alternative splicing and protein expression. *Human molecular genetics,* 7, 1301-1309.
Nishimura, H., Kim, E., Nakanishi, T. and Baba, T. (2004) Possible function of the ADAM1a/ADAM2 Fertilin complex in the appearance of ADAM3 on the sperm surface. *The Journal of biological chemistry,* 279, 34957-34962.
Nonhoff, U., Ralser, M., Welzel, F., Piccini, I., Balzereit, D., Yaspo, M. L., Lehrach, H. and Krobitsch, S. (2007) Ataxin-2 interacts with the DEAD/H-box RNA helicase DDX6 and interferes with P-bodies and stress granules. *Molecular biology of the cell,* 18, 1385-1396.
Nonis, D., Schmidt, M. H., van de Loo, S., Eich, F., Dikic, I., Nowock, J. and Auburger, G. (2008) Ataxin-2 associates with the endocytosis complex and affects EGF receptor trafficking. *Cellular signalling,* 20, 1725-1739.
Oprea, G. E., Krober, S., McWhorter, M. L., Rossoll, W., Muller, S., Krawczak, M., Bassell, G. J., Beattie, C. E. and Wirth, B. (2008) Plastin 3 is a protective modifier of autosomal recessive spinal muscular atrophy. *Science (New York, N.Y,* 320, 524-527.
Ordway, J. M., Tallaksen-Greene, S., Gutekunst, C. A. et al. (1997) Ectopically expressed CAG repeats cause intranuclear inclusions and a progressive late onset neurological phenotype in the mouse. *Cell,* 91, 753-763.
Orozco Diaz, G., Nodarse Fleites, A., Cordoves Sagaz, R. and Auburger, G. (1990) Autosomal dominant cerebellar ataxia: clinical analysis of 263 patients from a homogeneous population in Holguin, Cuba. *Neurology,* 40, 1369-1375.
Orr, H. T. (2012) The cell biology of disease: Cell biology of spinocerebellar ataxia. *The Journal of cell biology,* 197, 167-177.
Orr, H. T., Chung, M. Y., Banfi, S. et al. (1993) Expansion of an unstable trinucleotide CAG repeat in spinocerebellar ataxia type 1. *Nature genetics,* 4, 221-226.
Orr, H. T. and Zoghbi, H. Y. (2007) Trinucleotide repeat disorders. *Annual review of neuroscience,* 30, 575-621.
Pang, J. T., Giunti, P., Chamberlain, S. et al. (2002) Neuronal intranuclear inclusions in SCA2: a genetic, morphological and immunohistochemical study of two cases. *Brain,* 125, 656-663.
Payami, H., Nutt, J., Gancher, S. et al. (2003) SCA2 may present as levodopa-responsive parkinsonism. *Mov Disord,* 18, 425-429.

Pearson, C. E. (2011) Repeat associated non-ATG translation initiation: one DNA, two transcripts, seven reading frames, potentially nine toxic entities! *PLoS genetics,* 7, e1002018.

Pearson, C. E., Nichol Edamura, K. and Cleary, J. D. (2005) Repeat instability: mechanisms of dynamic mutations. *Nat Rev Genet,* 6, 729-742.

Pende, M., Kozma, S. C., Jaquet, M., Oorschot, V., Burcelin, R., Le Marchand-Brustel, Y., Klumperman, J., Thorens, B. and Thomas, G. (2000) Hypoinsulinaemia, glucose intolerance and diminished beta-cell size in S6K1-deficient mice. *Nature,* 408, 994-997.

Perez-Avila, I., Fernandez-Vieitez, J. A., Martinez-Gongora, E., Ochoa-Mastrapa, R. and Velazquez-Manresa, M. G. (2004) [Effects of a physical training program on quantitative neurological indices in mild stage type 2 spinocerebelar ataxia patients]. *Revista de neurologia,* 39, 907-910.

Picciotto, M. R. and Wickman, K. (1998) Using knockout and transgenic mice to study neurophysiology and behavior. *Physiological reviews,* 78, 1131-1163.

Pujana, M. A., Corral, J., Gratacos, M., Combarros, O., Berciano, J., Genis, D., Banchs, I., Estivill, X. and Volpini, V. (1999) Spinocerebellar ataxias in Spanish patients: genetic analysis of familial and sporadic cases. The Ataxia Study Group. *Human genetics,* 104, 516-522.

Pulst, S. M., Nechiporuk, A., Nechiporuk, T. et al. (1996) Moderate expansion of a normally biallelic trinucleotide repeat in spinocerebellar ataxia type 2. *Nature genetics,* 14, 269-276.

Pulst, S. M., Santos, N., Wang, D., Yang, H., Huynh, D., Velazquez, L. and Figueroa, K. P. (2005) Spinocerebellar ataxia type 2: polyQ repeat variation in the CACNA1A calcium channel modifies age of onset. *Brain,* 128, 2297-2303.

Ragothaman, M., Sarangmath, N., Chaudhary, S. et al. (2004) Complex phenotypes in an Indian family with homozygous SCA2 mutations. *Annals of neurology,* 55, 130-133.

Ralser, M., Albrecht, M., Nonhoff, U., Lengauer, T., Lehrach, H. and Krobitsch, S. (2005a) An integrative approach to gain insights into the cellular function of human ataxin-2. *Journal of molecular biology,* 346, 203-214.

Ralser, M., Nonhoff, U., Albrecht, M., Lengauer, T., Wanker, E. E., Lehrach, H. and Krobitsch, S. (2005b) Ataxin-2 and huntingtin interact with endophilin-A complexes to function in plastin-associated pathways. *Human molecular genetics,* 14, 2893-2909.

Ramos, E. M., Keagle, P., Gillis, T. et al. (2012) Prevalence of Huntington's disease gene CAG repeat alleles in sporadic amyotrophic lateral sclerosis patients. *Amyotroph Lateral Scler*.

Ranum, L. P. and Cooper, T. A. (2006) RNA-mediated neuromuscular disorders. *Annual review of neuroscience,* 29, 259-277.

Ravikumar, B., Berger, Z., Vacher, C., O'Kane, C. J. and Rubinsztein, D. C. (2006) Rapamycin pre-treatment protects against apoptosis. *Human molecular genetics,* 15, 1209-1216.

Reynaldo-Arminan, R. D., Reynaldo-Hernandez, R., Paneque-Herrera, M., Prieto-Avila, L. and Perez-Ruiz, E. (2002) [Mental disorders in patients with spinocerebellar ataxia type 2 in Cuba]. *Revista de neurologia,* 35, 818-821.

Richter, J. D. and Sonenberg, N. (2005) Regulation of cap-dependent translation by eIF4E inhibitory proteins. *Nature,* 433, 477-480.

Ristori, G., Romano, S., Visconti, A., Cannoni, S., Spadaro, M., Frontali, M., Pontieri, F. E., Vanacore, N. and Salvetti, M. (2010) Riluzole in cerebellar ataxia: a randomized, double-blind, placebo-controlled pilot trial. *Neurology,* 74, 839-845.

Ross, O. A., Rutherford, N. J., Baker, M. et al. (2011) Ataxin-2 repeat-length variation and neurodegeneration. *Human molecular genetics,* 20, 3207-3212.

Ruvinsky, I. and Meyuhas, O. (2006) Ribosomal protein S6-phosphorylation: from protein synthesis to cell size. *Trends in biochemical sciences,* 31, 342-348.

Ruvinsky, I., Sharon, N., Lerer, T., Cohen, H., Stolovich-Rain, M., Nir, T., Dor, Y., Zisman, P. and Meyuhas, O. (2005) Ribosomal protein S6-phosphorylation is a determinant of cell size and glucose homeostasis. *Genes & development,* 19, 2199-2211.

Sachs, A. B., Davis, R. W. and Kornberg, R. D. (1987) A single domain of yeast poly(A)-binding protein is necessary and sufficient for RNA binding and cell viability. *Molecular and cellular biology,* 7, 3268-3276.

Sahba, S., Nechiporuk, A., Figueroa, K. P., Nechiporuk, T. and Pulst, S. M. (1998) Genomic structure of the human gene for spinocerebellar ataxia type 2 (SCA2) on chromosome 12q24.1. *Genomics,* 47, 359-364.

Sanpei, K., Takano, H., Igarashi, S. et al. (1996) Identification of the spinocerebellar ataxia type 2 gene using a direct identification of repeat expansion and cloning technique, DIRECT. *Nature genetics,* 14, 277-284.

Sasaki, H., Wakisaka, A., Sanpei, K. et al. (1998) Phenotype variation correlates with CAG repeat length in SCA2--a study of 28 Japanese patients. *Journal of the neurological sciences,* 159, 202-208.

Sato, K., Kashihara, K., Okada, S., Ikeuchi, T., Tsuji, S., Shomori, T., Morimoto, K. and Hayabara, T. (1995) Does homozygosity advance the onset of dentatorubral-pallidoluysian atrophy? *Neurology,* 45, 1934-1936.

Satterfield, T. F., Jackson, S. M. and Pallanck, L. J. (2002) A Drosophila homolog of the polyglutamine disease gene SCA2 is a dosage-sensitive regulator of actin filament formation. *Genetics,* 162, 1687-1702.

Satterfield, T. F. and Pallanck, L. J. (2006) Ataxin-2 and its Drosophila homolog, ATX2, physically assemble with polyribosomes. *Human molecular genetics,* 15, 2523-2532.

Saudou, F., Finkbeiner, S., Devys, D. and Greenberg, M. E. (1998) Huntingtin acts in the nucleus to induce apoptosis but death does not correlate with the formation of intranuclear inclusions. *Cell,* 95, 55-66.

Schmidt, T., Lindenberg, K. S., Krebs, A., Schols, L., Laccone, F., Herms, J., Rechsteiner, M., Riess, O. and Landwehrmeyer, G. B. (2002) Protein surveillance machinery in brains with spinocerebellar ataxia type 3: redistribution and differential recruitment of 26S proteasome subunits and chaperones to neuronal intranuclear inclusions. *Annals of neurology,* 51, 302-310.

Schols, L., Bauer, P., Schmidt, T., Schulte, T. and Riess, O. (2004) Autosomal dominant cerebellar ataxias: clinical features, genetics, and pathogenesis. *Lancet neurology,* 3, 291-304.

Seidel, K., Brunt, E. R., de Vos, R. A., Dijk, F., van der Want, H. J., Rub, U. and den Dunnen, W. F. (2009) The p62 antibody reveals various cytoplasmic protein aggregates in spinocerebellar ataxia type 6. *Clinical neuropathology,* 28, 344-349.

Seidel, K., Meister, M., Dugbartey, G. J. et al. (2011) Cellular protein quality control and the evolution of aggregates in SCA3. *Neuropathology and applied neurobiology*.

Seznec, H., Lia-Baldini, A. S., Duros, C., Fouquet, C., Lacroix, C., Hofmann-Radvanyi, H., Junien, C. and Gourdon, G. (2000) Transgenic mice carrying large human genomic sequences with expanded CTG repeat mimic closely the DM CTG repeat intergenerational and somatic instability. *Human molecular genetics,* 9, 1185-1194.

Shan, D. E., Soong, B. W., Sun, C. M., Lee, S. J., Liao, K. K. and Liu, R. S. (2001) Spinocerebellar ataxia type 2 presenting as familial levodopa-responsive parkinsonism. *Annals of neurology,* 50, 812-815.

Shibata, H., Huynh, D. P. and Pulst, S. M. (2000) A novel protein with RNA-binding motifs interacts with ataxin-2. *Human molecular genetics,* 9, 1303-1313.

Shima, H., Pende, M., Chen, Y., Fumagalli, S., Thomas, G. and Kozma, S. C. (1998) Disruption of the p70(s6k)/p85(s6k) gene reveals a small mouse phenotype and a new functional S6 kinase. *The EMBO journal,* 17, 6649-6659.

Shinomiya, H. (2012) Plastin family of actin-bundling proteins: its functions in leukocytes, neurons, intestines, and cancer. *International journal of cell biology,* 2012, 213492.

Slow, E. J., Graham, R. K., Osmand, A. P. et al. (2005) Absence of behavioral abnormalities and neurodegeneration in vivo despite widespread neuronal huntingtin inclusions. *Proceedings of the National Academy of Sciences of the United States of America,* 102, 11402-11407.

Smyth, G. K. (2005) Limma: linear models for microarray data. In: Bioinformatics and Computational Biology Solutions using R and Bioconductor R. (Gentleman, V. Carey, S. Dudoit, R. Irizarry, W. Huber). pp 397-420. Springer: New York.

Sobue, G., Doyu, M., Nakao, N., Shimada, N., Mitsuma, T., Maruyama, H., Kawakami, S. and Nakamura, S. (1996) Homozygosity for Machado-Joseph disease gene enhances phenotypic severity. *Journal of neurology, neurosurgery, and psychiatry,* 60, 354-356.

Tadauchi, T., Inada, T., Matsumoto, K. and Irie, K. (2004) Posttranscriptional regulation of HO expression by the Mkt1-Pbp1 complex. *Molecular and cellular biology,* 24, 3670-3681.

Thangima Zannat, M., Bhattacharjee, R. B. and Bag, J. (2011) Depletion of cellular poly (A) binding protein prevents protein synthesis and leads to apoptosis in HeLa cells. *Biochemical and biophysical research communications,* 408, 375-381.

Thomas, E. A., Coppola, G., Desplats, P. A. et al. (2008) The HDAC inhibitor 4b ameliorates the disease phenotype and transcriptional abnormalities in Huntington's disease transgenic mice. *Proceedings of the National Academy of Sciences of the United States of America,* 105, 15564-15569.

Trejo, A., Tarrats, R. M., Alonso, M. E., Boll, M. C., Ochoa, A. and Velasquez, L. (2004) Assessment of the nutrition status of patients with Huntington's disease. *Nutrition (Burbank, Los Angeles County, Calif,* 20, 192-196.

Tsuda, H., Jafar-Nejad, H., Patel, A. J. et al. (2005) The AXH domain of Ataxin-1 mediates neurodegeneration through its interaction with Gfi-1/Senseless proteins. *Cell,* 122, 633-644.

Tsukiyama-Kohara, K., Poulin, F., Kohara, M. et al. (2001) Adipose tissue reduction in mice lacking the translational inhibitor 4E-BP1. *Nature medicine,* 7, 1128-1132.

Tsutsumi, T., Kuwabara, H., Arai, T., Xiao, Y. and Decaprio, J. A. (2008) Disruption of the Fbxw8 gene results in pre- and postnatal growth retardation in mice. *Molecular and cellular biology,* 28, 743-751.

Tuin, I., Voss, U., Kang, J. S. et al. (2006) Stages of sleep pathology in spinocerebellar ataxia type 2 (SCA2). *Neurology,* 67, 1966-1972.

Turnbull, V. J., Storey, E., Tarlac, V., Walsh, R., Stefani, D., Clark, R. and Kelly, L. (2004) Different ataxin-2 antibodies display different immunoreactive profiles. *Brain research,* 1027, 103-116.

Uchida, N., Hoshino, S., Imataka, H., Sonenberg, N. and Katada, T. (2002) A novel role of the mammalian GSPT/eRF3 associating with poly(A)-binding protein in Cap/Poly(A)-dependent translation. *The Journal of biological chemistry,* 277, 50286-50292.

Um, S. H., Frigerio, F., Watanabe, M. et al. (2004) Absence of S6K1 protects against age- and diet-induced obesity while enhancing insulin sensitivity. *Nature,* 431, 200-205.

Underwood, J. G., Boutz, P. L., Dougherty, J. D., Stoilov, P. and Black, D. L. (2005) Homologues of the Caenorhabditis elegans Fox-1 protein are neuronal splicing regulators in mammals. *Molecular and cellular biology,* 25, 10005-10016.

van de Loo, S., Eich, F., Nonis, D., Auburger, G. and Nowock, J. (2009) Ataxin-2 associates with rough endoplasmic reticulum. *Experimental neurology,* 215, 110-118.

Velazquez-Perez, L., Rodriguez-Labrada, R., Garcia-Rodriguez, J. C., Almaguer-Mederos, L. E., Cruz-Marino, T. and Laffita-Mesa, J. M. (2011) A comprehensive review of spinocerebellar ataxia type 2 in Cuba. *Cerebellum (London, England),* 10, 184-198.

Verkerk, A. J., Pieretti, M., Sutcliffe, J. S. et al. (1991) Identification of a gene (FMR-1) containing a CGG repeat coincident with a breakpoint cluster region exhibiting length variation in fragile X syndrome. *Cell,* 65, 905-914.

Voineagu, I., Wang, X., Johnston, P. et al. (2011) Transcriptomic analysis of autistic brain reveals convergent molecular pathology. *Nature,* 474, 380-384.

Wadia, N. H. and Swami, R. K. (1971) A new form of heredo-familial spinocerebellar degeneration with slow eye movements (nine families). *Brain,* 94, 359-374.

Watase, K., Gatchel, J. R., Sun, Y. et al. (2007) Lithium therapy improves neurological function and hippocampal dendritic arborization in a spinocerebellar ataxia type 1 mouse model. *PLoS medicine,* 4, e182.

Watase, K., Weeber, E. J., Xu, B. et al. (2002) A long CAG repeat in the mouse Sca1 locus replicates SCA1 features and reveals the impact of protein solubility on selective neurodegeneration. *Neuron,* 34, 905-919.

Watase, K. and Zoghbi, H. Y. (2003) Modelling brain diseases in mice: the challenges of design and analysis. *Nat Rev Genet,* 4, 296-307.

Whaley, N. R., Fujioka, S. and Wszolek, Z. K. (2011) Autosomal dominant cerebellar ataxia type I: a review of the phenotypic and genotypic characteristics. *Orphanet journal of rare diseases,* 6, 33.

Wiedemeyer, R., Westermann, F., Wittke, I., Nowock, J. and Schwab, M. (2003) Ataxin-2 promotes apoptosis of human neuroblastoma cells. *Oncogene,* 22, 401-411.

Xia, H., Mao, Q., Eliason, S. L. et al. (2004) RNAi suppresses polyglutamine-induced neurodegeneration in a model of spinocerebellar ataxia. *Nature medicine,* 10, 816-820.

Yoo, S. Y., Pennesi, M. E., Weeber, E. J. et al. (2003) SCA7 knockin mice model human SCA7 and reveal gradual accumulation of mutant ataxin-7 in neurons and abnormalities in short-term plasticity. *Neuron,* 37, 383-401.

Zhuchenko, O., Bailey, J., Bonnen, P. et al. (1997) Autosomal dominant cerebellar ataxia (SCA6) associated with small polyglutamine expansions in the alpha 1A-voltage-dependent calcium channel. *Nature genetics,* 15, 62-69.

8 Appendix

8.1 List of figures and tables

List of figures

List of tables

8.2 Abbreviations

129Sv	inbred mouse strain
A2BP1	Ataxin-2 binding protein 1
ADCA	autosomal dominant cerebellar ataxia
ALS	Amyotrophic Lateral Sklerosis
Atxn	Ataxin
Atxn1l	Ataxin-1 like
bas	basal
BCA	bicinchoninic acid
BGS	bovine growth serum
BLAST	Basic Local Alignment Search Tool
bp	base pair
BRCA1	breast cancer 1
BSA	bovine serum albumin
C57BL/6	inbred mouse strain; created by Dr. CC Little from the mating of female 57, black, subline 6
CAA	cytosine-adenine-adenine
CAG	cytosine-adenine-guanine
cDNA	complementary DNA
CHX	cycloheximide
cm	centimeter
CNS	central nervous system
Co-IP	Co-Immunoprecipitation
COS	CV-1 in Origin carrying SV40
Cre	cyclization recombination
CTG	cytosine-thymine-guanine
D	day
DAB	3,3'-Diaminobenzidine
DDX6	DEAD box polypeptide 6
DMEM	Dulbecco's Modified Eagle Medium
DMSO	Dimethyl solfoxide
DNA	deoxyribonucleic acid
dNTP	deoxyribonucleic triphosphates
DRPLA	Dentatorubral-pallidoluysian atrophy
DTA	Diphtheria Toxin A
ECL	enhanced chemiluminescence
EDTA	Ethylenediaminetetraacetic acid
e.g.	exempli gratia
EGTA	ethyleneglycoltetraacetic acid
eIF	eukaryotic initiation factor
ER	endoplasmic reticulum
ES cell	embryonic stem cell
et al.	et alii
ex	exon
exp	expected
FCS	fetal calf serum
FAM	fluorescein amidite
Flp	Flippase
FMR1	fragile X mental retardation 1
FMRP	fragile X mental retardation protein
FRT	Flippase recognition target
g	Earth's gravitational acceleration
G418	geneticin
h	hour

HEK293	human embryonic kidney cells
HeLa	cervical cancer cells derived from the patient Henrietta Lacks
HEPES	4-(2-hydroxyethyl)-1-piperazineethanesulfonic acid
hnRNP	heterogeneous nuclear ribonucleoproteins
IHC	Immunohistochemistry
IP	Co-immunoprecipitation
Hprt	Hypoxanthine-guanine phosphoribosyltransferase
Ins	insulin
LCM	Laser capture microdissection
kb	kilo bases
kDa	kilo Dalton
KO	knock-out
KRAB	Krüppel-associated box
LA	long homology arm
LoxP	locus of crossover in P1
LSm	Like Sm
LSmAD	Like Sm associated domain
µCi	micro Curie
µF	micro Farad
µg	microgram
µl	microliter
µm	micro metre
µM	micromolar
M	marker
M	molar
MEM	Modified Eagle Medium
mg	milligram
min	minutes
miRNA	micro RNA
ml	milliliter
mm	millimetre
mM	millimolar
mRNA	messenger RNA
n.a.	not analyzed
NaCl	sodium chloride
NCBI	National Center for Biotechnology Information
NEAA	non-essential amino acids
NII	neuronal intranuclear inclusions
Neo	neomycin
ng	nanogramm
NLS	nuclear localization signal
nM	nanomol
Nr	Number
n.s.	not significant
PABPC1	Poly(A) binding protein, cytoplasmic 1
Paip	Poly(A) binding protein interacting protein
PAM	PABP interacting motif
PAN	Poly(A) nuclease
PB	processing body
Pbp1	Pab binding protein 1
PBS	Phosphate-buffered saline
PBST	Phosphate-buffered saline, Tween
PCR	polymerase chain reaction
PDL	population doubling levels
Pen/Strep	Penicillin Streptomycin
PFA	paraformaldehyde

pmol	picomolar
PMSF	Phenylmethylsulfonylfluorid
Poly(A)	polyadenine
polyQ	polyglutamine
PRD	proline-rich domain
PVDF	Polyvinylidenfluorid
rER	rough endoplasmic reticulum
RIPA	radioimmunoprecipitation assay
RNA	ribonucleic acid
rpm	revolutions per minute
RRM	RNA recognition motif
rRNA	ribosomal RNA
RT	room temperature
SA	short homology arm
SBMA	Spinal bulbar muscle atrophy
SCA	Spinocerebellar Ataxia
$Sca2^{-/-}$	Sca2 deficient
SDS	sodium dodecyl sulfate
sec	seconds
Sens	senseless
SG	stress granule
SH3	Src homology 3
SMA	Spinal muscular atrophy
SMN1	survival motor neuron 1
SN	supernatant
SSC	saline sodium citrate
T	trial
TIA-1	T-cell restricted intracellular antigen-1
TCA	Trichloroacetic acid
TEMED	N,N,N',N'-Tetramethylethylendiamin
Tris	Tris(hydroxymethyl)-aminomethan
TM	Tunicamycin
TOP	terminal oligopyrimidine
UTR	untranslated region
V	Volt
vol	volume
WB	Western blot
WT	wild-type
ZBRK1	Zinc finger and BRCA1-interacting protein with a KRAB domain 1
ZFE	Zentrale Forschungseinrichtung

8.3 Microarray 18 months

Cerebellum			
ID	**Symbol**	**Name**	**log2 fold change**
1426944_PM_at	Fbxw8	F-box and WD-40 domain protein 8	**1.35**
1436732_PM_s_at	Fbxw8	F-box and WD-40 domain protein 8	**1.32**
1437397_PM_at	Prlr	prolactin receptor	**0.92**
1438198_PM_at	Bri3bp	Bri3 binding protein	**0.42**
1419406_PM_a_at	Bcl11a	B-cell CLL/lymphoma 11A (zinc finger protein)	**0.39**
1435935_PM_at	NA	NA	**-0.50**
1446948_PM_at	NA	NA	**-0.59**
1457155_PM_at	Aldh2	aldehyde dehydrogenase 2, mitochondrial	**-0.61**
1454561_PM_at	9430087B13Rik	RIKEN cDNA 9430087B13 gene	**-0.63**
1440206_PM_at	A930024E05Rik	RIKEN cDNA A930024E05 gene	**-0.73**
1443378_PM_s_at	Adam1a	a disintegrin and metallopeptidase domain 1a	**-0.82**
1423790_PM_at	Dap	death-associated protein	**-0.85**
1427790_PM_at	Adam1a	a disintegrin and metallopeptidase domain 1a	**-0.93**
1446137_PM_at	Gbas	glioblastoma amplified sequence	**-1.01**
1439787_PM_at	P2rx7	purinergic receptor P2X, ligand-gated ion channel, 7	**-1.14**
1446429_PM_at	P2rx4	purinergic receptor P2X, ligand-gated ion channel 4	**-1.27**
1447526_PM_at	D5Ertd255e	DNA segment, Chr 5, ERATO Doi 255, expressed	**-1.71**
1444750_PM_at	NA	NA	**-1.72**
1445307_PM_at	NA	NA	**-1.99**
1443905_PM_at	Hpvc-ps	human papillomavirus 18 E5 central sequence motif, pseudogene	**-2.07**

Brainstem			
ID	**Symbol**	**Name**	**log2 fold change**
1450483_PM_at	Gjc2	gap junction protein, gamma 2	**0.95**
1438198_PM_at	Bri3bp	Bri3 binding protein	**0.41**
1443378_PM_s_at	Adam1a	a disintegrin and metallopeptidase domain 1a	**-0.55**
1435935_PM_at	NA	NA	**-0.63**
1446137_PM_at	Gbas	glioblastoma amplified sequence	**-0.64**
1457557_PM_at	A330076H08 Rik	RIKEN cDNA A330076H08 gene	**-0.76**
1444750_PM_at	NA	NA	**-0.80**
1446429_PM_at	P2rx4	purinergic receptor P2X, ligand-gated ion channel 4	**-1.03**
1439787_PM_at	P2rx7	purinergic receptor P2X, ligand-gated ion channel, 7	**-1.13**
1457155_PM_at	Aldh2	aldehyde dehydrogenase 2, mitochondrial	**-1.25**
1447526_PM_at	D5Ertd255e	DNA segment, Chr 5, ERATO Doi 255, expressed	**-1.56**
1445307_PM_at	NA	NA	**-1.60**
1443905_PM_at	Hpvc-ps	human papillomavirus 18 E5 central sequence motif, pseudogene	**-1.61**
1452968_PM_at	Cthrc1	collagen triple helix repeat containing 1	**-1.88**

Liver			
ID	**Symbol**	**Name**	**log2 fold change**
1424775_PM_at	NA	NA	**2.56**
1459861_PM_s_at	NA	NA	**2.47**
1440921_PM_at	Nlrp12	NLR family, pyrin domain containing 12	**1.95**
1452956_PM_a_at	Ifi27l1	interferon, alpha-inducible protein 27 like 1	**1.71**
1454757_PM_s_at	Ifi27l1	interferon, alpha-inducible protein 27 like 1	**1.68**
1452198_PM_at	Kdm2b	lysine (K)-specific demethylase 2B	**1.52**
1419573_PM_a_at	Lgals1	lectin, galactose binding, soluble 1	**1.18**
1455439_PM_a_at	Lgals1	lectin, galactose binding, soluble 1	**1.10**
1418320_PM_at	Prss8	protease, serine, 8 (prostasin)	**1.06**
1438743_PM_at	Cyp7a1	cytochrome P450, family 7, subfamily a, polypeptide 1	**0.94**
1427410_PM_at	Dleu2	deleted in lymphocytic leukemia, 2	**0.81**
1452753_PM_at	Foxk2	forkhead box K2	**0.59**
1426406_PM_at	Setd8	SET domain containing (lysine methyltransferase) 8	**0.59**
1426670_PM_at	Agrn	agrin	**0.56**
1436981_PM_a_at	Ywhaz	tyrosine 3-monooxygenase/tryptophan 5-monooxygenase activation protein, zeta polypeptide	**0.45**
1419406_PM_a_at	Bcl11a	B-cell CLL/lymphoma 11A (zinc finger protein)	**-0.36**
1447526_PM_at	D5Ertd255e	DNA segment, Chr 5, ERATO Doi 255, expressed	**-0.46**
1451271_PM_a_at	Acat1	acetyl-Coenzyme A acetyltransferase 1	**-0.51**
1433470_PM_a_at	Immt	inner membrane protein, mitochondrial	**-0.54**
1424183_PM_at	Acat1	acetyl-Coenzyme A acetyltransferase 1	**-0.58**
1433855_PM_at	Abat	4-aminobutyrate aminotransferase	**-0.59**
1416570_PM_s_at	Gfm1	G elongation factor, mitochondrial 1	**-0.64**
1424182_PM_at	Acat1	acetyl-Coenzyme A acetyltransferase 1	**-0.66**
1439787_PM_at	P2rx7	purinergic receptor P2X, ligand-gated ion channel, 7	**-0.68**
1416049_PM_at	Gldc	glycine decarboxylase	**-0.82**
1419144_PM_at	Cd163	CD163 antigen	**-1.20**
1457155_PM_at	Aldh2	aldehyde dehydrogenase 2, mitochondrial	**-1.23**
1425689_PM_at	Dpys	dihydropyrimidinase	**-1.49**
1420447_PM_at	Sult1e1	sulfotransferase family 1E, member 1	**-1.83**
1453287_PM_at	Ankrd33b	ankyrin repeat domain 33B	**-2.06**

9 Acknowledgements

10 Publications

Scientific publications and presentations

Publications

Parts of this work were already published in:

In revision
"ATXN2-CAG42 sequesters PABPC1 into insolubility and induces FBXW8 in cerebellum of old ataxic knock-in mice"
Damrath E, Heck MV, Gispert S, Nowock J, Seifried C, Rüb U, Auburger G
PLoS Genetics

"The $(CAG)_{102}$ knock-in mouse as a model of Spinocerebellar Ataxia Type 2"
Damrath E, Gispert S, Nonis F, Lastres-Becker I, Nowock J, Rüb U, Auburger G
Journal of Neural Transmission, Vol. 116, No.2, 2009

Background: Spinocerebellar ataxia type 2 (SCA2) is an autosomal dominant neurodegenerative disease which is caused by an expanded polyglutamine tract in ataxin-2, a protein implicated in mRNA processing and endocytosis. The exon 1 in the human SCA2 gene usually contains the trinucleotide repeat (CAG)8CAA(CAG)4CAA(CAG)8, which is expanded to a pure (CAG)-repeat of more than 31 units in patients. Methods: To elucidate the pathogenesis of SCA2, a knock-in mouse model on a C57BL/6J-129SvPas background was generated by introduction of (CAG)102 repeat into the mouse Sca2 gene. Heterozygous and homozygous mice were analyzed for ataxin-2 expression in brain, and for behaviour anomalies until age 3 months. Results: Homozygous knock-in mice at ages 10 days, 20 days and 6 weeks showed a significant decrease in their body weight as well as locomotor hyperactivity in rotarod testing, but no longer at 3 months. Although polyglutamine expansion proteins tend to form neuronal inclusion bodies, ataxin-2 aggregates were not detectable in Western blots of SDS-soluble or SDS-insoluble protein extracts in this age period. The wild-type variant and the expanded variant of the ataxin-2 protein as well as its mRNA were expressed. Conclusions: Tissue from homozygous (CAG)102-Sca2 knock-in mice is now available for analysis, making a detailed comparison between the wild-type variant and the expanded variant of ataxin-2 possible, regarding their processing, subcellular localization and protein/RNA interactions. Its joint analysis with brain tissue from SCA2 patients should help to elucidate early events of the disease mechanism.

Further publications

In revision
"Ataxin-2 modulates the levels of Grb2 and Src"
Jessica Drost, David Nonis, Florian Eich, Oliver Leske, Ewa Damrath, Ewout R. Brunt, Isabel Lastres-Becker, Rolf Heumann, Joachim Nowock, Georg Auburger
Experimental Neurology

In preparation
“Ataxin-2 modulates global translation at initiation”
Isabel Lastres-Becker, David Nonis, Ewa Damrath, Florian Eich, Myriam Gorospe, Peter Kötter, Fabrice A. Klein, Nancy Kedersha, Georg Auburger

Presentations

Oral presentations

IMPRS for Neural Circuits - Q and A session, 04.10.2011, Goethe University, Campus Riedberg, Frankfurt am Main, Germany
Educational program of IMPRS “Modern Topics in neuroscience”
“A (CAG)42-SCA2 Knock-In mouse as a model for Spinocerebellar Ataxia type 2”

Immunopharmacology 2011 - The Fourth Symposium on Hereditary Ataxias, Varadero, Cuba, 29.07.2011
“A (CAG)42-SCA2 Knock-In mouse as a model for Spinocerebellar Ataxia type 2”

European A-T Workshop, 29.01.2011, Frankfurt am Main, Germany
“A model of Spinocerebellar Ataxia type 2 (SCA2): The (CAG)42-SCA2 knock-in mouse”

ICNF symposium at Neuro Science Center, 11.06.2010, Goethe University Medical School, Frankfurt am Main, Germany
“A (CAG)42-SCA2 Knock-In mouse as a model for Spinocerebellar Ataxia type 2”

Poster presentations

Gordon Research Conference, 05.-10.06.2011, Lucca, Italy
Damrath E, Gispert S, Nowock J, Auburger G
“A model of Spinocerebellar Ataxia type 2 (SCA2): The (CAG)42-SCA2 knock-in mouse”

Gordon Research Seminar, 04.-05.06.2011, Lucca, Italy
Damrath E, Gispert S, Nowock J, Auburger G
“A model of Spinocerebellar Ataxia type 2 (SCA2): The (CAG)42-SCA2 knock-in mouse”

Post-transcriptional control: mRNA translation, localization and turnover, Edinburgh, Scotland, 08.-10.06.2010
Damrath E, Lastres-Becker I, Fittschen M, Auburger G
“Ataxin-2 is implicated in translation”

IV. Meeting on Molecular Mechanisms of Neurodegeneration, Milan, Italy, 08.-10.05.2009
Damrath E, Gispert S, Nonis FD, Lastres-Becker I, Nowock J, Auburger G
“A model of Spinocerebellar Ataxia Type 2 (SCA2): The (CAG)102-Sca2 knock-in mouse”

6. Deutscher Parkinson Kongress, Marburg, Germany, 05.-07.03.2009
Damrath E, Gispert S, Nowock J, Auburger G
“The (CAG)102-Sca2 knock-in mouse as a model of Spinocerebellar Ataxia Type 2”

EUROSCA final meeting, Palma, Mallorca, 05.-06.12.2008
Damrath E, Gispert S, Nowock J, Auburger G
The (CAG)102-Sca2 knock-in mouse as a model of Spinocerebellar Ataxia Type 2

ICNF Symposia 2008-2011
Goethe University Medical School, Frankfurt am Main, Germany

11 Curriculum vitae